November 2016

The Fate of Haloacetonitriles in Drinking Waters

Yun Yu
University of Massachusetts Amherst

THE FATE OF HALOACETONITRILES IN DRINKING WATERS

A Dissertation Presented

by

YUN YU

Submitted to the Graduate School of the
University of Massachusetts Amherst in partial fulfillment
of the requirements for the degree of

DOCTOR OF PHILOSOPHY

September 2016

Environmental and Water Resources Engineering
Department of Civil and Environmental Engineering
University of Massachusetts Amherst

THE FATE OF HALOACETONITRILES IN DRINKING WATERS

A Dissertation Presented

by

YUN YU

Approved as to style and content by:

_____
David A. Reckhow, Chair

_____
John E. Tobiason, Member

_____
Paul K. Barten, Member

_____
Erich Hinlein, Member

_____
Richard N. Palmer, Department Head
Civil and Environmental Engineering Department

ACKNOWLEDGEMENTS

I would like to express my deepest gratitude to my advisor, Dr. David A. Reckhow, for his understanding, kindness, unwavering support, and generous guidance throughout my graduate education. It was his trust and encouragement that allowed me to develop as an experimentalist, an environmental chemist, and more importantly, as an independent researcher. His expertise and well-rounded experiences paved the path before me and lightened me up through the darkness when my steps faltered. Without his mentorship, the completion of this dissertation would not have been possible.

Thanks also extend to the member of my committee, Dr. John E. Tobiason for providing insightful comments and constructive criticisms at all stages of my research. I am grateful to him for focusing me to my ideas and holding me to a high standard. His continuous encouragement and selfless support to my professional development is also sincerely appreciated. My gratitude is also due to Dr. Paul K. Barten for his invaluable input to my dissertation. Many of the discussions with Dr. Barten enriched me and have certainly broadened my horizons which laid me the foundation for becoming a more interdisciplinary researcher.

I also want to take this opportunity to express my most sincere appreciation to Sherrie Webb-Yagodzinski for her assistance and her friendship. I am very thankful for her endeavors to maintain all the analytical instruments in the lab that much of my research was based on. Her unyielding devotion and care truly made the laboratory a safe, collaborative, and friendly place to work at for the past many years. Without her contributions, the completion of my dissertation research would have been immeasurably

more difficult. I also greatly value her friendship and I deeply appreciate her belief in me and her unending support that helped me overcome those setbacks and stay focused on my graduate study.

I am also grateful to many friends, Patrick Wittbold, Cynthia Castro, Caitlin Spence, Stephanie Zimmers, Ran Zhao, Soonmi Kim, Houbao Li, and Elizabeth Adams for their various forms of help and support that adjusted me to this new country. I would also like to acknowledge the former research associate emeritus, Larry Kramer and Kaoru Ikuma who got my graduate career started on the right foot and provided many helpful advices to improve my skill sets in this area. I am also indebted to Dr. David W. Ostendorf and Dr. Erich Hinlein for the financial support, Scott Steinschneider for developing the Bayesian modeling framework with me, and the rest of the research team at Environmental Water and Resources Engineering who I worked closely with, Varun Srinivasan, Arianne Bazilio, Camelia Rotaru, and Will Lukas.

Finally, and most importantly, this dissertation is also dedicated to my family, without whom none of this would have been achieved. I would like to express my heartfelt thanks to my parents, for their faith in me and allowing me to be as ambitious as I wanted. They have been a constant source of love, patience, concern, support, and strength throughout these difficult years and it was under their watchful eyes that I gained so much drive and ability to tackle challenges head on.

ABSTRACT

THE FATE OF HALOACETONITRILES IN DRINKING WATERS

SEPTEMBER 2016

YUN YU

B.A., SHANGHAI UNIVERSITY

M.S., UNIVERSITY OF MASSACHUSETTS AMHERST

PH.D., UNIVERSITY OF MASSACHUSETTS AMHERST

Directed by: Dr. David A. Reckhow

The identification and control of halogenated nitrogenous disinfection byproducts (N-DBPs) in drinking waters is of increasing interest over the past decade due to their more substantial carcinogenic potencies than the currently regulated trihalomethanes (THMs) and the haloacetic acids (HAAs), which offset their relatively low-level occurrence in drinking waters to be considered as important emerging DBPs.

Among the major N-DBP families, haloacetonitriles (HANs) are most ubiquitous and they usually occur at the highest levels in US drinking waters. The formation of HANs is always found to be positively correlated with dissolved organic nitrogen (DON) content in source waters. In particular, early research on HAN formation has recognized free amino acids, such as aspartic acid, tyrosine, tryptophan, as well as some of their metabolites (e.g. kynurenine and kynurenic acid) as prolific HAN producers. With the presence of free amino nitrogen, amino acids are demonstrated to be highly reactive with chlorine and can lead to rapid formation of HANs via dichloramination and

decarboxylation reactions. However, free amino acids are probably not the primary precursors for HANs, mainly because their actual concentrations in natural waters are too low to sufficiently account for significant amounts of HANs that actually occur in finish water supplies. On the contrary, combined amino acids including peptides, proteins, and those that are associated with humic substances, are four to five times as common as the free forms. Regardless of their much higher abundance, it is ambiguous if combined amino acids can contribute to the formation of HANs, especially with all the essential amino nitrogens bound in peptide linkages. In fact, many have shown that the amide nitrogen within peptide bonds is unreactive with aqueous chlorine. For this reason, one of the key objectives of this study was to clarify the reactivity of combined amino acids with chlorine particularly in terms of HAN formation. Results indicated that combined amino acids could actually produce dichloroacetonitrile (DCAN) during chlorination, but the rate of DCAN formation was much slower compared to that from free amino acids. The key to the formation of HANs from combined amino acids was found to be a chlorine-induced peptide degradation process, which removes each amino acid residue from the peptide backbone in a slow stepwise fashion, thus continuously creating reactive free amino nitrogens at the *N*-terminal end.

Simultaneous to their continuous formation, HANs are chemically unstable and can undergo considerable decomposition via several types of degradation reactions. It is commonly acknowledged that the rate of HAN loss generally increases with increasing pH but varies among different analogues depending on the nature of their halogenated substituents. Additionally, free chlorine was shown to be an important factor and HAN degradation was accelerated in its presence. Despite the prevailing understanding that

HANs are reactive, the chemical stability of HANs has not been systematically evaluated and kinetically characterized to allow quantitative prediction of their lifetime under typical drinking water conditions. Furthermore, HAN decomposition mechanisms have not been fully elucidated and reconciled with the postulated reaction pathways. Therefore, a more comprehensive kinetic analysis is necessary to understand the reaction kinetics as well as the reaction mechanisms for a more complete set of HANs. Through this study, a mathematical kinetic model was established for seven chlorinated and brominated HAN species and their individual reaction rate constants were estimated using the Bayesian modeling framework as a more robust means of parameter estimation than classic least squares regression. Moreover, the nucleophilic nature of HAN reactions was summarized by developing linear free energy relationships (LFERs) for both HAN hydrolysis and chlorination pathways.

Perhaps most importantly, as HANs degrade, they leave other reaction products in their place. Depending on the nature and lifetime of these sequential products, they may survive drinking water distribution and become important DBPs in their own right. Hence, understanding the concentrations, relations, and stability of these secondary reaction products is of great significance. Although it has been exclusively proposed that HAN degradation produces the corresponding haloacetamides (HAMs) and haloacetic acids (HAAs) as reaction intermediates and endpoint products, a group of previously misidentified N-DBPs, the *N-chloro*-haloacetamides (*N-Cl*-HAMs) were discovered to be the actual HAN reaction intermediates in this study. The *N-Cl*-HAMs exhibited substantial stability under pH conditions that are typical for drinking water treatment with and without the presence of chlorine. However, their nitrogen-bound chlorine was found

to be highly labile and could be readily dechlorinated by common reducing agents to form HAMs, which resulted in the erroneous identification of HAMs as emerging DBPs in prior occurrence studies.

In brief, this study traced the footprints of HANs in drinking waters from their precursors in source waters to their decomposition products in consumers' tap. The obtained findings from this study bridged several knowledge gaps regarding both HAN formation and degradation and are of practical importance especially in terms of quantitative prediction of their actual occurrence in finished water supplies and evaluation of overall drinking water toxicity as a result of their transformation into secondary DBPs. Moreover, some of the proposed kinetic modeling approaches are generic methodologies, which can be applicable to any instance where the formation and decomposition of reactive drinking water DBPs are to be assessed under varying conditions.

TABLE OF CONTENTS

Page

LIST OF TABLES

Table Page

LIST OF FIGURES

Figure Page

CHAPTER 1

KINETIC ANALYSIS OF HAN STABILITY IN DRINKING WATERS[1]

1.1. Introduction

To date, approximately 600-700 drinking water disinfection byproducts (DBPs) have been reported from the use of major disinfectants (i.e., chlorine, chloramines, etc.) as well as their combinations (Richardson & Postigo, 2011; Stevens et al., 1990; Krasner et al., 1989; Krasner et al., 2006). However, none of the hitherto identified DBPs has been recognized to have sufficient carcinogenic potency to account for the cancer risks to drinking water consumers that are projected from epidemiological studies (Bull et al., 2011). In the search for potential DBPs that might fill this risk gap, increasing interest has been focused on nitrogenous disinfection byproducts (N-DBPs), which are several orders of magnitude more genotoxic and cytotoxic than the regulated trihalomethanes (THMs) and the haloacetic acids (HAAs) (Plewa et al., 2004; Plewa et al., 2007; Muellner et al., 2007).

Among the major N-DBP families, haloacetonitriles (HANs) are the most ubiquitous and they usually occur at the highest levels in US drinking waters. In general, the total mass of HANs represents approximately 10% of the THMs (Krasner et al., 1989; Oliver, 1983). According to a national survey conducted under the Information Collection Rule (ICR), the median concentration for four HANs, including dichloroacetonitrile (DCAN),

[1] Yu, Y.; Reckhow, D.A. Kinetic Analysis of Haloacetonitrile Stability in Drinking Waters. *Environ. Sci. Technol.* **2015,** *49* (18), 11028-11036.

bromochloroacetonitrile (BCAN), dibromoacetonitrile (DBAN), and trichloroacetonitrile (TCAN), ranged from 0.5 μg/L to 41.0 μg/L in finished water supplies for 296 large-scale public water systems and DCAN was recognized to be the most prevalent species (Blank et al., 2002). Regardless of their much lower level of occurrence as compared to THMs, HANs are up to two orders of magnitude more toxic than the regulated HAAs (Muellner et al., 2007), which offsets their importance as emerging non-regulated DBPs.

HANs were first identified in US tap water in 1975 (McKinney et al., 1976). Free amino acids (Trehy & Bieber, 1981; Trehy et al., 1986; Ueno et al., 1996; Yang et al., 2010), algal suspensions that are rich in proteinaceous material (Oliver, 1983; Plummer & Edzwald, 1998), and to a lesser extent, heterocyclic nitrogen in nucleic acids (Young & Uden, 1994; Yang et al., 2012) were recognized as important HAN precursors. Simultaneous to the discovery of HANs, it was noticed that this group of compounds were absent in finished waters with high pHs (Trehy & Bieber, 1981; Bieber & Trehy, 1983). It was later revealed that the absence of HANs was attributed to their chemical instability as they could undergo considerable degradation on time scales relevant to distribution system residence times and the rate of HAN decomposition increases with increasing pH (Glezer et al., 1999; Reckhow et al., 2001).

In addition to pH, chlorine is another important factor and it has been demonstrated that HAN decomposition was accelerated in its presence (Oliver, 1983; Glezer et al., 1999; Reckhow et al., 2001). It was proposed that independent of base-catalyzed DCAN hydrolysis, chlorine can also react with DCAN via direct addition of hypochlorous acid (i.e. HOCl) onto the cyano group, forming the *N-chloro*-dichloroacetamide (*N-Cl*-DCAM; Peters et al., 1990). Alternatively, hypochlorite (i.e., OCl^-) will first catalyze

DCAN hydrolysis, producing the corresponding dichloroacetamide (DCAM), which further reacts with HOCl to form the *N-Cl*-DCAM (Peters et al., 1990). Despite the postulated HAN reaction mechanisms, none of the reaction intermediates have been verified and quantified to elucidate their relations and stabilities under typical drinking water conditions.

On the other hand, there are a large number of US drinking water utilities that have switched from free chlorine to chloramines in order to minimize the formation of THMs and HAAs, driven by more stringent federal regulations (e.g., Stage 2 Disinfectants/Disinfection Byproducts Rule; USEPA, 2003). However, there are concerns that chloramines could enhance the formation of N-DBPs whereas they are effective in inhibiting THM and HAA formation, because the nitrogen in N-DBPs can be derived either from organic precursors, or in the case of chloramination, from the disinfectant (Yang et al., 2010; Yang et al., 2012). For instance, based on the ICR database, an overall higher level of HAN_4 (i.e., DCAN, BCAN, DBAN and TCAN) was detected in surface water plants that used chloramines (both with and without chlorine) than those that only used chlorine (Blank et al., 2002). Nevertheless, the higher HAN occurrence was attributed to the higher level of precursors in the source water for those chloramination plants, and not necessarily to an inherent tendency of chloramines to form more HANs (Blank et al., 2002). In fact, laboratory research has shown a higher formation potential of DCAN from natural waters during free chlorination than during chloramination regardless of whether chloramines were pre-formed or formed in-situ (Hayes-Larson & Mitch, 2010). More importantly, the stability of HANs under conditions that are typical of those used by systems practicing chloramination has not been reported to clarify

whether the relatively higher HAN occurrence was due to their higher stability in the presence of chloramines or to the tendency of chloramines to increase the formation of HANs.

In spite of the general understanding that HANs are reactive under a wide range of pH conditions, their reaction kinetics have not been systematically characterized and the reaction mechanisms have not been fully elucidated. For these reasons, a more comprehensive kinetic analysis is necessary to quantitatively determine the HAN reaction kinetics, and to verify some of the reaction products to reconcile with the prevailing reaction pathways. Therefore, the purpose of this part of the study was to evaluate the chemical stability of a relatively complete set of HANs under different pH conditions (i.e., pH 6-9) with and without the presence of disinfectants (i.e., free chlorine and chloramines). Another key objective was to quantitatively characterize HAN reactions by developing a mathematical kinetic model and to summarize the HAN degradation mechanisms as well as to verify the major reaction intermediates and endpoint products.

1.2. Materials and Methods

1.2.1. Chemicals

Unless otherwise noted, all chemicals were purchased from Fisher Scientific Co. and were of analytical grade. Purified DBP standard compounds including monochloroacetonitrile (MCAN), monobromoacetonitrile (MBAN), dichloroacetonitrile (DCAN), and trichloroacetonitrile (TCAN) were purchased from Sigma-Aldrich. Bromochloroacetonitrile (BCAN) and dibromoacetonitrile (DBAN) were supplied by Crescent Chemical. Bromodichloroacetonitrile (BDCAN) and three of the brominated

HAMs were synthesized by CanSyn Chem. Corp. in Canada. The haloacetic acids mix was obtained from Sigma-Aldrich. Sources and purities of all the standard compounds are available in *Table 1*.

Table 1. Sources and purities of standard compounds.

Analytes	Molecular Formula	Purity	Source
Monochloroacetonitrile	$ClCH_2CN$	99%	Sigma-Aldrich
Monobromoacetonitrile	$BrCH_2CN$	97%	Sigma-Aldrich
Dichloroacetonitrile	Cl_2CHCN	98%	Sigma-Aldrich
Bromochloroacetonitrile	$BrClCHCN$	74%	Crescent Chemical
Dibromoacetonitrile	Br_2CHCN	95%	Crescent Chemical
Trichloroacetonitrile	Cl_3CCN	98%	Sigma-Aldrich
Bromodichloroacetonitrile	$BrCl_2CCN$	>85%	CanSyn Chem. Corp.
Monochloroacetamide	$ClCH_2CONH_2$	98%	Sigma-Aldrich
Monobromoacetamide	$BrCH_2CONH_2$	98%	Sigma-Aldrich
Dichloroacetamide	$Cl_2CHCONH_2$	98%	Sigma-Aldrich
Bromochloroacetamide	$BrClCHCONH_2$	>99%	CanSyn Chem. Corp.
Dibromoacetamide	$Br_2CHCONH_2$	>99%	CanSyn Chem. Corp.
Trichloroacetamide	Cl_3CCONH_2	99%	Sigma-Aldrich
Bromodichloroacetamide	$BrCl_2CCONH_2$	>99%	CanSyn Chem. Corp.

1.2.2. Experimental Conditions

All solutions were prepared in ultra-pure Milli-Q water (EMD Millipore Corp.) containing 10 mM phosphate buffer and were adjusted to the desired pH with sodium hydroxide or hydrochloric acid. One milliliter of mixed HAN stock solution (1 mg/mL in methanol) was introduced into 4 L buffered solutions at the start of each experiment, so that the initial concentration for individual HANs was approximately 250 μg/L. Chlorination of HANs was conducted by adding small volumes of acidified sodium hypochlorite solution to reach the target doses. The chlorine solutions were prepared on the day of use by diluting the sodium hypochlorite stock solution (5.65%-6%, laboratory grade, Fisher Scientific), followed by acidification to the target pHs using hydrochloric

acid, prior to which the actual free chlorine concentration of the stock solution was standardized based on the *N,N*-diethyl-*p*-phenylene diamine (DPD)-ferrous ammonium sulfate (FAS) titrimetric method (EPA Method 330.4). Chloramination was carried out by adding small amounts of a 40 mM chloramine stock solution to each sample, and the chloramines were pre-formed by mixing aqueous ammonium sulfate and sodium hypochlorite at a Cl_2/N ratio of 0.8 M/M, with pH of both solutions adjusted to 8.5 before mixing. After dosing with chlorine or chloramines, samples were partitioned off into 300 mL BOD bottles and were stored free of headspace in a dark 20 °C constant temperature chamber for a maximum of 19 days. At the prescribed reaction times, one bottle of sample would be sacrificed and analyzed immediately for disinfectant residual and DBP concentrations. Six sample replicates were analyzed in this study for the estimation of measurement uncertainties.

1.2.3. Sample Preparation and Chromatographic Analysis

The extraction and analysis of HANs was based on EPA Method 551.1. After the prescribed reaction time, 20 mL aliquots of sample were first acidified using 100 µL of 6 N hydrochloric acid. In the case of chlorination and chloramination of HANs, residual oxidant was quenched by 20 mg/L ascorbic acid after sample acidification. HANs were extracted by adding 4 mL of pentane with an internal standard (*1,2*-dibromopropane) into each sample, together with 15 g of anhydrous sodium sulfate. The samples were shaken at 300 rpm for 15 minutes and the upper organic layer was collected for chromatographic analysis. Haloacetic acids were quantified following the EPA 552.2 method. The standard operating procedures include pH adjustment and quenching of the disinfectant residual, acidification of 30 mL sample using 1.5 mL of 95.0-98.0% W/W sulfuric acid, and

extraction with methyl *tert-butyl* ether, followed by methylation using 5% acidic methanol for two hours. Analysis of the HAMs was conducted via a solid-phase extraction/gas chromatography-mass spectrometry (SPE/GC-MS) method that was developed during the course of this study. The SPE procedure involves initial conditioning of the cartridges (Bond Elut PPL, 200 mg, 3 mL, Agilent Technologies) using 9 mL of methanol followed by 6 mL of Milli-Q water, sample loading (100 mL at ~1 mL/min), nitrogen drying of the cartridges for 30 minutes, and final elution with 2 mL of ethyl acetate. HANs and the derivatized methyl haloacetates were analyzed using an Agilent 6980 gas chromatography with a linearized micro-electron capture detector (μ-ECD). HAMs were quantified by a Varian CP-3800 gas chromatography coupled with a Varian Saturn 2200 ion-trap mass spectrometer using chemical ionization. Detailed information about the capillary GC columns and oven temperature programs are provided in *Table 2*.

Table 2. GC columns and oven temperature programs for the analysis of all DBPs

	HANs	HAAs	HAMs
Analytical Column	DB-5	DB-1	DB-1/MS
Length	30 m	30 m	30 m
Internal Diameter	0.25 mm	0.25 mm	0.25 mm
Film Thickness	1.0 μm	0.25 μm	0.25 μm
Carrier Gas	N_2	N_2	He
Carrier Flow	3.9 mL/min	0.9 mL/min	1.2 mL/min
Injector Temp.	175°C	200°C	250°C
Detector Temp.	275°C	250°C	NA
Oven Program	Hold at 27°C for 10 min Ramp to 41°C at 3°C/min and hold for 6 min Ramp to 81°C at 5°C/min Ramp to 180°C at 25°C/min and hold for 6 min	Hold at 37°C for 21 min Ramp to 136°C at 5°C/min and hold for 3 min Ramp to 250°C at 20°C/min and hold for 3 min	Hold at 40°C for 9 min Ramp to 200°C at 20°C/min and hold for 13 min

1.3. Results and Discussion

1.3.1. Hydrolysis of Haloacetonitriles

The hydrolysis of seven HANs (MCAN, MBAN, DCAN, BCAN, DBAN, TCAN and BDCAN) was investigated at pH 6, 7, 8, 8.5, and 9 in phosphate buffered solutions for reaction times of a few minutes to a total of 19 days (456 hours). Residual HAN concentrations were consistent with a rate law that is first-order in HANs (*Figure 1*). All seven HANs were most stable at pH 6 and the rate of loss increased with both increasing pH and the number of halogens, which is congruent with the trend that has been reported before (Oliver, 1983; Trehy & Bieber, 1981; Glezer et al., 1999; Reckhow et al., 2001). The instant trihaloacetonitrile (THAN) hydrolysis even under slightly acidic and neutral pH conditions (i.e., pH 6-7) explains their general absence in most drinking water

systems as was noted during the ICR survey (Blank et al., 2002). In sharp contrast, concentrations of monochloroacetonitrile (MCAN) and monobromoacetonitrile (MBAN) remained nearly constant regardless of pH over the entire period of the hydrolysis experiment (*Figure 2*). Furthermore, with the same number of halogens, HAN hydrolysis rate decreased as the halogens shifted from chlorine to bromine, resulting in the following hierarchy in terms of HAN hydrolytic stability:

MBAN>MCAN>DBAN>BCAN>DCAN>BDCAN>TCAN.

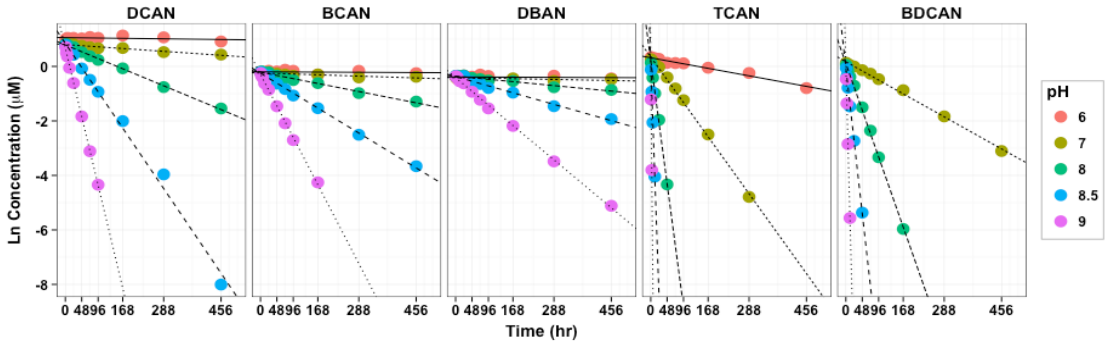

Figure 1. Semi-logarithmic plots of residual HAN concentrations versus reaction time under five hydrolysis pH conditions.

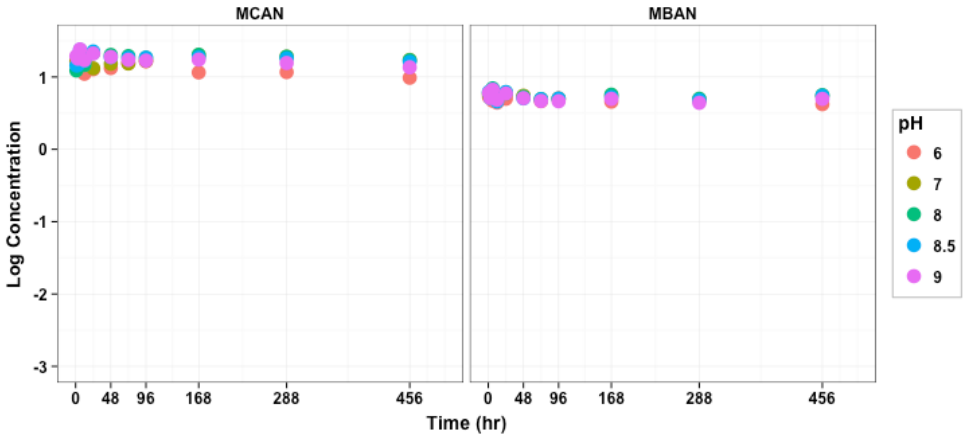

Figure 2. Semi-logarithmic plots of residual MHAN concentrations versus reaction time under hydrolysis conditions (i.e., pH 6-9).

Moreover, two putative hydrolysis products (i.e., the HAMs and the HAAs) were identified and quantified in the same samples, which verifies the prevailing HAN hydrolysis pathways (Reckhow et al., 2001). In general, results demonstrated that the loss of HANs was accompanied by a rapid increase in HAM concentrations, followed by a slower formation of the corresponding HAAs. As metastable reaction intermediates, the formed HAMs also underwent a certain extent of hydrolysis depending on pH and the number of halogens in the substituents. *Figure 3* shows the formation of DCAM (and TCAM) and DCAA (and TCAA) during DCAN (and TCAN) hydrolysis under four different pH conditions. It is evident in *Figure 3* that DCAM tended to hydrolyze when pH was above 8, and thus its concentration first increased and then decreased at pH 9 due to simultaneous DCAM formation and degradation. Compared to DCAM, TCAM started to hydrolyze at a lower pH (i.e., pH 8) due to its higher degree of halogenation, and its concentration profile was characterized by a distinct peak at pH 8 and only by its decomposition at pH 9. More importantly, the molar sum of residual HAN and the formed HAM and HAA remained almost constant over the entire reaction time for both DCAN and TCAN. This mass balance further confirms that hydrolysis of HANs only produces HAMs and HAAs as major reaction products (Glezer et al., 1999; Reckhow et al., 2001).

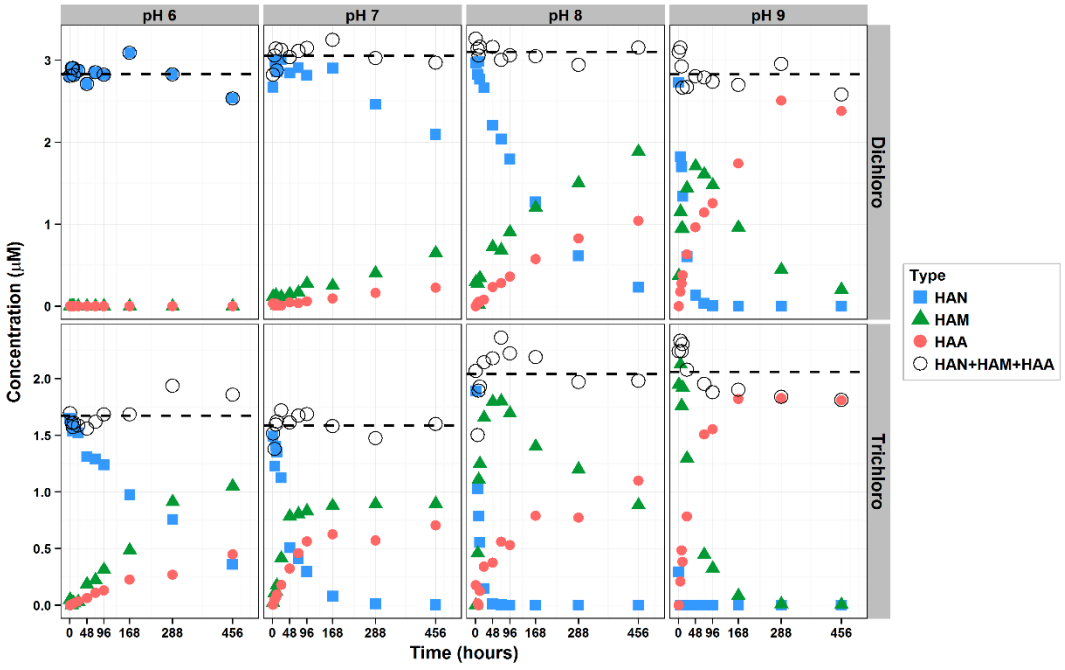

Figure 3. Formation of reaction products during the course of DCAN (top row) and TCAN (bottom row) hydrolysis. The dashed lines represent the initial DCAN and TCAN molar concentrations spiked at the beginning of each hydrolysis experiment.

Based on the first-order reaction kinetics consistent with the results in *Figure 1*, the full second-order HAN hydrolysis rate law can be proposed as follows:

$$\frac{d[HAN]}{dt} = -K_{obs} \cdot [HAN] = -k_{H_2O} \cdot [HAN] - k_{OH} \cdot [OH^-][HAN] \qquad (1)$$

In the above equation, k_{H_2O} and k_{OH} are the respective neutral and basic hydrolysis rate constants. Although it has been acknowledged that neutral water is about nine orders of magnitude less reactive with HANs than the anionic hydroxide (Reckhow et al., 2001), the neutral hydrolysis rate constant (i.e., k_{H_2O}) and the product of $k_{OH}[OH^-]$ can be similar in magnitude when pH is close to or below 5, and therefore can equally contribute to the hydrolysis rate of HANs. For this reason, the proposal of a neutral hydrolysis

pathway and the estimation of the corresponding reaction rate constant (i.e., k_{H_2O}) are necessary for quantitative characterization of HAN hydrolysis under slightly acidic pH conditions. The neutral and basic hydrolysis rate constants for the seven HANs were estimated using a Bayesian modeling approach (Yu et al., 2015) and the details of this statistic methodology are addressed in Chapter 2, while the resulting estimates of k_{H_2O} and k_{OH} are presented below.

In many cases, this hydrolysis model can be further stratified into a hierarchical structure (Yu et al., 2015) by parsing it into a first-order observed rate constant K_{obs} as shown by *Equation 2:*

$$K_{obs} = k_{H_2O} + k_{OH} \cdot [OH^-] \qquad (2)$$

Given that HAN hydrolysis has previously been investigated by several teams of researchers (Oliver 1983; Trehy & Bieber, 1981; Bieber & Trehy, 1983; Glezer et al., 1999; Reckhow et al., 2001), it is important to reconcile our results with those that have been reported. Generally, when pH was below or equal to 8, the first-order observed rate constants (i.e., K_{obs}) determined in this work were in general agreement with literature values (*Figure 4*). Certain disagreements were noted at higher pH levels, which are probably attributed to different experimental conditions such as temperature, sample matrix and measurement errors.

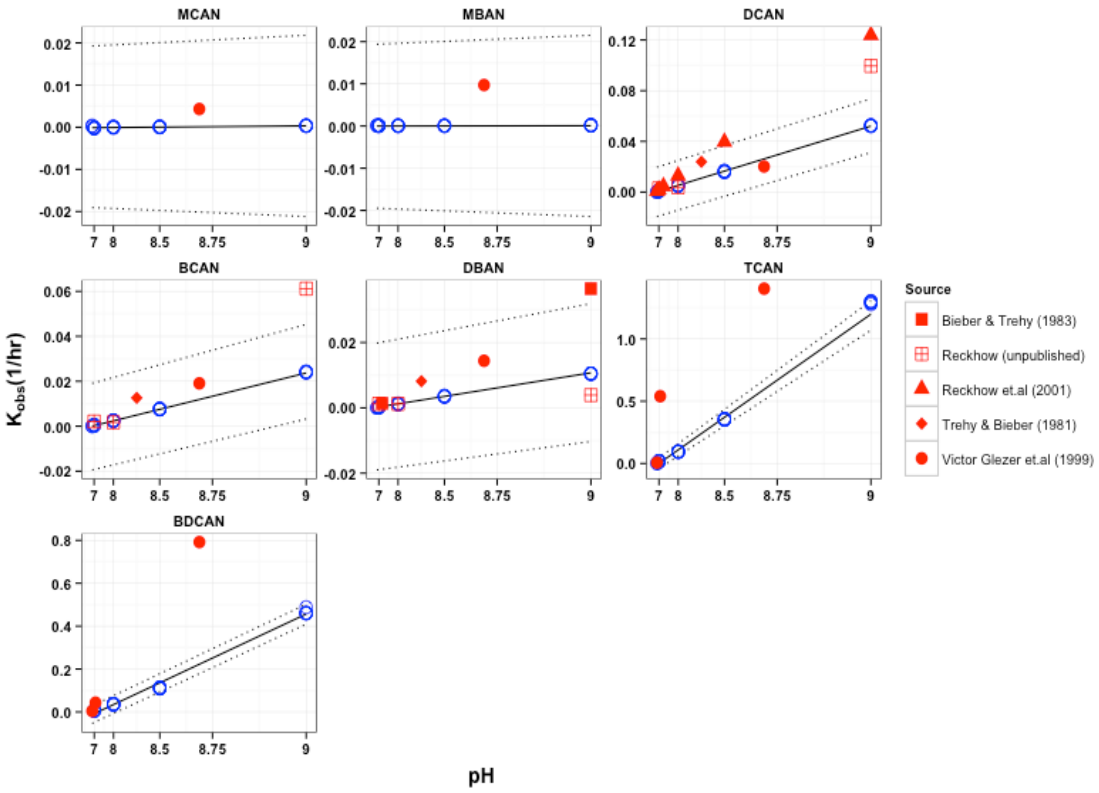

Figure 4. HAN hydrolysis kinetic model. Solid lines represent the modeled K_{obs} values as a function of pH and the dashed lines indicate the lower and upper bounds of a 95% confidence interval. Estimated K_{obs} values from individual lower-level hydrolysis experiments are shown in blue open circles. Literature values are shown in red symbols.

1.3.2. Degradation of Haloacetonitriles in the Presence of Free Chlorine

HAN reaction kinetics were further investigated under three pH conditions (i.e., pH 5, 6, and 7) in the presence of free chlorine (initial chlorine dose: 0.5 mg Cl_2/L ~ 4.0 mg Cl_2/L). It is evident in *Figure 5* that the presence of free chlorine caused rapid HAN degradation, particularly the THANs (i.e., TCAN and BDCAN), and the rate of HAN loss accelerated with both increasing pH and increasing chlorine dose. This chlorine-induced HAN degradation followed many of the trends noted for HAN hydrolysis, with THANs

degrading at the highest rates followed by DHANs and finally MHANs under all investigated conditions. Furthermore, within each of the three groups, more brominated HANs persisted longer than the chlorinated analogues. As a result, the stability hierarchy for the seven HANs remained the same regardless of the presence or the absence of chlorine. Perhaps more importantly, the alike HAN behavior under both hydrolysis and chlorination conditions implies that the two reactions may proceed by similar pathways. This is further validated by developing the respective liner free energy relationships (LFERs) below.

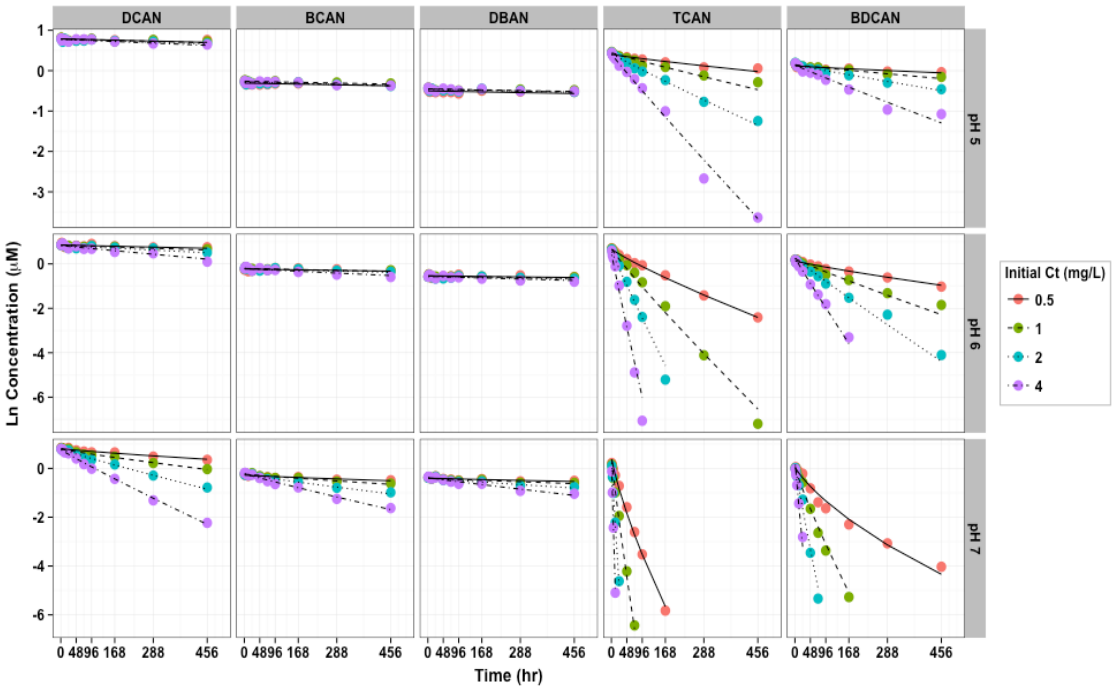

Figure 5. Semi-logarithmic plots of residual HAN concentrations versus reaction time under three pH conditions (i.e., pH 5, 6, and 7) with four different initial free chlorine doses (i.e., 0.5 mg Cl_2/L, 1.0 mg Cl_2/L, 2.0 mg Cl_2/L, and 4.0 mg Cl_2/L). Lines in the figure indicate the predicted HAN concentrations based on the developed HAN kinetic model.

Furthermore, during HAN chlorination, the corresponding HAMs and the HAAs were also quantified. *Figure 6* shows that both two dichloro- and trichloro-reaction products were formed, which partially compensated the loss of DCAN and TCAN under all chlorination conditions. In general, the higher the initial chlorine dose, the more HAN was degraded, and thus the more HAM and HAA were formed. On the other hand, the concentration of HAMs exhibited a slight decrease at longer reaction times. Particularly, TCAM concentration decreased after 96 hours at pH 6 with 4.0 mg Cl_2/L initial chlorine dose. This is probably because HAM themselves can be decomposed through reactions with chlorine (Peters et al., 1990). More importantly, there was a substantial discrepancy between the molar sum of the three HAN, HAM and HAA species and the initial HAN dose (*Figure 6*). Such a negative deviation is indicative of the formation of some other reaction intermediates that were not identified and quantified in this study. In Chapter 3, a full description of this reaction product is presented. Here, it is postulated that HAMs can be further *N*-chlorinated by chlorine to form the *N-chloro*-haloacetamides (*N-Cl*-HAMs; Peters et al., 1990). Moreover, the *N-Cl*-HAMs are weakly acidic (Menard & Lessard, 1978; $pK_{a,NClDCAM} = 3.71$; $pK_{a,NClTCAM} = 2.91$), and therefore will tend to deprotonate and stay relatively stable in the anionic forms within the pH range that is typical for drinking water treatment.

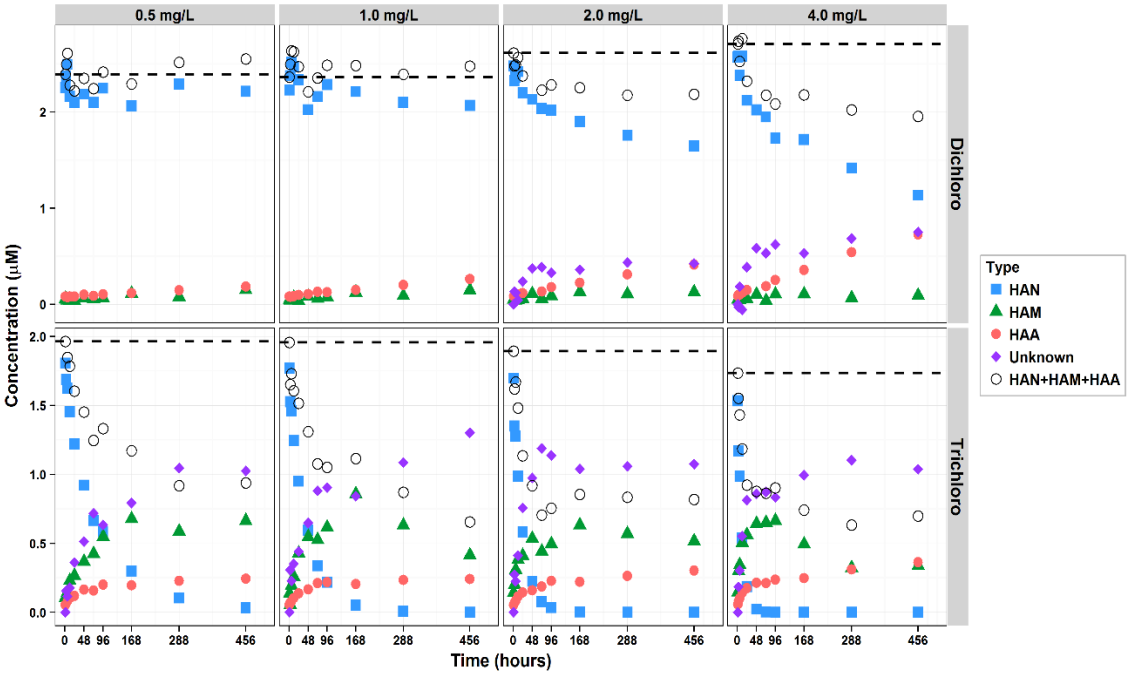

Figure 6. Formation of DCAM and DCAA (top row), TCAM and TCAA (bottom row) during DCAN and TCAN chlorination at pH 6. Purple diamonds represent the intermediates that were not identified and quantified in this investigation. The dashed lines indicate the initial DCAN and TCAN molar concentrations spiked at the beginning of individual chlorination experiments.

Analogous to HAN hydrolysis, the second-order chlorination rate law can be proposed as follows by assuming significant HAN reaction rates with both hypochlorous acid and hypochlorite:

$$\frac{d[HAN]}{dt} = -k_{H_2O}[HAN] - k_{OH}[OH^-][HAN] - k_{HOCl}[HOCl][HAN] - k_{OCl}[OCl^-][HAN] \quad (3)$$

To reflect the pH-dependent speciation between hypochlorous acid and hypochlorite (i.e., HOCl/OCl$^-$), *Equation 3* was reformulated using total free chlorine concentration

(i.e., C_t) and dissociation constant K_a (Morris, 1966) for hypochlorous acid with corrections for ionic strength (i.e., *I*):

$$\frac{d[HAN]}{dt} = -(k_{H_2O} + k_{OH}[OH^-] + k_{HOCl}\alpha_0 C_t + k_{OCl}\alpha_1 C_t) \cdot [HAN] \quad (4)$$

$$\alpha_0 = \frac{[H^+]}{[H^+] + K_{a,I}};\ \alpha_1 = \frac{K_{a,I}}{[H^+] + K_{a,I}} \quad (5)$$

In some of the chlorination experiments, significant depletion of chlorine occurred, particularly when the initial chlorine dose was low. As a result, its concentration cannot be treated as constant without introducing substantial error when the second-order reaction rate constants (i.e., k_{HOCl}.and k_{OCl}) are to be estimated. For this reason, residual chlorine was numerically integrated over time (i.e., $\int_0^t C_t dt$), which is defined as chlorine contact time (CT) and the final kinetic model can be formulated as *Equation 6* shown as follows. The estimated second-order reaction rate constants via Bayesian modeling are presented below.

$$\ln[HAN] = \ln[HAN]_0 - \left(k_{H_2O} + k_{OH}[OH^-]\right) \cdot t - (\alpha_0 k_{HOCl} + \alpha_1 k_{OCl}) \cdot \int_0^t C_t dt \quad (6)$$

1.3.3. Stability of Haloacetonitriles in the Presence of Chloramines

Because of their continuous reaction with chlorine, HANs are often detected at lower levels in systems that only use free chlorine (Blank et al., 2002). Nevertheless, the total amount of HANs that could initially form in those chlorination systems may otherwise be substantially higher (Reckhow et al., 2001; Hayes-Larson & Mitch, 2010). However, the reactivity of HANs with chloramines has not been assessed to clarify if the relatively higher HAN occurrence in most chloramination systems is attributed to their greater

stability in the presence of chloramines or to the greater tendency of chloramines to form more HANs. Therefore, a set of experiments was conducted for the evaluation of HAN stability at a typical chloramination pH (i.e., pH 8.5) with varying doses of preformed monochloramine. The use of preformed monochloramine instead of forming chloramines in-situ via ammonia addition was done to prevent HANs from reacting with transient free chlorine before the latter had a chance to fully combine with ammonia. Results indicated that there was no significant difference in HAN stability with or without the presence of chloramines at doses up to 4 mg/L (as Cl_2) (*Figure 7*), implying that the reaction between HANs and monochloramine was not significant enough to be detectable under the investigated conditions.

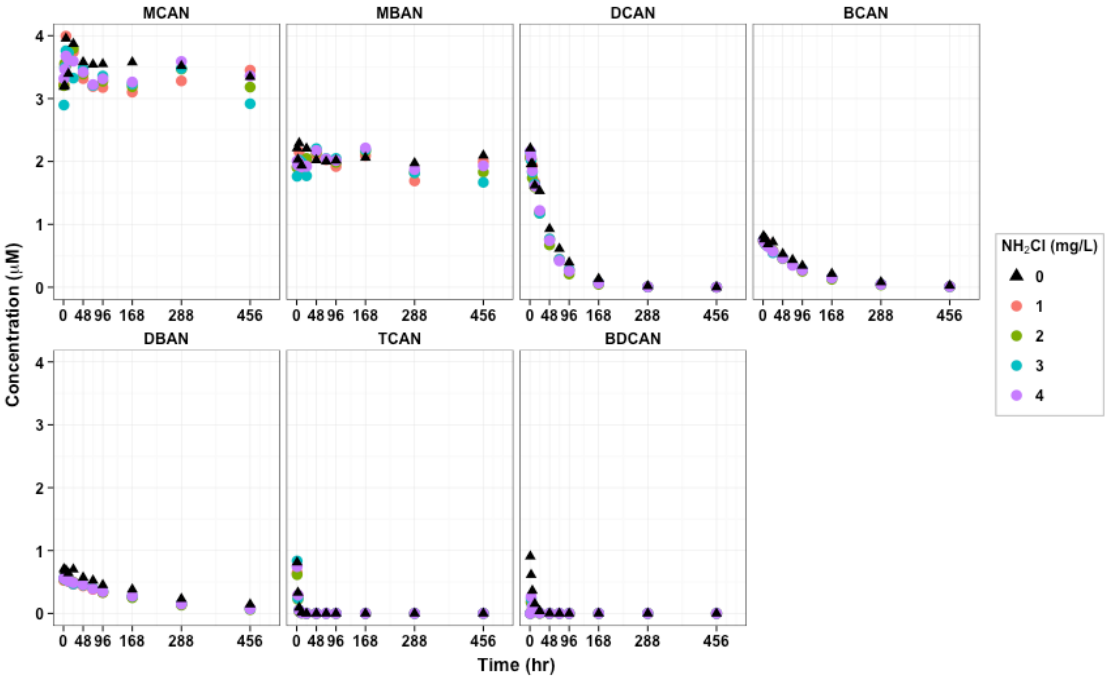

Figure 7. HAN degradation at pH 8.5 with and without the presence of preformed monochloramine.

1.3.4. Estimation of Second-Order Reaction Rate Constants Using Bayesian Modeling

In this study, the four second-order reaction rate constants (i.e., k_{H_2O}, k_{OH}, k_{HOCl}, and k_{OCl} in *Equation 6*) were estimated using a Bayesian framework, which is an alternative statistical approach to the classic least squares regression for the estimation of model parameters. The main benefits of parameter estimation using Bayesian statistics are fully discussed in Chapter 2.

The final distribution of all model parameters, known as the joint posterior distribution (*Figure 8*) shows that the basic hydrolysis rate constant (i.e., k_{OH}) and the hypochlorite chlorination rate constant (i.e. k_{OCl}) for individual HANs were of the same order of magnitude. Moreover, both of the second-order reaction rate constants ranked in reverse order to the HAN stability hierarchy. On the other hand, all estimated neutral hydrolysis rate constants (i.e.,k_{H_2O}) and hypochlorous acid chlorination rate constants (i.e., k_{HOCl}) were not only several orders of magnitude smaller, but also had some fluctuation in terms of following the stability hierarchy. Perhaps most importantly, for all seven HANs, the k_{HOCl} estimates were normally distributed around zero, suggesting that given the size of the dataset collected in this study, this second-order reaction rate constant is not statistically different from zero. As a result, the HAN kinetic model can be simplified to *Equation 7* by dropping the HOCl chlorination term, which will in turn leave the data with higher degrees of freedom to allow for more precise estimation for the remaining three reaction rate constants. The resulting joint posterior distribution of k_{H_2O}, k_{OH}, and k_{OCl} (*Figure 9*) shows that the three second-order reaction rate constants for MBAN were not statistically different from zero due to its remarkably high stability

under all investigated conditions. Furthermore, for MCAN, only k_{OH} is statistically significant and therefore can be estimated with sufficient precision. Lastly, the neutral hydrolysis rate constants (i.e., k_{H_2O}) for the two THANs (i.e., BDCAN and TCAN) were also noted to be small compared to k_{OH} and k_{OCl}. Following the previous methodology, all the reaction rate constants were re-estimated by dropping the insignificant terms to leave the dataset with more freedom. The final posterior estimates of k_{H_2O}, k_{OH}, and k_{OCl} for the seven HANs are listed in *Table 3* with 95% confidence intervals.

$$\ln[HAN] = \ln[HAN]_0 - \left(k_{H_2O} + k_{OH}[OH^-]\right) \cdot t - \alpha_1 k_{OCl} \cdot \int_0^t C_t dt \quad (7)$$

Table 3. The estimated neutral, basic hydrolysis rate constants (k_{H_2O} and k_{OH}), and hypochlorite chlorination rate constant (k_{OCl}) for 7 HANs.

	k_{H_2O} (hr^{-1})		k_{OH} ($M^{-1}hr^{-1}$)		k_{OCl} ($M^{-1}hr^{-1}$)	
	Median	95% C.I.	Median	95% C.I.	Median	95% C.I.
MBAN		NS		NS		NS
MCAN		NS	4.14E+01	(0.89, 7.35) E+01		NS
DBAN	1.38E-04	(0.46, 2.31) E-04	1.09E+03	(1.03, 1.16) E+03	1.54E+02	(1.23, 1.86) E+02
BCAN	1.36E-04	(0.42, 2.35) E-04	2.57E+03	(2.43, 2.72) E+03	3.24E+02	(2.91, 3.58) E+02
DCAN	1.68E-04	(0.66, 2.70) E-04	5.60E+03	(5.29, 5.91) E+03	6.85E+02	(6.40, 7.30) E+02
BDCAN		NS	4.45E+04	(4.20, 4.71) E+04	1.36E+04	(1.30, 1.42) E+04
TCAN		NS	1.23E+05	(1.17, 1.31) E+05	3.91E+04	(3.77, 4.06) E+04

*NS – not significant

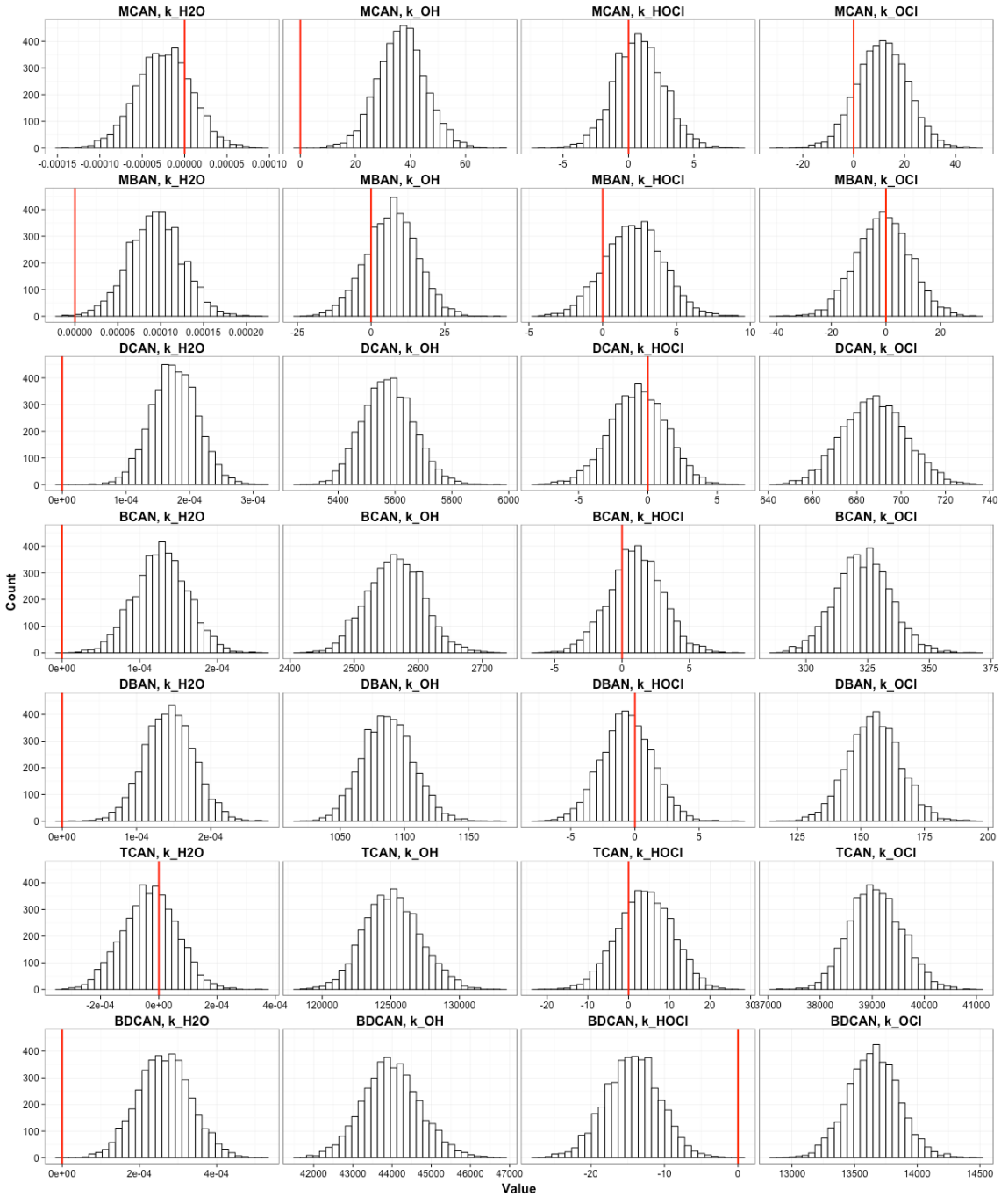

Figure 8. Joint posterior distribution of k_{H_2O}, k_{OH}, k_{HOCl}, and k_{OCl} estimates through Bayesian estimation. Red lines in the figure indicate the zero abscissa.

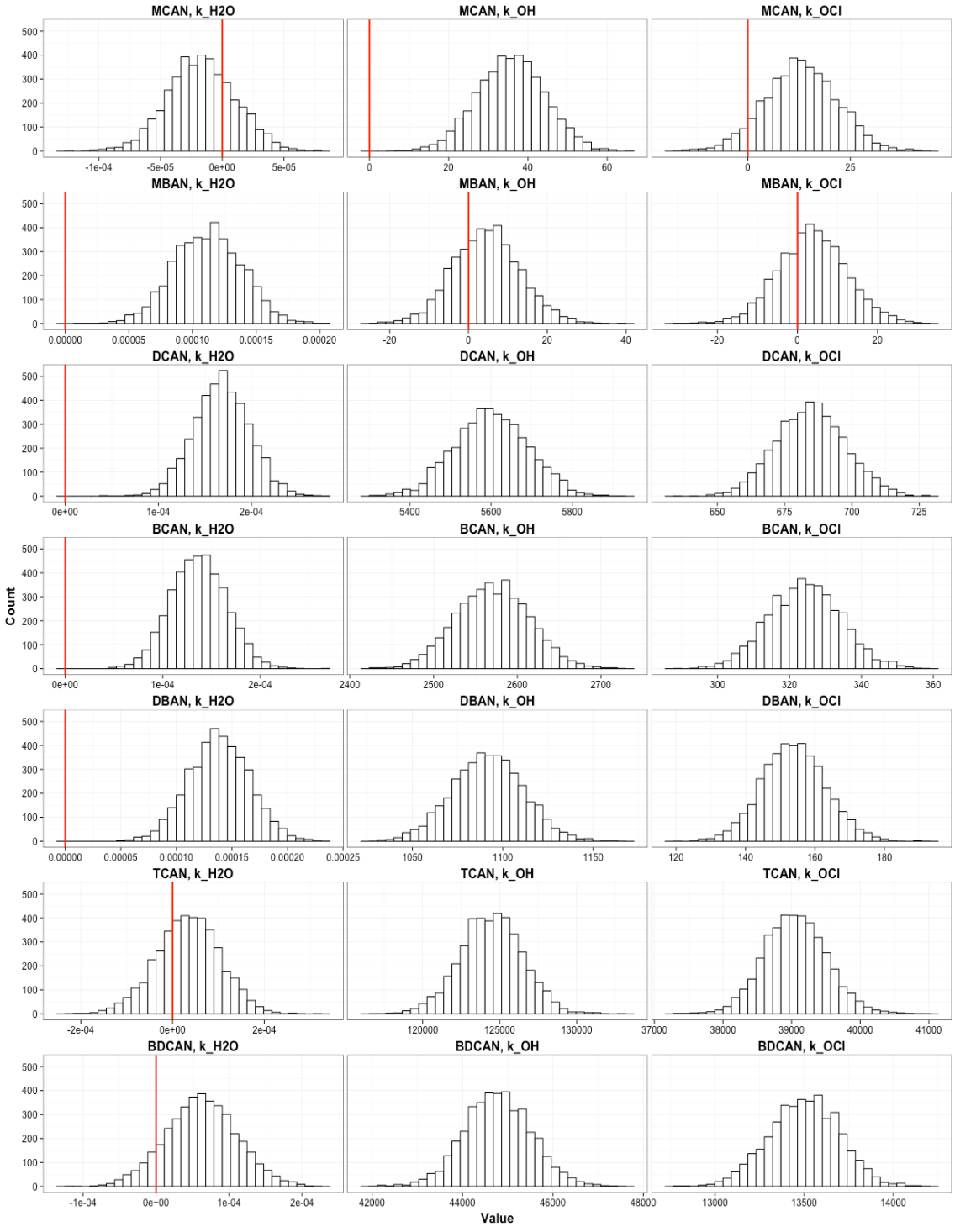

Figure 9. Joint posterior distribution of k_{H_2O},k_{OH}, and k_{OCl} estimates through Bayesian estimation, assuming trivial second-order reaction rates between HANs and HOCl under the investigated conditions. Red lines indicate the zero abscissa.

1.3.5. Taft Linear Free Energy Relationships (LFERs)

The impact of reactant structure on the kinetic properties of the corresponding reaction is usually assessed using LFERs. Establishing LFERs also helps to understand reaction mechanisms and to predict unknown reaction rates assuming that compounds with structural similarities behave alike (Chen, 2011; Deborde & von Gunten, 2008; Schwarzenbach et al, 2003; Zhang & Minear, 2002). The Taft equation (*Equation 8*) was selected for HANs because it has been previously used for the evaluation of substituent inductive and steric effect on the reactivity of aliphatic acetonitriles (Glezer et al., 1999; Taft, 1952; Taft, 1956). In the Taft equation, K_0 is the reaction rate constant for unsubstituted acetonitrile, *k* is the pathway-specific second-order reaction rate constant for a particular HAN with substituent R. σ^* and E_s are Taft's polar and steric substituent constants. The polar and steric sensitivity factors, ρ and δ, are resulting model parameters reflecting the sensitivity of the reaction rate to the substituent polar and steric properties across the entire family of HANs.

$$\log\frac{k}{K_0} = \rho\sigma^* + \delta E_s \qquad (8)$$

Since the Taft's polar substituent constant, σ^*, was only documented for $ClCH_2$-, Cl_2CH-, Cl_3C- and $BrCH_2$- groups (Taft, 1956), its value for mixed bromochloro-substituent was calculated based on proposed correlations between the inductive component of Hammett constant, σ_1, and Taft's polar substituent constant, σ^*, as listed in *Table 4*. On the other hand, the Taft's steric substituent constants, E_s, for CH_2Cl-, CH_2Br-, $CHCl_2$-, $CHBr_2$-, CCl_3- and CBr_3- substituents have been reported (Taft, 1956). E_s for the other mixed bromine- and chlorine-containing substituents was calculated

assuming that the steric effect of di- and tri-halo substituents is a combination of the individual steric contribution of all comprising halogen atoms. As a result, the contribution of a single chlorine atom to the overall steric effect equals half of $E_{s,CHCl_2}$ for dihalogenated compounds and a third of E_{s,CCl_3} for trihalogenated ones. Detailed calculations of the Taft steric substituent constant, E_s, are shown in *Table 5*.

Table 4. Calculation of Taft's polar substituent constants, σ*.

Hammett σ_I		Substituent	Correlation	Taft σ*
$\sigma_{I(Cl)}$	0.47	CH_2Cl	$\sigma^*_{(CH_2X)} = \sigma_{I(X)}/0.45$[1]	1.04
$\sigma_{I(Br)}$	0.45	CH_2Br		1.00
		$CHCl_2$	$\sigma^*_{(CHX_1X_2)} = A(\sigma_{I(X_1)} + \sigma_{I(X_2)})/0.45$[2]	1.94
		CHBrCl	$(A = 0.93)$	1.90
		$CHBr_2$		1.86
		CCl_3	$\sigma^*_{(CX_1X_2X_3)} = B(\sigma_{I(X_1)} + \sigma_{I(X_2)} + \sigma_{I(X_3)})/0.45$[3]	2.65
		CBr_2Cl		2.59
		$CBrCl_2$	$(B = 0.85)$	2.62
		CBr_3		2.55

[1] $\sigma_{I(X)}$ is the inductive component of the Hammett constant and 0.45 is an empirical factor (Lowry & Richardson, 1981; Hansch et al., 1991).

[2] The correlation coefficient, *A*, is evaluated based on the known value of σ^* for $CHCl_2$- substituent: $A = \sigma^*_{(CHCl2)} \cdot \frac{0.45}{2\sigma_{I(Cl)}} = 1.94 \cdot \frac{0.45}{2 \cdot 0.47} = 0.93$ (Glezer et al., 1999.)

[3] The correlation coefficient, *B*, is similarly calculated based on the known value of σ^* for CCl_3- substituent: $B = \sigma^*_{(CCl3)} \cdot \frac{0.45}{3\sigma_{I(Cl)}} = 2.65 \cdot \frac{0.45}{3 \cdot 0.47} = 0.85$ (Glezer et al., 1999).

Table 5. Calculation of Taft's steric substituent constants, E_s.

	E_s (Taft, 1956)		Individual Contribution		E_s (Calculated)	
Monohalo-	$E_{s\ (CH2Cl)}$	-0.24				
	$E_{s\ (CH2Br)}$	-0.27				
Dihalo-	$E_{s\ (CHCl2)}$	-1.54	$E_{s\ (Cl)}$	-0.77		
	$E_{s\ (CHBr2)}$	-1.86	$E_{s\ (Br)}$	-0.93		
					$E_{s\ (CHBrCl)}$	(-0.77)+(-0.93)=-1.70
Trihalo-	$E_{s\ (CCl3)}$	-2.06	$E_{s\ (Cl)}$	-0.69		
	$E_{s\ (CBr3)}$	-2.43	$E_{s\ (Br)}$	-0.81		
					$E_{s\ (CBrCl2)}$	2(-0.69)+(-0.81)=-2.19
					$E_{s\ (CBr2Cl)}$	2(-0.81)+(-0.69)=-2.31

Figure 10 shows the estimated ρ and δ values based on the median second-order reaction rate constants that were determined in this study (*Table 3*). For the two major HAN degradation pathways (i.e., basic hydrolysis and hypochlorite chlorination), since the product of $\rho\sigma^*$ is always greater than the product of δE_s, it can be inferred that both reactions are more sensitive to the polar than to the steric property of the halogenated substituents. For this reason, the higher hydrolysis and chlorination rates for more halogenated HANs can be explained by the higher electron-withdrawing effect from the halogen aggregate, which activates the nitrile carbon and renders it more electrophilic. Although the steric hindrance of the substituent also increases with increasing number of halogens, it has less impact on both of the reaction rates compared to the aforementioned polar effect. Perhaps most importantly, positive ρ estimates for the two LFERs reveal that both HAN hydrolysis and chlorination reactions are nucleophilic reactions. In other words, HANs react with hydroxide and hypochlorite through nucleophilic attack of the latter on the nitrile carbon.

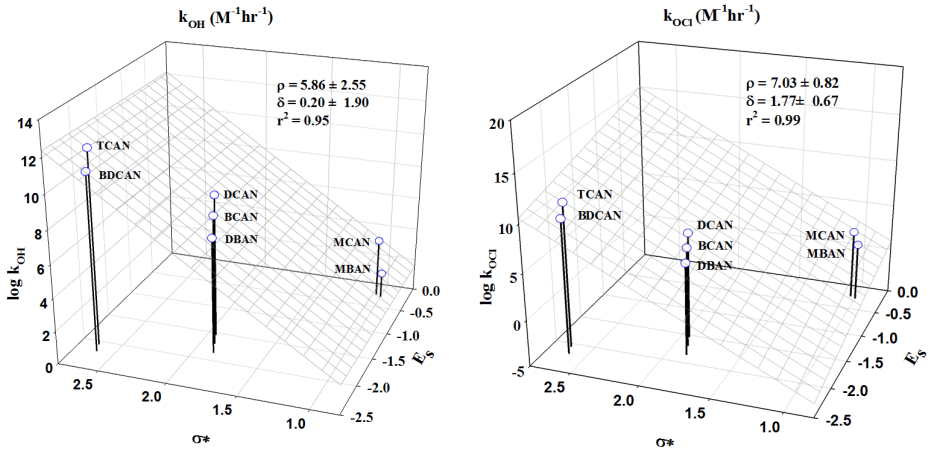

Figure 10. Taft LFERs based on median k_{OH} and k_{OCl} estimates shown in *Table 3*.

1.3.6. Implications of HAN Degradation Kinetics with Respect to Drinking Water Treatment and System Management

With HAN reaction kinetics fully characterized above, the persistence of this group of compounds in drinking water distribution systems can therefore be quantitatively predicted. When exact chlorine exposure (i.e., CT) for distributed water is not readily available, an averaged chlorine residual $\overline{C_t}$ can be assumed and a predictive model (*Equation 10*) is proposed on the basis of this pseudo-constant $\overline{C_t}$:

$$\overline{C_t} = \frac{\int_0^t C_t dt}{t} \quad (9)$$

$$\ln[HAN] = \ln[HAN]_0 - \left(k_{H_2O} + k_{OH} \cdot [OH^-] + k_{OCl}\alpha_1 \cdot \overline{C_t}\right) \cdot t \quad (10)$$

Depending on the pH and the chlorine residual that are specific to individual systems, there exists a predominant reaction pathway to which the majority of HAN loss can be attributed. *Figure 11* presents a summary of HAN half-lives over the range of pH and chlorine residual that are relevant to drinking water, where the half-lives were calculated according to *Equation 11*. Also shown on the figure are regions where each of the three major reactants results in the greatest amount of HAN loss (i.e., the predominant pathway).

$$t_{0.5} = \frac{\ln(2)}{k_{H_2O} + k_{OH} \cdot [OH^-] + k_{OCl}\alpha_1 \cdot \overline{C_t}} \quad (11)$$

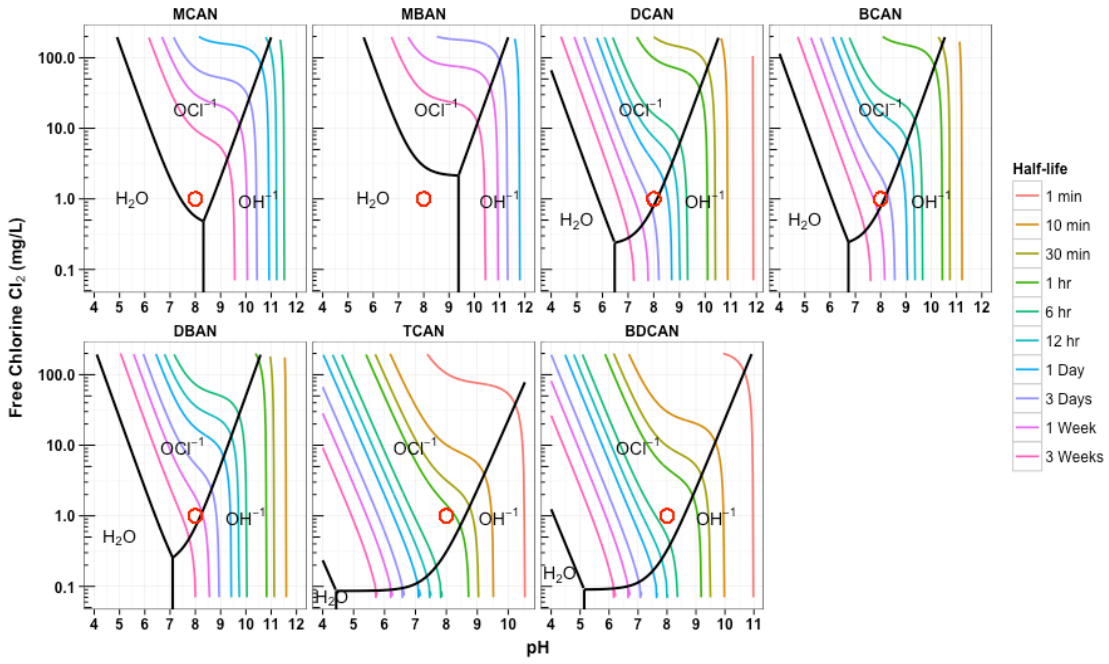

Figure 11. Predominance diagram of HAN half-lives showing all three degradation pathways. Red open circles indicate a typical set of conditions (pH 8 with 1.0 mg Cl_2/L averaged chlorine residual), under which the persistence of HANs was predicted in the following figure.

As an example, *Figure 12* draws from the predictive model (*Equation 10*) under a typical set of conditions for finished waters (i.e., pH 8 with 1 mg Cl_2/L averaged residual chlorine, red circles in *Figure 11*) and projects the decrease in normalized HAN concentrations over water age up to 3 weeks. *Figure 12* illustrates that under this set of conditions, TCAN and BDCAN will decompose rather rapidly even at low water ages and will completely disappear within a day. DCAN and BCAN will be lost only in relatively old water (from several days to a week), while DBAN, MBAN and MCAN will essentially remain stable during the entire distribution period. It is also important to recognize that very different results will be observed for systems distributing water at

higher pH levels (e.g., softening systems, or those using high pH for corrosion control) and those using chloramines as secondary disinfectant. Additionally, the above prediction solely considers HAN degradation kinetics and did not account for their simultaneous formation, which may also occur when both HAN precursors and residual disinfectant are present. Finally, as HANs degrade, they leave other DBPs in their place (i.e., HAMs, *N-Cl*-HAMs, and HAAs) and the concentrations, relations, and stability of these sequential byproducts should also be considered to assess their associated health risks to drinking water consumers.

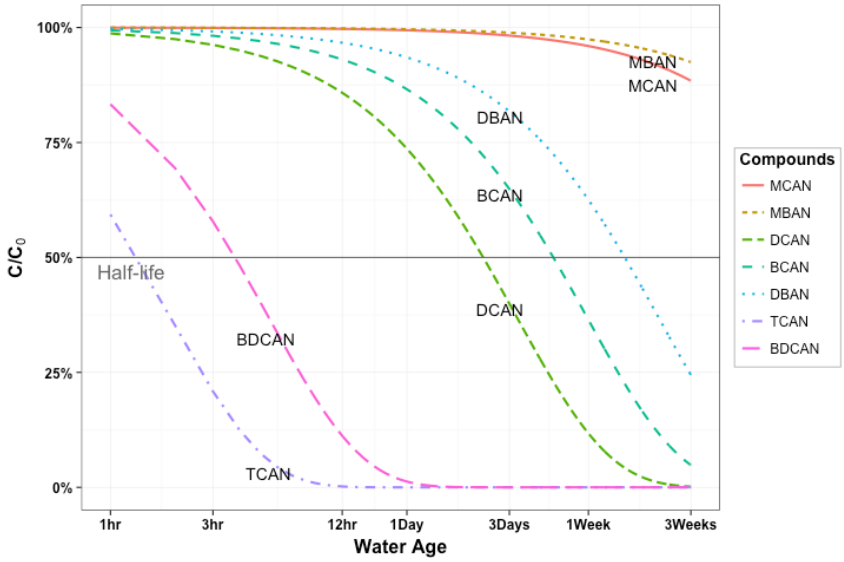

Figure 12. Predicted persistence of HANs under a typical set of conditions: pH 8 with 1.0 mgCl_2/L averaged chlorine residual.

CHAPTER 2

EVALUATION OF DISINFECTION BYPRODUCT REACTION KINETICS USING HIERARCHICAL BAYESIAN MODELING[2]

2.1. Introduction

Since the adverse health effects of drinking water DPBs are associated not only with their specific toxic potencies but also with their actual occurrence, it is therefore critical to understand their stability under various conditions that are relevant to drinking water treatment and distribution. The stability of individual DBPs is often inferred from kinetic studies that monitor and model its degradation reactions. The kinetic experiments can be conducted across different conditions (e.g. varying pH levels) to develop a predictive degradation kinetic model based on the experimental circumstances (Reckhow et al., 2001). This modeling framework is known as a hierarchical model, that is, a multilevel statistical model in which reaction rate constants characterize compound degradation kinetics for individual, "lower-level" time-based kinetic experiments but also exhibit a "higher-level" structure across different experimental conditions.

The method of least squares is often preferred when kinetic models are fitted to temporal concentration measurements (Englezos, 2001). This method is simple and computationally straightforward, can be extended to nonlinear kinetic models (Englezos, 2001), and provides a valid estimation of sampling variability and predictive uncertainty under independent and identically distributed (i.i.d.) Gaussian errors. Despite its wide

[2] Yu, Y.; Steinschneider, S.; Reckhow, D.A. Evaluation of Environmental Degradation Kinetics Using Hierarchical Bayesian Modeling. *J. Environ. Eng.* **2015,** 06015008.

appeal and application in kinetic studies, there are several challenges associated with the use of least squares when trying to construct hierarchical models. These limitations are addressed below and a hierarchical Bayesian modeling framework is forwarded in this Chapter as a more robust method to manage such problems. Hierarchical Bayesian models have been introduced in many environmental engineering and public health disciplines, including pharmacokinetics (Lunn & Aarons, 1998), epidemiology (Lawson, 2009), ecology (Wikle, 2003), and hydrology (Steinschneider & Lall, 2015), but they have not yet been extended to the DPB degradation kinetics literature. Here, a hierarchical Bayesian model with novel components for non-constant variance is proposed, with special focus on its ability to propagate all uncertainties through to the predictive distribution of apparent reaction rate constants under different experimental conditions. More importantly, the hierarchical modeling framework is proposed as a generic methodology applicable to any instance where compound degradation reaction rate constants are to be estimated under varying conditions. As a specific example, the method is demonstrated for a particular instance examining the hydrolysis reaction rate constants for haloacetamides (HAMs) as an important group of emerging nitrogenous DBPs (N-DBPs).

2.1.1. The Hierarchical Model

The hierarchical model considered here relates reaction rate constants *k* of a compound (e.g., a DBP) to the experimental conditions under which those reaction rates are observed. Let $\boldsymbol{X}_i$ be a vector of experimental factors (e.g., pH, chlorine residual, etc.) for the ith experiment, with $i = 1, 2, \cdots, N$. Let $Y_{i,t}$ be the concentration of a compound measured at time points $t = 1, 2, \cdots, T$ under the ith experimental condition. In the lower-

level regression, the compound reaction rate law for the i[th] experiment can be expressed as a function of time, given the reaction rate constant vector $\boldsymbol{k}_i$ hypothesized to vary with $\boldsymbol{X}_i$, as well as i.i.d. normal residual noise ε_t with mean 0 and variance σ_ε^2:

$$Y_{i,t} = f\left(t\middle|\boldsymbol{k_i}(\boldsymbol{X_i})\right) + \varepsilon_t \quad (12)$$

The function $f(t|\boldsymbol{k_i}(\boldsymbol{X_i}))$ can be a simple linear model, as in the case of first-order reaction under a logarithmic transformation, or it can be nonlinear for mixed-order reactions. The higher-level regression then relates compound reaction rate constants to the experimental conditions that were varied across the different experiments:

$$k_i^j = \beta_0^j + \boldsymbol{X}_i^j\boldsymbol{\beta}_1^j + \xi_i^j \quad (13)$$

Here, *j* indexes the vector of reaction rate constants, although for simplicity vector notation for $\boldsymbol{k}$ will be omitted in later discussion. The term $\boldsymbol{\beta}_1^j$ is written as a vector to allow for multiple predictors in $\boldsymbol{X}_i^j$. The relationship between reaction rate constants and experimental conditions is assumed linear, although this is not required. Finally, it is assumed that the error term ξ_i^j is normally distributed with zero mean. Assumptions regarding the variance, $\sigma_{\xi_i}^2$ of ξ_i^j are addressed later. *Equation 13* is of particular interest, as this is the model that will be used to predict compound reaction rates under conditions that were not experimentally determined.

2.1.2. Challenges in Estimating Hierarchical Models in Stages Using Least Squares

The development of a hierarchical kinetic model is often carried out in two stages, first with the lower-level estimation of reaction rate constants (i.e., *k*) for all individual experiments and replicates, followed by the higher-level regression of *k* on experimental

conditions. However, there are several challenges in developing such a model using a two-stage approach.

First, it is critical to recognize that the *k* values are not observations, but rather they are estimated quantities from a regression with an associated level of sampling uncertainty. When developing the regression in *Equation 13*, this sampling uncertainty in *k* needs to be accounted for so that the higher-level regression does not give more weight than justified to inherently uncertain predictands.

In a frequentist framework, this can be accomplished using weighted least squares (Stedinger & Tasker, 1985) and standard error estimates for each *k*. However, the use of standard errors depends on a symmetric approximation of the sampling distribution for regression parameters (Tellinghuisen, 2000), yet nonlinear kinetic models often have asymmetric sampling distributions (Görlitz, et.al, 2011). Thus, the use of weighted least squares in this context may not always be straightforward.

Furthermore, the higher-level regression can also exhibit behavior that violates assumptions of a standard linear model, such as non-constant variance (i.e., heteroscedasticity). Methods such as general weighted least squares (Tellinghuisen, 2000) or iteratively reweighted least squares (IRLS) (Gao, et.al, 2011) are available to correct for heteroscedasticity, but these methods were developed assuming the predictand is an observed value, not an estimated parameter with sampling uncertainty. Unfortunately, the existence of a method designed to weight *k* values in *Equation 13* based simultaneously on their sampling uncertainty and the heteroscedasticity in the model residuals ξ_i is so far unavailable.

Perhaps most importantly, the staged estimation of the hierarchical model leaves the predictive model in *Equation 13* sensitive to both outliers and limited data. Given the complexity of experimental procedures to quantify most DBPs at trace levels, the potential for substantial measurement error is nontrivial, and a small number of samples are often all that can be processed. Outlier estimates of k can undermine the predictive model in *Equation 13*, while a limited number of k values across experimental conditions can reduce model precision.

2.1.3. Hierarchical Bayesian Modeling

Hierarchical Bayesian modeling is an alternative approach to manage the challenges of hierarchical modeling described above, providing a flexible and robust means to estimate the predictive model in *Equation 13*. A brief overview of hierarchical Bayesian models is provided here, but a more thorough introduction to hierarchical Bayesian modeling is found in the following literature (Gelman, 1995; Carlin & Louis, 2008). In a Bayesian framework, all parameters are considered as random variables with uncertainty that can be described by a probability density function (pdf). Before considering any available data, all previous knowledge regarding the model parameters $\boldsymbol{\theta} = \{k_i, \beta_0, \beta_1, \sigma_\varepsilon^2, \sigma_{\xi_i}^2 \,|i = 1,2,\cdots,N\}$ is summarized in a prior distribution, denoted $P(\boldsymbol{\theta})$. If no prior information is available, then vague priors can be used so that estimation is driven by the data. However, prior information based on expert knowledge is available in many situations and will reduce the uncertainty in model estimation (Choy et al., 2009; Kuhnert et al., 2010). For instance, in the case study presented below, linear free energy relationship (LFER) reveals that the HAM hydrolysis reaction is nucleophilic, implying that the hydrolysis reaction rates should be higher under more basic conditions where

hydroxide ions predominate as strong nucleophiles. This information can be included into the model by specifying a non-negative prior on the coefficient for pH in *Equation 13*.

A likelihood function, $L(\boldsymbol{Y}|\boldsymbol{\theta},\boldsymbol{X})$, is defined based on the joint distribution of the residuals $\{\varepsilon,\xi\}$ of both the lower-level and higher-level regression models:

$$\mathrm{L}(\mathbf{Y}|\boldsymbol{\theta},\mathbf{X}) = \prod_{i=1}^{N} \frac{1}{\sqrt{2\pi}\sigma_{\xi_i}} exp\left(\frac{\left(k_i - (\beta_0 + \beta_1 \cdot X_i)\right)^2}{2\sigma_{\xi_i}^2}\right) \prod_{t=1}^{T_i} \frac{1}{\sqrt{2\pi}\sigma_{\varepsilon}} exp\left(\frac{\left(Y_{i,t} - f\left(t|\boldsymbol{k_i}(\mathrm{Xi})\right)\right)^2}{2\sigma_{\varepsilon}^2}\right) \quad (14)$$

Here, the likelihood function simultaneously considers both the fit of each individual *k* value to the residual concentration profile in the ith experiment (i.e., the lower-level regressions), as well as the likelihood of all *k* values in the regression against experimental conditions **X** across the *N* experiments (i.e., the higher-level regression).

The final distribution of all model parameters, known as the joint posterior distribution, is evaluated using Bayes theorem, which combines information from both the likelihood and the prior:

$$\boldsymbol{P}(\boldsymbol{\theta}|\boldsymbol{Y},\boldsymbol{X}) = \frac{\mathrm{L}(\mathbf{Y}|\boldsymbol{\theta},\mathbf{X}) \cdot \mathrm{P}(\boldsymbol{\theta}|\mathbf{X})}{\int_{\boldsymbol{\theta}} \mathrm{L}(\mathbf{Y}|\boldsymbol{\theta},\mathbf{X}) \cdot \mathrm{P}(\boldsymbol{\theta}|\mathbf{X}) d\boldsymbol{\theta}} \quad (15)$$

The integral in the denominator is a constant of proportionality required to ensure that the right hand side term is a well-defined pdf. This integral often cannot be solved using analytical methods. However, this challenge has been largely overcome using Markov Chain Monte Carlo (MCMC) techniques that can efficiently sample parameter values to describe the joint posterior space. However, it is noted that convergence of MCMC sampling to the posterior distribution is not immediately guaranteed and requires convergence testing (Gelman & Rubin, 1992).

Uncertainty propagation between the lower-level estimates of *k* and the higher-level regression is immediate in the Bayesian framework, as the posterior distribution is evaluated jointly across all model parameters. Also, the Bayesian approach does not need to make any explicit assumptions about the shape of the sampling distribution of reaction rate constants, which, as argued earlier, is useful in most nonlinear reaction kinetics where this distribution is often asymmetric (Görlitz, et.al, 2011).

By considering both the lower and higher level regressions simultaneously in the likelihood function, the hierarchical Bayesian model can pool information across experiments to lessen the influence of outliers. Estimates of k_i (based on the data $\boldsymbol{Y}_{i,\cdot}$) that appear inconsistent with the higher-level regression (based on data from the remaining experiments $\boldsymbol{Y}_{-i,\cdot}$) will be partially pulled, or shrunk, toward the higher-level regression estimate, $\beta_0 + \boldsymbol{X}_i\boldsymbol{\beta_1}$. This occurs simultaneously for all *N* values of k_i. In so doing, the higher-level relationship is made more robust by reducing the effects of "outlier" *k* values (Gelman & Hill, 2007). This effectively acts as a compromise between completely including or completely removing outliers at the higher level, which is believed to be justified given the nontrivial measurement variability and data scarcity for most trace-level drinking water DBPs.

In *Equation 16*, it is highlighted that the residual variance $\sigma_{\xi_i}^2$ for the higher-level regression is allowed to vary linearly with experimental condition to entertain heteroscedasticity in the error term ξ_i:

$$\sigma_{\xi_i}^2 = \gamma_0 + \boldsymbol{X_i\gamma_1} \quad (16)$$

These additional parameters, and their uncertainty, can be estimated along with the other model parameters in the Bayesian framework.

Finally, a predictive distribution for an out-of-sample value of k_i associated with a new experimental condition $\boldsymbol{X}_i$ can be estimated by posterior sampling. First, $\sigma_{\xi_i}^2$ is estimated using posterior samples of γ_0 and $\boldsymbol{\gamma}_1$ and *Equation 16*. Then, a sample for k_i is developed via *Equation 13* by adding a random deviate $N(0, \sigma_{\xi_i}^2)$ to the quantity $(\beta_0 + \boldsymbol{X}_i\boldsymbol{\beta}_1)$ after sampling from the posteriors of β_0 and $\boldsymbol{\beta}_1$. This process can be repeated many times to estimate the predictive distribution of k_i.

2.2. Case Study: Hydrolysis of Haloacetamides under Different pH Conditions

The hierarchical Bayesian model described above is applied in a case study examining the second-order hydrolysis reaction rate constants for HAMs. HAMs are an important group of N-DBPs that can form during the chlorination or chloramination of source waters that are rich in organic nitrogen content (Chu et al., 2010a). Furthermore, it was proposed that HAMs are reactive under conditions that are relevant to drinking water treatment and can undergo substantial degradation to form the corresponding haloacetic acids under alkaline pH conditions (Glezer et al., 1999; Reckhow et al., 2001). However, their reaction kinetics have not been characterized to allow quantitative prediction of their lifetimes in drinking water supplies. Therefore, the key objective of this case study was to establish a quantitative predictive model to evaluate HAM hydrolytic stability without the presence of chlorine or chloramines.

2.2.1. Experimental Conditions

All reaction solutions were prepared in 10 mM phosphate buffer and were adjusted to the desired pH levels using sodium hydroxide or sulfuric acid. Small volumes of HAM stock solution (i.e., 0.5 mg/mL) were introduced into 4 L buffer at the start of each experiments so that the initial concentration for individual HAMs was 250 μg/L. After the addition of HAMs, samples were partitioned off into 300 mL biochemical oxygen demand (BOD) bottles and were then stored free of headspace in a dark 20ºC incubator for a maximum of 19 days. At prescribed reaction times, a single bottle of sample was sacrificed for immediate analysis of residual HAM concentrations. For each pH condition and time point, at least two sample duplicates were analyzed for the determination of measurement uncertainties. Quantification of HAMs was conducted using a solid-phase extraction/ gas chromatography–mass spectrometry (SPE/GC-MS) method that was previously developed.

2.2.2. Hierarchical HAM Hydrolysis Kinetic Model

The hydrolysis of two brominated HAMs, monobromoacetamide (MBAM) and tribromoacetamide (TBAM), was investigated under 6 pH conditions (pH=6, 7, 7.5, 8, 8.5, and 9). The fully second-order hydrolysis reaction rate law can be described by *Equation 17*, with k_{H_2O} and k_{OH} representing the respective neutral and basic hydrolysis rate constants:

$$\frac{d[HAM]}{dt} = -k_{H_2O}[HAM] - k_{OH}[OH^-][HAM] = -\left(k_{H_2O} + k_{OH}[OH^-]\right)[HAM] \quad (17)$$

Therefore, the overall reaction is first-order in HAM. The hierarchical model (*Equations 12-16*) can be developed with $Y_{i,t}$ being the residual HAM concentration

measured at time, t, and X_i being the hydroxide concentration variable (i.e., $X_i = [OH^-] = 10^{-(14-pH)}$) for the ith experiment. In *Equation 13*, β_0 and β_1 are then equivalent to the neutral and basic hydrolysis rate constants k_{H_2O} and k_{OH} that are to be estimated.

The k_{H_2O} and k_{OH} were estimated via two different approaches: the Bayesian approach and the least squares regression in two stages. The Bayesian model was fitted in the JAGS programming language (Plummer, 2011). All parameters were given vague, uniform priors except for $\boldsymbol{\beta_1}$, which was given a non-negative uniform prior to reflect our knowledge about the positive correlation between the HAM hydrolysis rate and hydroxide concentration. To account for sampling uncertainty in the least squares approach, the *k* values were weighted in the second stage by the square of their inverted standard errors estimated in the first stage. The resulting parameter estimates and predictive intervals were examined under both approaches, focusing on the influence of outliers, the effects of heteroscedasticity, and the simultaneous propagation of all uncertainties into model predictions.

2.3. Results and Discussion

Figure 13(a) and *(b)* show the apparent MBAM and TBAM first-order hydrolysis rates as a function of pH predicted by two-stage least squares regression. The expected linear relationship and the 95% predictive intervals are also presented by solid and dashed lines in *Figure 13*. It has to be noted that the predictive intervals were developed without the inverse-variance weighting because the predictive bounds for out-of-sample estimates were of interest. Similarly, the respective posterior mean estimates and

predictive intervals for the apparent first-order hydrolysis rate constants, *k,* resulted from hierarchical Bayesian modeling are shown in *Figure 1(c)* and *(d)*. The intercept and slope for the higher-level regression for both compounds and the two methods are listed in *Table 6*.

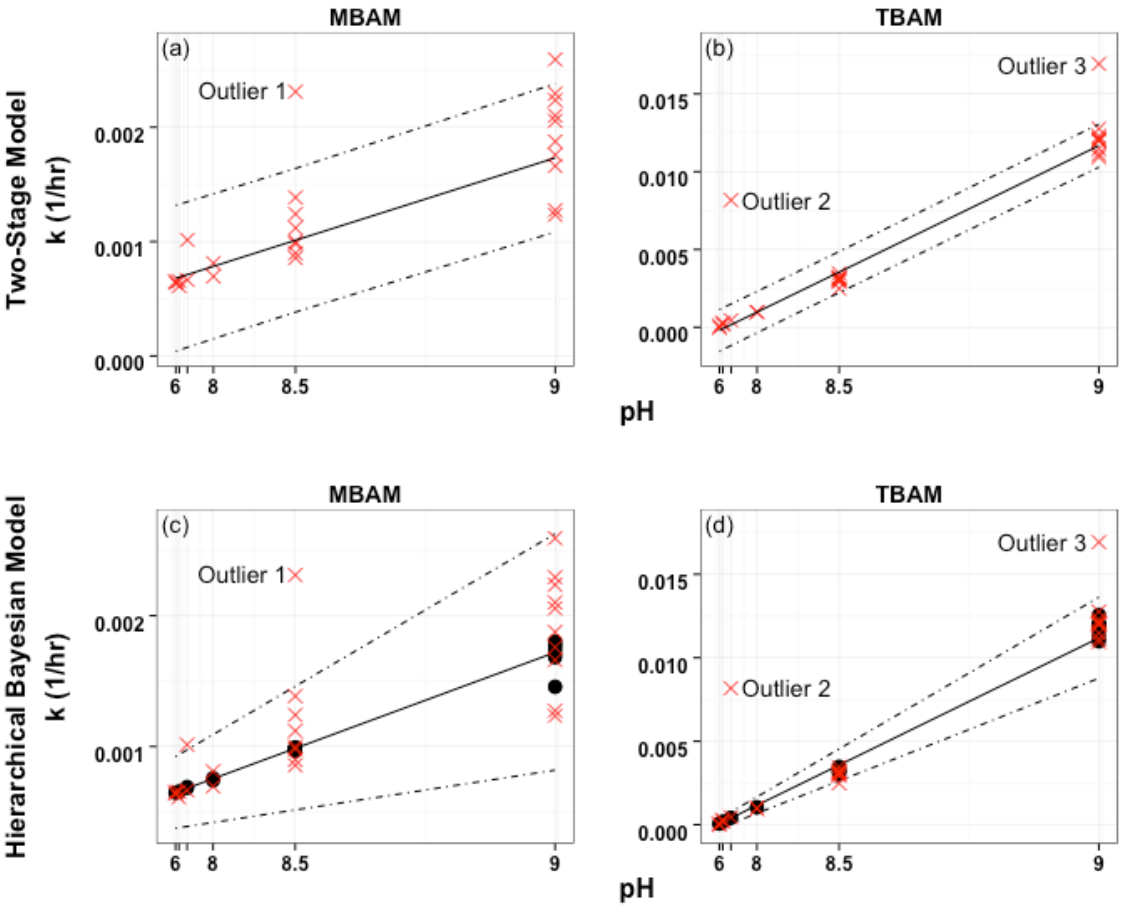

Figure 13. Comparison between the predictive kinetic hydrolysis models from the staged least squares regressions ((a) and (b)) and Bayesian hierarchical model ((c) and (d)) for MBAM ((a) and (c)) and TBAM ((b) and (d)). Also shown in the figure are estimates of *k* from the staged least squares (red crosses) and Bayesian modeling (black circles). Three potential outlier *k* values are numbered as 1, 2, and 3.

Table 6. Estimated values of k_{H_2O} and k_{OH} from the two methods. Standard errors are given in parentheses. For the Bayesian approach, the posterior mean estimates are shown, and standard errors are estimated as the standard deviation of the posterior distribution.

	Compound	k_{H_2O}	k_{OH}
Staged Least Squares	MBAM	1.0E-03 (8.7E-05)	82.7 (14.8)
	TBAM	1.4E-05 (1.20E-04)	1137.7 (26.9)
Hierarchical Bayesian	MBAM	0.001 (0.0001)	102.5 (23.1)
	TBAM	0.0002 (0.0001)	1103.5 (41.2)

In general, the posterior predictive intervals (indicated by dashed lines in *Figure 13*) for both haloacetamides were much narrower using the Bayesian method than the staged least squares regression, especially under lower pH conditions. The Bayesian method provided higher precision at lower pHs mainly because it explicitly accounted for heteroscedasticity in the error term ξ. As seen in the staged least squares estimates of *k* (red crosses in *Figure 13*), the apparent first-order MBAM and TBAM hydrolysis rates were significantly smaller under lower pH conditions, as was their variability (particularly for TBAM), thus validating the necessity of a heteroscedastic error term. However, the non-constant variance cannot be readily included in the second stage least squares regression because the *k* values were already weighted according to their sampling uncertainty. This sampling uncertainty is nontrivial and varies across *k* estimates, and therefore should be considered when estimating the higher-level relationship. For instance, the coefficient of variation (CV) for *k* values, calculated as the standard error divided by the least squares *k* estimate, had an interquartile range of [0.22,0.31] and [0.03,0.16] for MBAM and TBAM, respectively. Both compounds had some *k* estimates with a CV greater than 0.5. The Bayesian estimation accounts for

sampling uncertainty and heteroscedasticity simultaneously, allowing the method to correctly weight each *k* value in the higher-level regression.

Figure 13 also highlights three potential outlier values of *k* for the two compounds, which were estimated in the staged least squares approach. These outliers originated from outlying concentration measurements in the lower-level time-based kinetic experiments (*Figure 14*). The lower-level residual concentrations are shown as a function of reaction time on a semi-logarithmic scale for one outlier of MBAM (*Figure 14(a)*) and two of TBAM (*Figures 14(b) and (d)*). It is obvious in *Figure 14* that the least squares regression was quite sensitive to the individual outlying concentration measurements, leading to higher *k* estimates than what data would suggest based on a straight visual analysis. The artificial upward bias in the *k* estimates propagated into the higher-level regression of *k* on pH in the staged least squares approach (see regression estimates in *Table 6*). In contrast, the hierarchical Bayesian analysis was less sensitive to the effects of these outliers because it can pool information across different pH conditions. The Bayesian model shrunk the *k* estimates toward the higher-level regression estimate (i.e., $\beta_0 + \boldsymbol{\beta_1 X_i}$), as shown by the solid blue line in *Figure 14(a-c)*. The higher-level relationship is then made more robust because the effects of these individual outlying concentration data are discounted. This partial pooling allowed the posterior predictive distribution for *k* to become tighter, as seen when comparing *Figures 13(a)* and *13(c)* for MBAM at pH 8.5 and *Figures 13(b)* and *13(d)* for TBAM at pH 7.5 and 9.

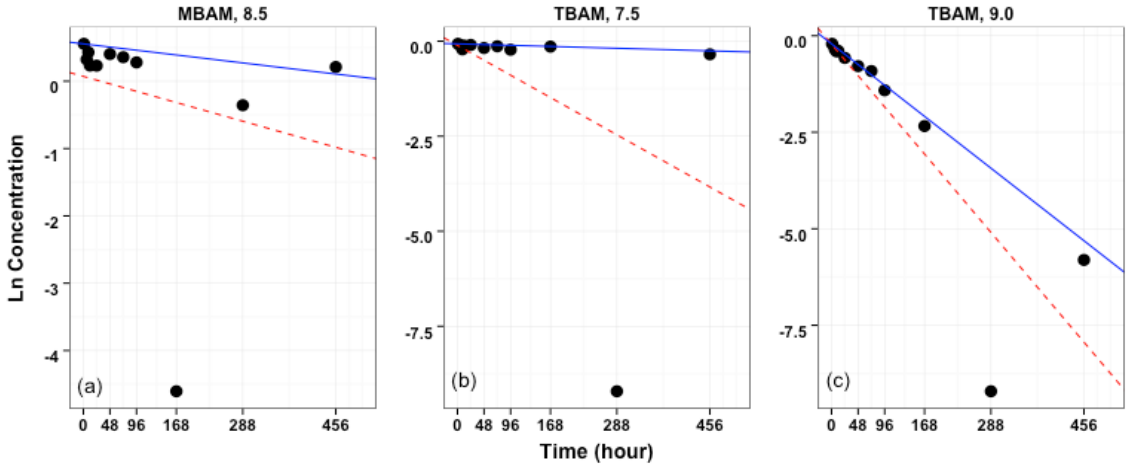

Figure 14. Lower-level residual MBAM and TBAM concentrations as a function of reaction time for the three outliers 1, 2, and 3 in Figure 13. Also shown in the figure are the least squares (red dashed) and posterior mean (solid blue) estimates of *k*.

CHAPTER 3

HAN CHLORINATION PRODUCTS: THE *N-CHLORO*-HALOACETAMIDES INSTEAD OF HALOACETAMIDES[3]

3.1. Introduction

Disinfection of drinking water provides an effective barrier in the control of microbial growth and therefore protects consumers from waterborne pathogens. However, the presence of a disinfectant can lead to the formation of potentially carcinogenic disinfection byproducts (DBPs). To date, approximately 600-700 DBPs have been identified in US drinking waters from the use of major disinfectants (i.e., chlorine, chloramines, chlorine dioxide, etc.) as well as their combinations (Richardson, 1998; Stevens et al., 1990; Krasner et al., 1989; Krasner et al., 2006). However, none of those hitherto reported DBPs has been recognized to have sufficient carcinogenic potency to account for the cancer risks that are projected from epidemiological studies (Bull et al., 2011). In the meanwhile, haloacetamides (HAMs) have received lots of attention as an emerging group of nitrogenous DBPs (N-DBPs) mainly because they are one order of magnitude more genotoxic while two orders of magnitude more cytotoxic than the corresponding haloacetic acids (Plewa et al., 2007), which are currently regulated by the USEPA as surrogates for drinking water toxicity.

[3] Yu, Y.; Reckhow, D.A. The Formation and Occurrence of *N-chloro-2,2*-dichloroacetamide Instead of 2,2-dichloroacetamide in Chlorinated Drinking Waters. Manuscript in preparation, to be submitted to *Environ. Sci. Technol.*

The occurrence of HAMs was first reported in a 2000-2002 DBP survey that was conducted at 12 US drinking water treatment plants (Weinberg et al., 2002; Krasner et al., 2006). The median and maximum concentrations for a collective of five chlorinated and brominated HAMs were 1.4 μg/L and 7.4 μg/L, respectively, among which *2,2*-dichloroacetamide (DCAM) occurred at the highest levels with a median concentration of 1.3 μg/L. More recently, *2,2,2*-trichloroacetamide (TCAM) was found to be ubiquitously present in English drinking water supply systems (Bond et al., 2015), albeit at a relatively lower level compared to DCAM (respective median concentrations for these two HAMs were 0.4 μg/L and 0.6 μg/L). Furthermore, the concentrations of both DCAM and TCAM were noted to be slightly higher in distribution systems than in finished waters, even though the differences were too trivial to make any significant inferences about their stability during drinking water distribution.

Perhaps most importantly, in most occurrence studies, HAMs exhibited strong positive correlations with the corresponding haloacetonitriles (HANs) and these two groups of compounds were often detected at comparable levels (Krasner et al., 2006; Chu et al., 2010; Bond et al., 2015). This is consistent with the prevailing understanding that HAMs in drinking waters result primarily from base-catalyzed HAN hydrolysis (Glezer et al., 1999; Reckhow et al., 2001). For instance, laboratory research has verified that dichloroacetonitrile (DCAN) can hydrolyze to form DCAM and ultimately to dichloroacetic acid (DCAA) in the absence of free chlorine when pH is above neutral (Yu & Reckhow, 2015). However, in the presence of chlorine, hypochlorite (i.e., OCl^-) becomes the dominant reactant in DCAN decomposition and the reaction between DCAN and free chlorine forms the putative *N-chloro-2,2*-dichloroacetamide (*N-Cl*-DCAM) as

reaction product (Yu & Reckhow, 2015). In fact, the formation of this halogenated nitrogenous compound has been proposed early in the 1990s as one of the major DCAN degradation products (Peters et al., 1990). Nevertheless, the identity of *N-Cl*-DCAM has not been substantiated and its presence in drinking waters has never been recognized or reported. Due to the similarity in their molecular structures except the presence and the absence of a nitrogen-bound chlorine, it was postulated that *N-Cl*-DCAM can be formed from DCAM via an *N*-chlorination reaction at the primary amide (Peters et al., 1990), whereas the actual *N-Cl*-DCAM formation mechanisms have not been elucidated heretofore. More importantly, the formation of an *N-Cl*-DCAM analogue, the *N,2*-dichloroacetamide (or *N-chloro-2*-monochloroacetamide) has been observed from the reaction between chloroacetaldehyde and monochloramine. This *N-chloro*-haloacetamide (*N-Cl*-HAM) was found to be very unstable and was readily reduced to the corresponding *2*-chloroacetamide (or monochloroacetamide) in the presence of sodium thiosulfate (Kimura et al., 2013). This finding further brings about the following question: will the other *N-Cl*-HAM species, especially the *N-Cl*-DCAM, have similar behavior, thus being dechlorinated to the corresponding HAMs when a reducing agent is used for sample preservation? Moreover, if *N-Cl*-HAMs can initially form but subsequently reduce, then what proportion of HAMs that has previously been identified and reported was actually due to *N-Cl*-HAM reduction? Therefore, the extent of *N-Cl*-HAM reduction in the presence of common reducing agents, such as sodium sulfite, ascorbic acid, ammonium chloride, and sodium thiosulfate needs to be further clarified.

For these reasons, the main objectives of this study were to confirm the existence of *N-Cl*-DCAM in chlorinated drinking waters, and to quantitatively characterize and

reconcile its formation kinetics with the respective DCAN and DCAM degradation kinetics. Furthermore, with the third chlorine bound to the amide nitrogen, *N*-*Cl*-DCAM can be defined as an organic monochloramine. Since organic chloramines are capable of transferring the *N*-*chloro* group to other chemicals such as the exocyclic nitrogens in DNA and RNA (Hawkins and Davies, 1999), it is commonly acknowledged that they are toxicologically active and may pose special health concern to drinking water consumers regarding chronic diseases (Bull et al., 2011) if they have sufficient stability to survive drinking water distribution. For this reason, aside from its formation kinetics and mechanisms, the stability of *N*-*Cl*-DCAM was also evaluated under typical drinking water pH conditions with and without the presence of chlorine and its decomposition pathways were proposed accordingly. Additionally, the impact of common reducing agents on the persistence of *N*-*Cl*-DCAM during sample preservation was also assessed in this study. Another key purpose of this investigation was to develop an analytical method that will enable the quantification of *N*-*Cl*-DCAM, or more ideally, a family of *N*-*Cl*-HAMs at concentrations that are comparable to their expected occurrence levels. To further validate this method, a set of real tap water samples collected from seven private residences in the US were analyzed to examine the presence of *N*-*Cl*-HAMs in actual chlorinated drinking waters.

3.2. Materials and Methods

3.2.1. Chemicals and Reagents

Dichloroacetamide (DCAM) and trichloroacetamide (TCAM) were purchased from Sigma-Aldrich (St. Louis, MO). Bromochloroacetamide (BCAM), dibromoacetamide (DBAM), bromodichloroacetamide (BDCAM), dibromochloroacetamide (DBCAM), and

tribromoacetamide (TBAM) were synthesized and supplied by CanSyn Chem. Corp. from Canada. General laboratory chemicals including Optima LC/MS grade organic solvents and formic acid (FA) were obtained from Fisher Scientific (Pittsburgh, PA). Purified *N-chloro*-haloacetamide (*N-Cl*-HAM) standard compounds are not commercially available, and they were individually prepared by reacting equal stoichiometric amount (Cl_2/N=1:1) of free chlorine with the corresponding haloacetamides (Kimura et al., 2013; Kimura et al., 2015), with pH of both solutions adjusted to 9.0 before mixing.

3.2.2. Chlorination of Dichloroacetamide

All DCAM reaction solutions were prepared in ultrapure Milli-Q water (EMD Millipore Corp.), containing 10 mM phosphate buffer and were adjusted to the desired pHs with sodium hydroxide or hydrochloric acid. At the start of each chlorination experiment, 3 mL of DCAM reaction solution (0.505 mM) was introduced into a quartz cuvette with 1 cm path length. Chlorination of DCAM was conducted by adding a small volume (30 μL) of acidified sodium hypochlorite solution (50.5 mM as Cl_2) into the cuvette containing the aforementioned DCAM reaction solution, so that the initial concentrations for both reactants were 0.5 mM. The chlorine solutions (50.5 mM as Cl_2) were prepared on the day of use by diluting the sodium hypochlorite stock solution (5.65%-6%, laboratory grade, Fisher Scientific), followed by acidification to the predetermined pHs using hydrochloric acid, prior to which the actual free chlorine concentration in the stock solution was standardized based on the *N,N*-diethyl-*p*-phenylene diamine (DPD)-ferrous ammonium sulfate (FAS) titrimetric method (EPA Method 330.4). Immediately after the introduction of chlorine, absorption spectrum was scanned in a continuous kinetic mode once every 5 seconds from 200 nm to 400 nm using

an Agilent 8453 diode array UV-visible spectrophotometer. All DCAM chlorination reactions were monitored at ambient room temperature (i.e., 20 °C). Reaction rate constants were determined from the kinetic UV absorbance measurements at 292 nm.

3.2.3. Stability of *N-chloro-2,2*-dichloroacetamide

The stability of *N-Cl*-DCAM was assessed in phosphate buffered solutions (10 mM, pH 4-8) with and without the presence of chlorine. Initial *N-Cl*-DCAM concentration was 40 μM and a small volume of acidified sodium hypochlorite solution was introduced at the beginning of each stability test to reach the same molar concentration of 40 μM. The chlorinated and unchlorinated *N-Cl*-DCAM solutions were repeatedly injected into the ultra performance liquid chromatography (UPLC)-quadrupole time-of-flight mass spectrometer (qTOF) once every 15 minutes for a total of 8 hours. Reduction of *N-Cl*-DCAM by sodium sulfite, sodium thiosulfate, ammonium chloride, and ascorbic acid was investigated in the same fashion via repeated sample injections into the UPLC/qTOF.

3.2.4. Sample Pretreatment

For the quantification of a group of seven *N-Cl*-HAMs, a solid phase extraction (SPE)-ultra performance liquid chromatography/mass spectrometry (UPLC/MS) method was developed during the course of this study. Before analysis, the *N-Cl*-HAMs in aqueous samples were first concentrated by SPE using the Oasis mixed-mode, reversed-phase, strong anion-exchange (MAX) cartridges (60 mg, 3 mL, 30 μm; Waters, Milford, MA) that were mounted on an Agilent VacElut SPS 24 SPE manifold. Prior to sample loading, each MAX cartridge was conditioned with 3 mL of methanol followed by one wash using 3 mL of ultrapure Milli-Q water. Each sample (100 mL) was drawn through

the cartridges under vacuum at a flow rate of approximately 1 mL/min. After sample loading, the cartridges were washed with 2 mL of methanol/NH_4OH (v/v=95/5) and then dried for 1 minute under vacuum. Subsequently, the retained *N-Cl*-HAMs were eluted with 2 mL of acetonitrile/water (v/v=90/10, with 25% formic acid). The acetonitrile extract was reconstituted by adding 0.5 mL of water/NH_4OH (v/v=85/15) and was then evaporated down to 1.0 mL under a gentle nitrogen stream (TurboVap LV).

3.2.5. Ultra Performance Liquid Chromatography/Quadrupole Time-of-Flight Mass Spectrometry

An ACQUITY UPLC (Waters, Milford, MA) system was used for LC separation with an ACQUITY UPLC HSS T3 column (1.8 μm, 100 Å, 2.1×100 mm; Waters), coupled with a 1.8 μm, 2.1×5 mm VanGuard pre-column (ACQUITY UPLC HSS T3; Waters). Column temperature was maintained isothermally at 35 °C. The mobile phases were 5 mM ammonium acetate (solvent A) and 100% methanol (solvent B) at a constant flow rate of 0.3 mL/min. The initial gradient was 0-2 min, 5% B, curve 6; increased from 5% to 90% B between 2 and 7 min, curve 6; 7-8 min 90% B, curve 6; switch back to 5% B in 0.1 min, curve 11; 11-15 min for equilibration, 5% B. The injection volume for each sample was 5 μL. A quadrupole time-of-flight mass spectrometer (Xevo G2-XS qTOF; Waters) with an electrospray ionization (ESI) source was used to obtain the accurate mass measurements of *N-Cl*-HAM parent ions. Negative ESI-TOFMS mode was applied with typical conditions optimized as follows: capillary voltage 2.50 kV; sampling cone, 25 arbitrary units; source offset, 80 arbitrary units; source temperature, 120 °C; desolvation temperature 400 °C; cone gas, 80 L/hour; desolvation gas flow, 800 L/hour.

3.2.6. Method Validation

To determine the method detection limits (MDLs) and recoveries for the seven *N*-*Cl*-HAMs using the SPE-UPLC/ESI/qTOF method, three sets of tap water samples (100 mL each) were prepared: (1) eight calibration standards spiked with seven *N*-*Cl*-HAMs; (2) seven replicate samples spiked with 0.02 μM of each *N*-*Cl*-HAM; (3) unspiked blanks. All samples were extracted and analyzed at the same time using the method described above. The SPE recovery rate for each *N*-*Cl*-HAM was determined according to the standard addition method (Hrudey, 2004). Furthermore, to validate the SPE-UPLC/ESI/qTOF method, 11 tap water samples collected from seven private residences in the US were analyzed for *N*-*Cl*-HAMs. Prior to sampling, 100 mg of ammonium chloride (i.e., NH_4Cl) was added to each 1 L glass bottle as the preservative. All samples were collected without headspace, stored at 4 °C, extracted within 72 hours, and analyzed by UPLC/ESI/qTOF immediately after sample pretreatment.

3.3. Results and Discussion

3.3.1. Identification and Verification of *N-chloro-2,2*-dichloroacetamide and *N-chloro*-haloacetamides

The discovery of *N*-*Cl*-DCAM stemmed from a preliminary kinetic study where the stability of DCAM was evaluated under a range of pH conditions with and without the presence of chlorine. When DCAM was chlorinated and residual chlorine was quenched by ascorbic acid to stop the chlorination reaction at prescribed reaction times, no significant decrease in DCAM concentration was observed over time. In contrast, residual DCAM was immeasurable at identical reaction times when chlorinated samples

were immediately analyzed by liquid-liquid extraction-gas chromatography/mass spectrometry (LLE-GC/MS; Yu & Reckhow, unpublished method) without the addition of any reducing agent. This suggests that DCAM chlorination may have formed a labile reaction intermediate, which was converted back into the initial DCAM by the addition of ascorbic acid. To identify this reaction intermediate, unquenched DCAM chlorination solution was directly infused into the high resolution quadrupole time-of-flight mass spectrometer (Xevo G2-XS qTOF). Under negative electrospray ionization (ESI^-), a unique isotope cluster was observed, reflecting the presence of three chlorine atoms in this unknown compound. Through isotopic modeling, both the exact masses and the isotopic pattern of these measured $[M-H]^-$ ions were found to agree with the mass spectrum for *2,2,2*-trichloroacetamide (TCAM).

Nonetheless, TCAM behaved very differently from this unidentified compound in many ways and therefore was unlikely the DCAM chlorination product. First of all, the unknown compound was well retained on an UPLC column (Waters ACQUITY HSS T3 column) with a stationary phase that promotes polar compound retention. On the contrary, purified TCAM standard compound was eluted near the dead volume over the entire mobile phase composition range, thus indicating different chemical polarities between these two compounds. More importantly, TCAM didn't dechlorinate to form DCAM in the presence of ascorbic acid, whereas conversion of the unknown to DCAM was found to be a more generic result from the addition of other reductants as well (e.g., potassium iodide, sodium sulfite, and sodium thiosulfate), and was not otherwise specific to ascorbic acid. In fact, it was noticed that this DCAM chlorination product exhibited a very similar behavior as inorganic dichloramine (i.e., $NHCl_2$) in terms of slowly

oxidizing iodide to form triiodide that reacted with *N,N*-Diethyl-p-phenylene diamine (DPD) to produce a relatively stable free radical species with an intense pink color. In contrast, TCAM didn't react with the DPD indicator to form colored free radicals either directly or indirectly via the triiodide intermediate.

Alternative to TCAM formation via chlorine substitution on the alkyl carbon, chlorination of DCAM may also result in bonding of chlorine to the amide nitrogen (Wayman & Thomm, 1969; Thomm & Wayman, 1969), forming the *N-chloro-2,2*-dichloroacetamide (*N-Cl*-DCAM) as a constitutional isomer of TCAM (*Figure 15*). Particularly, trihaloacetamides (THAMs) including trichloroacetamide (TCAM), bromodichloroacetamide (BDCAM), dibromochloroacetamide (DBCAM), and tribromoacetamide (TBAM) cannot be *C*-chlorinated due to the absence of a substitutable hydrogen on the trihalogenated tertiary carbon. However, *N*-chlorination of THAMs may otherwise still be possible, leading to the formation of *N-chloro*-trihaloacemides (*N-Cl*-THAMs) that are distinctively tetrahalogenated. In this regard, if THAMs can be further chlorinated to form those unique tetrahalogenated acetamides, the HAM *N*-chlorination pathway can therefore be verified and *N-Cl*-DCAM can be confirmed as the DCAM chlorination product. To substantiate our speculation that DCAM and the other HAMs are *N*-chlorinated by free chlorine to form the corresponding *N-chloro*-haloacetamides (*N-Cl*-HAMs), seven dihalogenated and trihalogenated HAMs (i.e., DCAM, BCAM, DBAM, TCAM, BDCAM, DBCAM, and TBAM) were chlorinated and the resulting HAM chlorination solutions were directly infused into the qTOF mass spectrometer and were screened for *N-Cl*-HAMs.

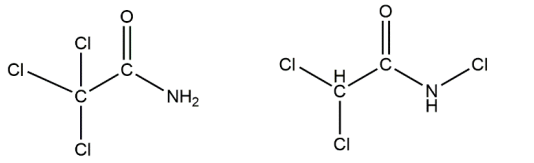

Figure 15. *2,2,2*-trichloroacetamide (TCAM) and its constitutional isomer, *N-chloro-2,2*-dichloroacetamide (*N-Cl*-DCAM).

Figure 16 shows the obtained isotope clusters for the four THAM chlorination products on the bottom row and all the isotopic distributions are in support of the presence of a total of four chlorine or bromine atoms in their molecular structures. Furthermore, the measured exact masses of all $[M-H]^-$ ions were in perfect agreement with the calculated values for *N-Cl*-THAMs. It therefore can be concluded that free chlorine reacts with THAMs by *N*-chlorinating their primary amides instead of *C*-chlorinating the tertiary alkyl carbons. In the same way, chlorination of dihaloacetamides (DHAMs), including DCAM, BCAM, and DBAM, is expected to produce the corresponding *N-chloro*-dihaloacetamides (*N-Cl*-DHAMs) instead of the THAM isomers (i.e., TCAM, BDCAM, and DBCAM). As a result, the identity of *N-Cl*-DCAM as DCAM chlorination product is confirmed herein.

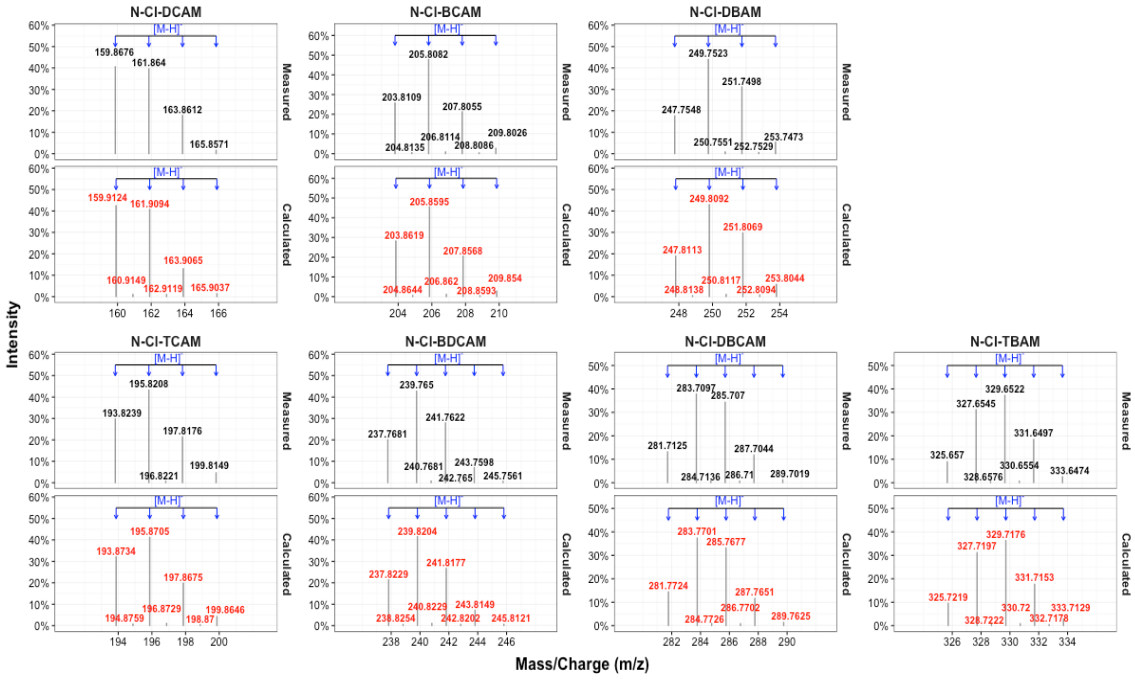

Figure 16. Obtained isotope clusters for the seven HAM chlorination products (i.e., *N*-*Cl*-HAMs) using Xevo G2-XS qTOF. All *N*-*Cl*-HAMs were formed individually by reacting equal stoichiometric amount of free chlorine with the corresponding HAMs (i.e., 100 µM Cl_2:100 µM HAM) and were ionized under the negative ESI mode. For each *N*-*Cl*-HAM, the measured exact masses (shown in black) were compared with the calculated values (shown in red) and all halogen isotopes are indicated by the blue arrows.

3.3.2. Dichloroacetamide Chlorination Kinetics

In the preliminary study, it was noted that residual chlorine was exhausted almost instantaneously when DCAM was chlorinated by equal stoichiometric amount of chlorine, implying that the formation of *N*-*Cl*-DCAM might be very rapid during DCAM chlorination. In order to quantitatively determine the rate at which *N*-*Cl*-DCAM is formed, DCAM *N*-chlorination kinetics were investigated spectrophotometrically at four different pHs (i.e., pH 6, 7, 8, and 9) by reacting same molar concentration of DCAM and

aqueous chlorine (i.e., $[DCAM]_0=[Cl_2]_0$=0.5 mM). UV absorbance at 292 nm was monitored over reaction time at a sampling frequency of once every five seconds and the concentrations of residual hypochlorous acid (HOCl), hypochlorite (OCl^-), DCAM, and formed *N-Cl*-DCAM at each reaction time point can be determined as follows according to their individual molar absorptivities at the given wavelength (i.e., ε_λ):

$$Abs_{\lambda,t} = \varepsilon_{HOCl,\lambda}[HOCl]_t + \varepsilon_{OCl^-,\lambda}[OCl^-]_t + \varepsilon_{DCAM,\lambda}[DCAM]_t + \varepsilon_{NClDCAM,\lambda}[NClDCAM]_t \quad (18)$$

Compared to chlorine, the same concentration of DCAM and *N-Cl*-DCAM didn't cause significant UV absorbance at 292 nm (*Figure 17*), suggesting very low molar absorptivities of these two compounds at this specific wavelength (i.e., 292 nm), although the actual values were not determined in this study. As a result, total residual chlorine concentration at each reaction time (i.e., C_t) can be calculated based on *Eq. 19*, assuming negligible contributions from both residual DCAM and formed *N-Cl*-DCAM to the total absorbance (i.e., $Abs_{\lambda,t}$) that was measured at 292 nm (i.e., $\varepsilon_{DCAM,\lambda}[DCAM]_t \approx \varepsilon_{NClDCAM,\lambda}[NClDCAM]_t \approx 0$ in *Eq.18*).

$$C_t = \frac{Abs_{\lambda,t}}{\alpha_{0,HOCl}\varepsilon_{HOCl} + \alpha_{1,OCl^-}\varepsilon_{OCl^-}} \quad (19)$$

$$\alpha_{0,HOCl} = \frac{[H^+]}{K_{a,HOCl} + [H^+]}; \quad \alpha_{1,OCl^-} = \frac{K_{a,HOCl}}{K_{a,HOCl} + [H^+]} \quad (20)$$

In *Eq. 19*, the respective molar absorptivities for hypochlorite and hypochlorous acid are 350.2 $M^{-1}cm^{-1}$ (Hand & Margerum, 1983) and 26.95 $M^{-1}cm^{-1}$ (Silverman & Gordon, 1980) at 292 nm. The two alpha values (denoted as α_0 and $\alpha_1$in following discussion for simplicity) represent the fractions of total residual chlorine that are actually in the form of hypochlorous acid (i.e., α_0) and hypochlorite (i.e., α_1) at any given pH, which can be

calculated using *Eq. 20* and a hypochlorous acid dissociation constant $K_{a,HOCl}$ of $10^{-7.582}$ at 20°C (Morris, 1966).

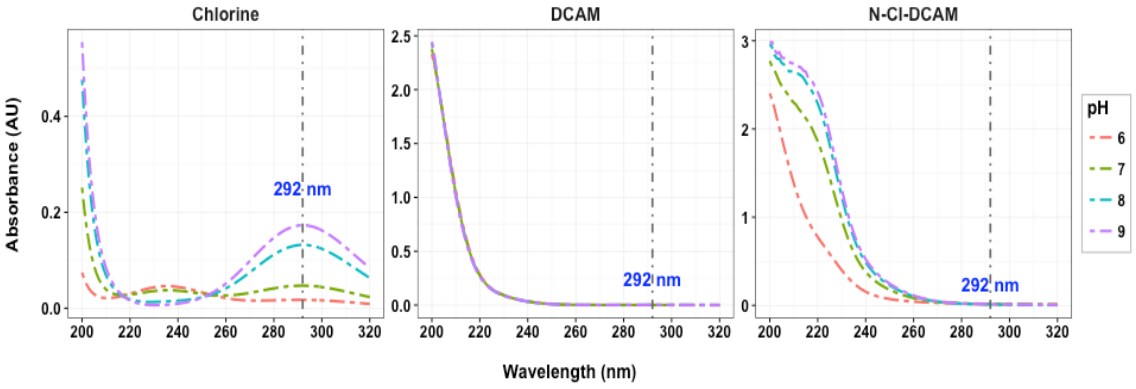

Figure 17. UV-vis spectra of total free chlorine, DCAM and *N-Cl*-DCAM in 10 mM phosphate buffered solutions at four pH levels. C_{t,Cl_2}= [DCAM] = [*N-Cl*-DCAM].

As is shown in *Figure 18(a)*, residual chlorine concentrations were consistent with a rate law that is second-order in chlorine. Since DCAM and total free chlorine were of same initial concentrations, the second-order behavior of residual chlorine indicates a 1:1 reaction stoichiometry between DCAM and chlorine. This was further confirmed on the basis of a fixed 1 mM Cl_2/mM DCAM chlorine demand when DCAM was chlorinated using excess molar equivalents of chlorine (*Figure 18(b)*). More importantly, it is clear from *Figure 18(a)* that hypochlorite is the only reactive form of chlorine in DCAM *N*-chlorination reaction, because chlorine decay was nearly immeasurable at pH 6 but was substantially accelerated when pH was above $pK_{a,HOCl}$ (i.e., 7.582; Morris, 1966). The specific participation of hypochlorite is consistent with the prevailing amide *N*-chlorination mechanism (Mauger & Soper, 1946), which indicates that formation of a hydrogen bond by the amino hydrogen with the hypochlorite oxygen is the rate-limiting

preliminary step. Moreover, hypochlorite is probably the only chlorinating agent since the oxygen atom in hypochlorous acid does not have enough electron-donating tendency to initially form a hydrogen bond with the amino hydrogen (Mauger & Soper, 1946). Therefore, the full second-order DCAM chlorination kinetics can be described as follows, reflecting the particular involvement of hypochlorite:

$$DCAM + OCl^- \xrightarrow{k_3} NClDCAM \quad (21)$$

$$\frac{d[DCAM]}{dt} = \frac{dC_t}{dt} = -k_3[DCAM][OCl^-] = -k_3 C_t \cdot \alpha_1 C_t = -k_3\alpha_1 \cdot C_t^2$$
$$Initial\ Condition: [DCAM]_0 = C_{t,0} \quad (22)$$

Based on the integrated form of this second-order reaction rate law (*Eq. 23*), the product of $k_3\alpha_1$ at any given pH can be derived by finding the corresponding slope of the linear regression line in *Figure 18(a)* (i.e., $\frac{1}{C_t}$ versus reaction time). Subsequently, the second-order DCAM *N*-chlorination rate constant, k_3, can be estimated by regressing the obtained $k_3\alpha_1$ products over α_1 (or reaction pH) with the intercept being forced through zero. *Figure 18(c)* shows the result of this linear regression (R^2=0.9972) and the estimated reaction rate constant, k_3 of 9.94×10^4 $M^{-1}hr^{-1}$ (or 0.0276 $mM^{-1}s^{-1}$).

$$\frac{1}{C_t} = \frac{1}{C_{t,0}} + k_3\alpha_1 \cdot t \quad (23)$$

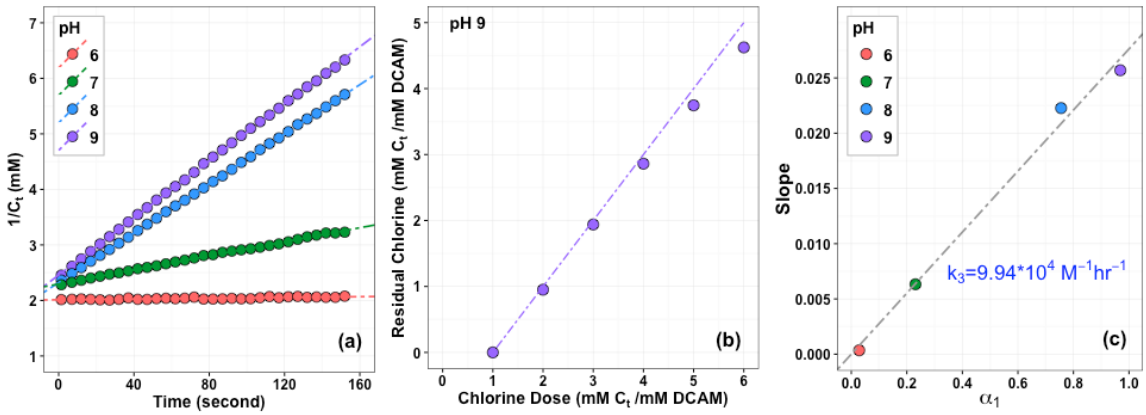

Figure 18. Analysis of DCAM chlorination kinetics. (a) Reversed residual chlorine concentration ($1/C_t$) versus reaction time at four DCAM chlorination pHs. (b) Verification of DCAM: Cl_2=1:1 reaction stoichiometry. (c) Estimation of second-order DCAM chlorination rate constant (i.e., k_3).

3.3.3. *N-chloro-2,2*-dichloroacetamide Degradation Kinetics

Aside from *N-Cl*-DCAM formation, its stability in drinking water on time scales that are relevant to system residence times is also of great significance. As a newly identified compound, it is necessary to understand if *N-Cl*-DCAM can persist for enough periods of time during drinking water distribution to reach the consumers' tap, or is it too short-lived to be considered as an important drinking water DBP.

N-Cl-DCAM was found to be quite stable under a range of pH conditions (i.e., pH 6-9) up to several weeks when chlorine was not present (data not shown). However, in the presence of chlorine, *N-Cl*-DCAM can decompose to form the corresponding DCAA especially at lower pHs (Peters et al., 1990). For this reason, the chlorine-induced *N-Cl*-DCAM degradation kinetics were further investigated at pH 4, 5, 6, 7, and 8 by reacting equal concentrations of *N-Cl*-DCAM with aqueous chlorine (i.e., 40 μM for each).

Figure 19(a) shows the normalized reversed residual *N*-*Cl*-DCAM concentration (i.e., C_0/C) as a function of reaction time, which supported a rate law that is second-order in *N*-*Cl*-DCAM. Analogous to the DCAM *N*-chlorination reaction, the second-order behavior of *N*-*Cl*-DCAM also suggests a 1:1 reaction stoichiometry between *N*-*Cl*-DCAM and free chlorine. Perhaps most importantly, unlike DCAM, *N*-*Cl*-DCAM is weakly acidic in water, and its estimated acid dissociation constant $K_{a,NClDCAM}$ is $10^{-3.71}$ at 25 °C (i.e., $pK_{a,NClDCAM}$=3.71; Menard & Lessard, 1978). Because of this relatively low pKa value, *N*-*Cl*-DCAM will tend to deprotonate into the corresponding anionic form (i.e., $Cl_2CHC(O)NCl^-$) within the pH range that is typical for drinking water (i.e., pH 6-9). Since both of the two reactants can either be protonated or deprotonated depending on the reaction pH, it is helpful to first determine the two respective forms of reactants that are actually reactive in this *N*-*Cl*-DCAM chlorination reaction.

As is evident in *Figure 19(a)*, the apparent *N*-*Cl*-DCAM chlorination rate substantially increased when pH was decreased. Accordingly, the Log C versus pH diagram (*Figure 19(b)*) shows all four possible combinations of the two participating reactants, among which, only when *N*-*Cl*-DCAM and aqueous chlorine are both in their protonated forms, their combined concentration (i.e., $[Cl_2CHC(O)NHCl][HOCl]$; the red line in *Figure 19(b)*) will also increase with decreasing pH. This strongly indicates that it is the hypochlorous acid (i.e., HOCl) that reacts with the neutral $Cl_2CHC(O)NHCl$ to form DCAA under acidic pH conditions. As a result, the full second-order *N*-*Cl*-DCAM chlorination kinetics can be proposed as follows:

$$\frac{dC_{t,NClDCAM}}{dt} = \frac{dC_{t,Cl_2}}{dt} = -k_4[Cl_2CHC(O)NHCl][HOCl]$$

$$= -k_4 \cdot \alpha_{0,NClDCAM} C_{t,NClDCAM} \cdot \alpha_{0,HOCl} C_{t,Cl_2}$$

$$= -k_4 \alpha_{0,NClDCAM} \alpha_{0,HOCl} \cdot C_{t,NClDCAM}^2$$

$$Initial\ Condition: C_{t,NClDCAM,0} = C_{t,Cl_2,0} \qquad (24)$$

$$\alpha_{0,NClDCAM} = \frac{[H^+]}{K_{a,NClDCAM} + [H^+]}; \quad \alpha_{1,NClDCAM} = \frac{K_{a,NClDCAM}}{K_{a,NClDCAM} + [H^+]} \qquad (25)$$

In *Eq. 24*, k_4 denotes the second-order *N-Cl*-DCAM chlorination rate constant. $\alpha_{0,HOCl}$ and $\alpha_{0,NClDCAM}$ represent the respective fractions of total residual chlorine (i.e., C_{t,Cl_2}) and total residual *N-Cl*-DCAM (i.e., $C_{t,NClDCAM}$) that are actually in the forms of HOCl and $Cl_2CHC(O)NHCl$, and these two values can be calculated according to *Eq. 20* and *Eq. 25*, respectively. The integrated form of this kinetic model is formulated in *Eq. 26*, on the basis of which, the second-order *N-Cl*-DCAM chlorination rate constant k_4 was estimated in two stages (Yu et al., 2015). Products of $k_4 \alpha_{0,HOCl} \alpha_{0,NClDCAM} C_{t,NClDCAM,0}$ were first estimated via lower-level linear least squares regressions of $\frac{C_{t,NClDCAM,0}}{C_{t,NClDCAM}}$ over reaction time at individual pH levels (*Figure 19(a)*). With known initial total *N-Cl*-DCAM concentration (i.e., $C_{t,NClDCAM,0} = 40\ \mu M$) and calculated alpha values (i.e., $\alpha_{0,HOCl}$ and $\alpha_{0,NClDCAM}$) at all investigated pHs (*Eq. 20* and *Eq. 25*), the higher-level linear regression shown in *Figure 19(c)* resulted in an estimated k_4 of 703.1 $M^{-1}hr^{-1}$.

$$\frac{C_{t,NClDCAM,0}}{C_{t,NClDCAM}} = 1 + k_4 \alpha_{0,HOCl} \alpha_{0,NClDCAM} C_{t,NClDCAM,0} \cdot t \qquad (26)$$

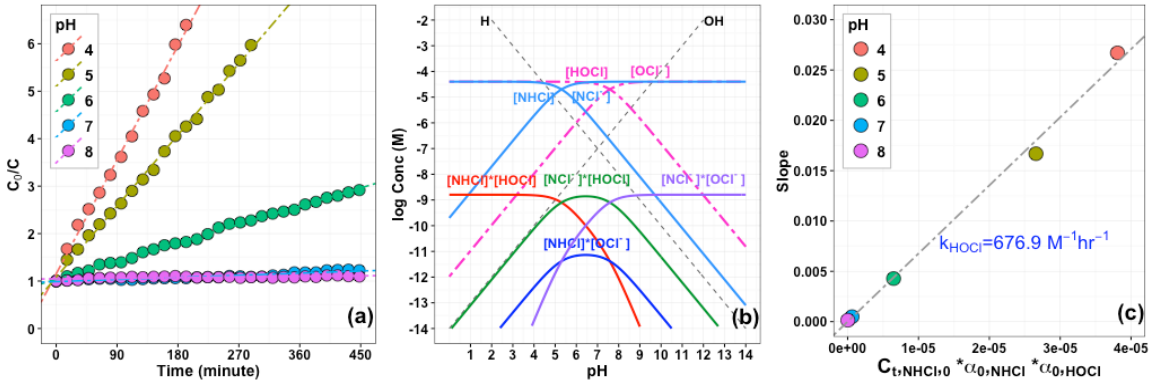

Figure 19. Analysis of *N-Cl*-DCAM chlorination kinetics. (a) Kinetic analysis of *N-Cl*-DCAM degradation in the presence of same molar concentration of aqueous chlorine under five different pH conditions. (b) Log C-pH diagram for a system containing 40 μM *N-Cl*-DCAM and 40 μM total free chlorine. (c) Estimation of *N-Cl*-DCAM chlorination rate constant (i.e., $k_{HOCl,NClDCAM}$).

Another transient chlorine species that needs to be considered in *N-Cl*-DCAM degradation is the H_2OCl^+, since its specific reactivity is estimated to be 10^5 times higher than that of HOCl at pH 7 and therefore is probably the species responsible for many acid-catalyzed reactions (Morris, 1975). If H_2OCl^+ is the major reactive species, the corresponding reactive form of *N-Cl*-DCAM will be the deprotonated $Cl_2CHC(O)NCl^-$ (*Figure 20(b)*) and the resulting second-order reaction rate constant k_4' is 1.1×10^9 $M^{-1}hr^{-1}$ (*Figure 20(c)*). As the HOCl/$Cl_2CHC(O)NHCl$ and the H_2OCl^+/ $Cl_2CHC(O)NCl^-$ combinations are both compatible, this can be interpreted that the extra proton can be either on the $Cl_2CHC(O)NCl^-$ or on the HOCl to decompose *N-Cl*-DCAM to DCAA. However, the actual speciation of these two reactants is not of great concern considering the scope of this work and the description of this reaction by the two neutral species (i.e., HOCl and $Cl_2CHC(O)NHCl$) might be relatively easier to perceive. Lastly, it has to be

addressed that the key to the estimation of k_4 using *Eq. 26* was to determine the acid dissociation constant, $K_{a,NClDCAM}$, for *N-Cl*-DCAM (i.e., $Cl_2CHC(O)NHCl$) at 20 °C, under which condition the *N-Cl*-DCAM chlorination rates were observed. The estimated $pK_{a,NClDCAM}$ value is 5.2 in this study, which exhibited certain disagreement with the value that was reported earlier ($pK_{a,NClDCAM}$=3.71 at 25 °C; Menard & Lessard, 1978). For this reason, this tentative acid dissociation constant needs to be further validated in a future work.

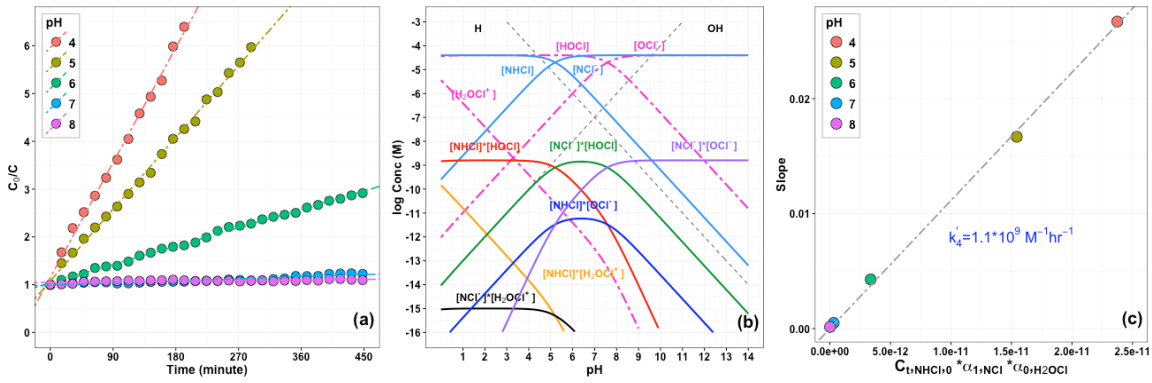

Figure 20. Analysis of *N-Cl*-DCAM reaction kinetics with H_2OCl^+.(a) Normalized reversed residual *N-Cl*-DCAM concentration (i.e., C_0/C) as a function of reaction time under five different pH conditions. (b) Log C-pH diagram for a system containing 40 μM *N-Cl*-DCAM and 40 μM total free chlorine. (c) Estimation of second-order *N-Cl*-DCAM chlorination rate constant (i.e., k_4').

3.3.4. The Fate of *N-chloro-2,2*-dichloroacetamide and *2,2*-dichloroacetamide in Chlorinated Drinking Waters

In *Chapter 1*, it has been proposed that chlorination of DCAN can lead to the formation of *N-Cl*-DCAM via direct nucleophilic addition of hypochlorite on the nitrile

carbon (*Figure 21*) and the estimated second-order reaction rate constant k_1 is (6.85±0.45) $\times 10^2$ $M^{-1}hr^{-1}$. Alternatively, DCAN can undergo base-catalyzed hydrolysis to form the corresponding DCAM by reacting with hydroxide (i.e., OH^-) at an estimated rate of (5.60± 0.31) $\times 10^3$ $M^{-1}hr^{-1}$ (i.e., k_2). According to the *N-Cl*-DCAM formation mechanism that has been elucidated above, the formed DCAM will further react with hypochlorite via the amide *N*-chlorination pathway, resulting in rapid *N-Cl*-DCAM formation (*Figure 21* & *Eq. 27*). Perhaps most importantly, reaction kinetics suggest that DCAM will not be able to persist as a long-lived reaction intermediate in this pathway, mainly because its reaction rate with hypochlorite is more than one order of magnitude higher than the rate at which DCAM can actually form via alkaline DCAN hydrolysis. As an example, *Table 7* compares the DCAM formation rate (i.e., $rate_F = k_2[DCAN][OH^-]$) with its subsequent reaction rate with hypochlorite (i.e., $rate_{Cl_2} = -k_3[DCAM][OCl^-]$) under a set of conditions that are typical for finished waters (i.e., pH 6-9 with 1 mg/L residual chlorine as Cl_2). Results indicated that under these conditions, DCAM will be *N*-chlorinated by free chlorine to form the corresponding *N-Cl*-DCAM at a rate that is 24 to 638 times faster than the rate at which it is initially formed from DCAN hydrolysis. As a result, it can be concluded that DCAM is so highly reactive with chlorine that it will not remain in systems with the presence of residual free chlorine for significant amount of time that is relevant to drinking water distribution.

$$DCAN + OH^- \xrightarrow[rate_F = k_2[DCAN][OH^-]]{DCAM\ foramtion} DCAM + OCl^- \xrightarrow[rate_{Cl_2} = -k_3[DCAM][OCl^-]]{DCAM\ chlorination} NClDCAM \qquad (27)$$

Table 7. Comparison of DCAM formation and chlorination rate at four different pH levels assuming a 1.0 mg Cl_2/L chlorine residual.

pH	C_{t,Cl_2}(mg/L)	α_{1,OCl^-}	$k_2[OH^-]$	$k_3[OCl^-]$	$\frac{rate_{F,DCAM}}{rate_{Cl_2,DCAM}}$
6	1.0	0.03	5.6E-05	3.6E-02	638
7		0.21	5.6E-04	2.9E-01	519
8		0.72	5.6E-03	1.0E+00	181
9		0.96	5.6E-02	1.3E+00	24

Furthermore, also reconciled in *Figure 21* are the *N-Cl*-DCAM chlorination pathway and the base-catalyzed DCAM hydrolysis pathway, both of which can lead to the formation of DCAA as final endpoint product. Owning to the very short lifetime of DCAM in chlorinated drinking waters, its hydrolysis pathway is considered as relatively unimportant, even though its second-order reaction rate constant has also been estimated in this study ($k_5 = 620\ M^{-1}hr^{-1}$; *Figure 22*). On the other hand, the rate of *N-Cl*-DCAM degradation via the HOCl chlorination pathway has also been estimated above ($k_4 = 703.1\ M^{-1}hr^{-1}$), and this reaction pathway is important only when the reaction pH is very low (i.e., $pH < pK_{a,NClDCAM} < pK_{a,HOCl}$), considering that the actual participating reactants are the uncharged neutral *N-Cl*-DCAM and hypochlorous acid (i.e., HOCl). When under ambient or slightly basic pH conditions (i.e., pH≥7), either *N-Cl*-DCAM is deprotonated, or both *N-Cl*-DCAM and chlorine are in their conjugated anionic forms, which inhibits the degradation of *N-Cl*-DCAM to DCAA. For this reason, *N-Cl*-DCAM are very stable in its deprotonated form under typical drinking water pH conditions regardless of the absence or the presence of residual chlorine. Accordingly,

Figure 23 draws the calculated half-lives of DCAN, DCAM, and *N-Cl*-DCAM based on the characterized reaction kinetics that are shown in *Figure 21* under identical conditions as listed in *Table 7* (i.e., pH 6-9 with 1 mg/L residual chlorine as Cl_2). As is illustrated in *Figure 23*, the half-lives of both DCAN and DCAM will substantially decrease with increasing pH and DCAM will decompose rather rapidly even at slightly acidic pH (i.e., pH 6), with its half-life ranging between 30 minutes to 1 day over decreasing pH. DCAN will degrade only in relatively alkaline waters (e.g., softened waters or finished waters with high pH for corrosion control). For instance, DCAN has a 1-day half-life when pH is increased to 8.5. This compares to a half-life of 10 days for DCAN at neutral pH (i.e., pH 7). In sharp contrast, *N-Cl*-DCAM will essentially remain stable regardless of the water pH, with a minimum half-life of 20 days at pH 6.

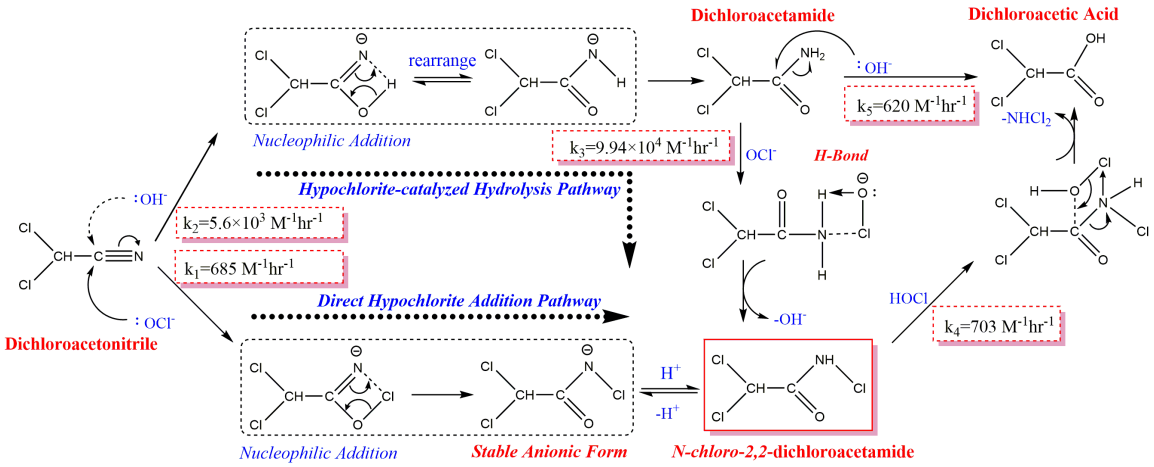

Figure 21. *N-chloro-2,2*-dichloroacetamide formation and degradation mechanisms.

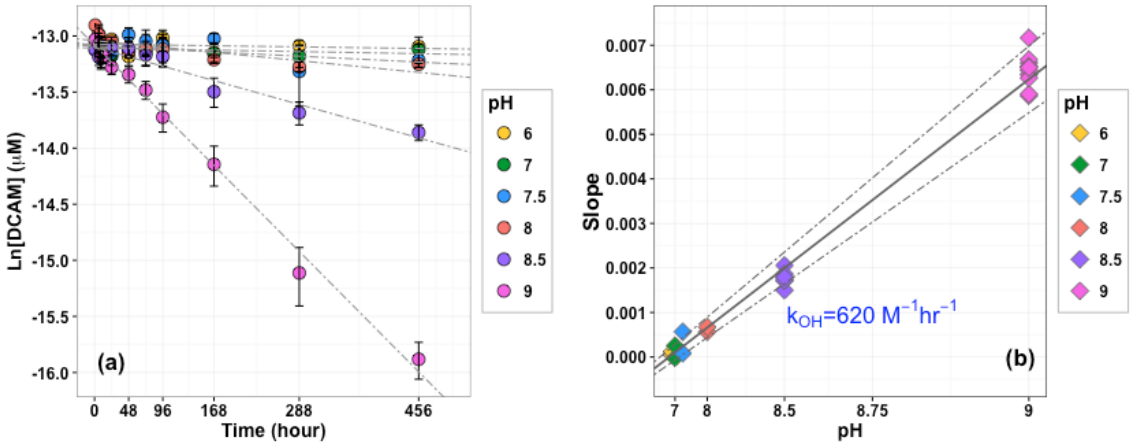

Figure 22. Kinetic analysis of second-order DCAM hydrolysis rate constant, k_5. (a) Semilogarithmic plot of residual DCAM concentration versus reaction time at six investigated pH levels. (b) Estimation of second-order DCAM hydrolysis rate constant, k_5 using heteroscedastic hierarchical Bayesian modeling (detailed methodology is referred to Chapter 2).

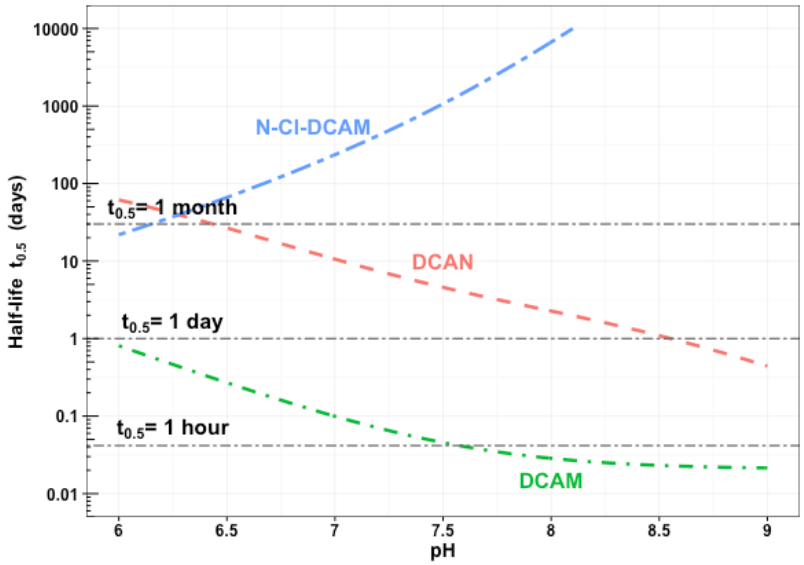

Figure 23. Predicted half-lives of DCAN, DCAM, and *N-Cl*-DCAM under a range of pH conditions (i.e., pH 6-9) with 1mg/L residual chlorine as Cl_2.

3.3.5. Quantification and Occurrence of *N-chloro*-haloacetamides in Drinking Waters

To examine the existence of *N-Cl*-DCAM, or more ideally, the family of *N-Cl*-HAMs in real drinking water supplies, a SPE-UPLC/ESI/qTOF method was developed and validated during the course of this study, which enables the quantification of seven chlorinated and brominated *N-Cl*-HAMs (*Figure 24*) in drinking waters at trace concentration levels. The optimized SPE procedures and UPLC/ESI conditions have been summarized above. All seven *N-Cl*-HAMs were separated within 4 minutes (*Figure 25*) and the performance of this SPE-UPLC/ESI/qTOF method was evaluated as shown in *Table 8*. When combined with SPE pre-enrichment, the estimated method detection limits (MDLs) for the seven analytes were between 0.13 μg/L and 1.40 μg/L, and recoveries ranged from 46% to 86% with standard deviations of 3%-7%, depending on the *N-Cl*-HAM species. Additionally, prior to sample pretreatment, ammonium chloride was found to be the only reducing agent that did not cause *N-Cl*-HAM reduction to HAMs even over a relatively long period of sample storage time (i.e., 14 days). On the contrary, complete disappearance of all seven analytes from the selected ion chromatogram was observed instantly after spiked ultrapure water (1 μM for each *N-Cl*-HAM) was treated with same concentrations of ascorbic acid, sodium sulfite, and sodium thiosulfate, respectively. This is probably because dechlorination by ammonium chloride is due to the combination of ammonium with residual free chlorine to form the inorganic monochloramine (i.e., NH_2Cl), which may not interact with *N-Cl*-HAMs also as chloramines, but organic ones.

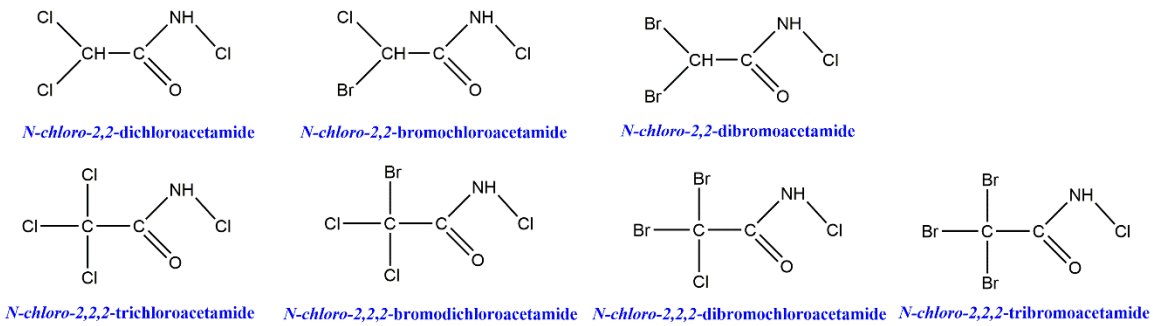

Figure 24. *N-chloro*-haloacetamide molecular structures.

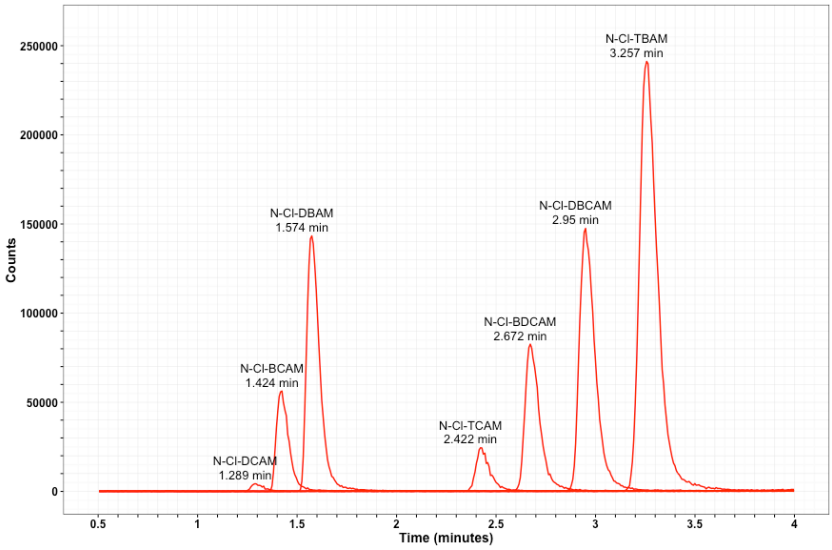

Figure 25. Typical selected ion chromatogram of *N-Cl-HAMs* using the optimized UPLC/ESI/qTOF method. The concentrations were 1 µM for each *N-Cl*-HAM.

Table 8. Retention times, method detection limits (MDLs), and recoveries of the developed SPE-UPLC/ESI/qTOF method.

Analytes	Retention Time (min)	MDL (μg/L)	Recovery (%)
N-chloro-2,2-dichloroacetamide	1.289	0.90	85±6
N-chloro-2,2-bromochloroacetamide	1.424	0.15	86±4
N-chloro-2,2-dibromoacetamide	1.574	0.13	84±4
N-chloro-2,2,2-trichloroacetamide	2.422	1.40	51±7
N-chloro-2,2,2-bromodichloroacetamide	2.672	0.82	49±4
N-chloro-2,2,2-dibromochloroacetamide	2.950	1.08	47±4
N-chloro-2,2,2-tribromoacetamide	3.257	0.81	46±3

To further validate this analytical method, 11 tap water samples collected from seven private US residences were analyzed to quantitatively determine the occurrence of *N-Cl*-HAMs. Among the seven *N-Cl*-HAM species, all three *N-Cl*-DHAMs, including *N-Cl*-DCAM, *N-Cl*-BCAM, and *N-Cl*-DBAM were detected for the first time (*Figure 26*), whereas the other four *N-Cl*-THAMs were absent in all of the samples that were analyzed. *N-Cl*-DCAM was present in 5 of the 11 samples at levels that are higher than its MDL, with averaged concentrations ranging between 1.40 μg/L to 3.48 μg/L. Interestingly, the two brominated *N-Cl*-DHAM analogues were detected more frequently (n=8) than the *N-Cl*-DCAM probably because the developed method is more sensitive to those two higher molecular weight compounds (i.e., lower MDLs). *N-Cl*-BCAM and *N-Cl*-DBAM also exhibited some moderate correlations with each other, since *N-Cl*-DBAM tended to occur at higher levels in samples with higher concentrations of *N-Cl*-BCAM, even though the median concentration of the former remained relatively lower than that

of the latter (respective median concentrations for *N-Cl*-DBAM and *N-Cl*-BCAM were 0.20 μg/L and 0.65 μg/L). The lower level *N-Cl*-DBAM occurrence is in agreement with the bromine substitution efficiency that was noted for other DBP families (Hua & Reckhow, 2012). Additionally, as has been demonstrated above, *N-Cl*-DCAM forms as DCAN degrades. Thus, concentrations of the three *N-Cl*-DHAMs are further compared in *Figure 26* with dihaloacetonitrile (DHAN) concentrations that were determined in the same sample. Although strong correlations between these two classes of N-DBPs were not observed given the very small pool of samples that were analyzed, the average concentrations of the *N-Cl*-DHAMs were consistently higher than those of the corresponding DHANs. This further supports the previous conclusion regarding the high chemical stability of *N-Cl*-HAMs (e.g., *Figure 23*). It is also noteworthy that all three *N-Cl*-DHAMs were not detected in three of the samples that were collected from systems using chloramine instead of free chlorine (i.e., sample 7, 8, and 10), nor were their corresponding DHANs, suggesting that the formation of these two groups compounds is more likely associated with the use of free chlorine instead of chloramines during drinking water disinfection.

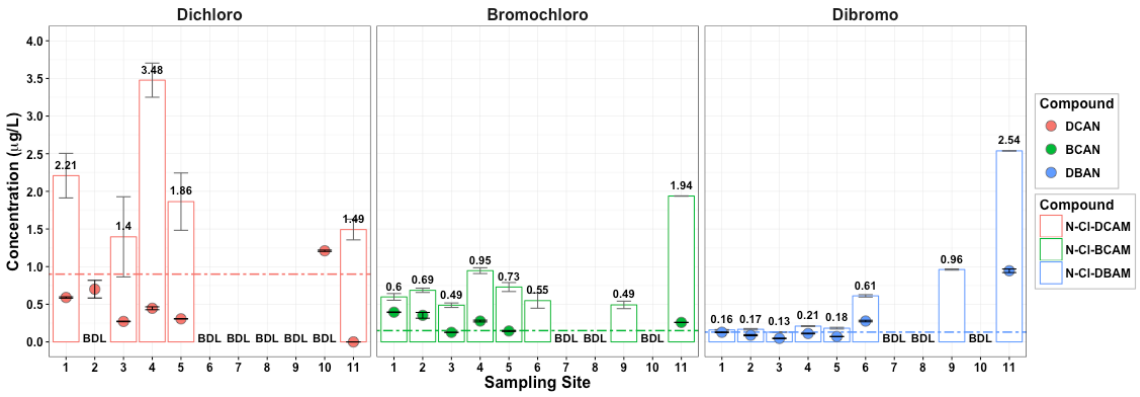

Figure 26. Measured concentrations of *N-Cl*-DCAM, *N-Cl*-BCAM, and *N-Cl*-DBAM (shown in bars) in 11 real tap water samples by SPE-UPLC/ESI/qTOF. Numbers above the bars denote the averaged *N-Cl*-DHAM concentrations between two sample duplicates. Dashed lines indicate the MDLs for each N-Cl-DHAM species. Concentrations of the three *N-Cl*-DHAMs were also compared to those of the corresponding dihaloacetonitriles (DHANs; shown in solid dots) that were determined in the same sample.

3.3.6. Implications for Future DBP Work

The existence of a previously misidentified nitrogenous disinfection byproduct, *N-chloro-2,2*-dichloroacetamide in chlorinated drinking waters was confirmed in this part of the study. The discovery of this compound is of great importance since *N-Cl*-DCAM exhibited very high stability under pH conditions that are relevant to drinking water treatment with and without the presence of chlorine. Furthermore, as an organic chloramine, *N-Cl*-DCAM is expected to be more toxicologically potent than the hitherto identified N-DBPs, and therefore may pose higher carcinogenic risks to drinking water consumers given its ubiquitous occurrence and high stability. Paradoxically, the escape of *N-Cl*-DCAM from previous detection by advanced analytical technologies is due to its

reduction by common reducing agents during sample preservation, which resulted in the erroneous identification of DCAM as an emerging drinking water DBP. The SPE-UPLC/ESI/qTOF method developed in this study can be used in the future as a strong analytical tool to create a larger scale of occurrence information for the *N*-*Cl*-HAM family. Lastly, with the underlying formation and degradation mechanisms elucidated herein, the remaining question is how toxic *N*-*Cl*-DCAM, or more broadly speaking, *N*-*Cl*-HAMs are and how the overall drinking water toxicity may alter as a result of inter-class transformation from HANs to *N*-*Cl*-HAMs and ultimately to HAAs. For this reason, quantitative toxicity assessment is needed in order to determine the potential health risks that may be imposed by *N*-*Cl*-HAMs.

CHAPTER 4

FORMATION AND DEGRADATION OF DICHLOROACETONITRILE DURING THE CHLORINATION OF FREE AND COMBINED ASPARTIC ACID: EFFECT OF PEPTIDE BOND[4]

4.1. Introduction

Different from the trihalomethanes (THMs) and the haloacetic acids (HAAs), which are mainly derived from activated aromatic moieties of natural organic matter (NOM) (Rook, 1974), the formation of haloacetonitriles (HANs) tends to correlate positively with the organic nitrogen content in NOM (Lee et al., 2007). In fact, early research on HAN formation has established α-amino acids as important HAN precursors in drinking water (Trehy & Bieber, 1981; Ueno et al., 1996; Yang et al., 2012). Of all the common amino acids, aspartic acid was found to be the most prolific HAN producer, especially for dichloroacetonitrile (DCAN; Trehy & Bieber, 1981; Bond et al., 2014; Chu et al., 2010b).

As is demonstrated in *Figure 25*, free aspartic acid can react very quickly with excess chlorine (Alouini & Seux; 1987) leading to rapid DCAN formation via the "decarboxylation pathway". In this pathway, chlorination of the α-amine first forms the *N,N*-dichloroaspartic acid. Subsequent decarboxylation of this dichloramine forms an *N*-chloroaldimine, which can dehydrohalogenate (i.e., elimination of hydrochloric acid) to yield the cyanoacetic acid. Due to the combined electron-withdrawing effect from both

[4] Yu, Y.; Reckhow, D.A. The Formation of Dichloroacetonitrile from Chlorination of Free and Combined Aspartic Acid: Effect of Peptide Bond. Manuscript in preparation, to be submitted to *Water Research*.

the carboxylic acid group and the nitrile group, the methylene carbon in cyanoacetic acid is very acidic (Shah & Mitch, 2011). Therefore, rapid dichlorination of this carbon followed by decarboxylation will ultimately lead to the formation of DCAN. In the meanwhile, aspartic acid can also react with one molar equivalent of free chlorine to form the *N*-chloroaspartic acid, which can undergo concerted decarboxylation to yield an imine. Imines are usually very unstable in water and can rapidly hydrolyze to form the corresponding aldehydes (Nweke & Scully, 1989). In this case, hydrolysis of the primary aldimine forms the *3*-oxopropanoic acid, which can be further chlorinated and decarboxylated to form the dichloroacetaldehyde. Although dichloroacetaldehyde is an important drinking water DBP in its own right, it tends to further react with chlorine to form the trichloroacetaldehyde (or chloral; Trehy, 1980), while the latter can readily form a hydroxyl adduct with water (i.e., chloral hydrate) and finally result in chloroform (i.e., $CHCl_3$) formation (Trehy, 1980).

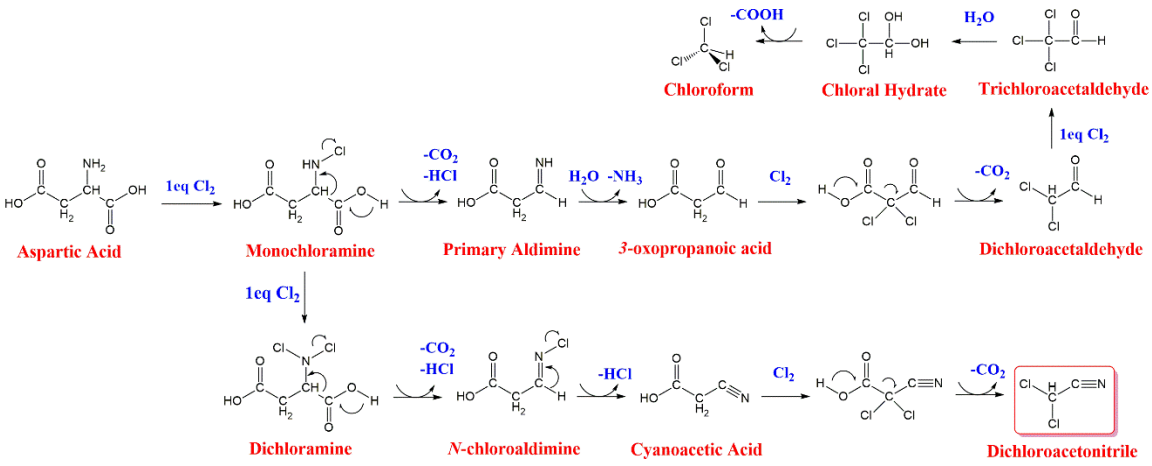

Figure 27. Scheme of reaction pathways for aspartic acid chlorination (summarized from Trehy & Bieber, 1981; Trehy et al., 1986; Peters et al., 1990; Hureike et al., 1994; Shah & Mitch, 2011; Bond et al., 2014).

Despite their relatively high reactivity with chlorine (Trehy & Bieber, 1981; Trehy et al., 1986; Peters et al., 1990; Hureike et al., 1994; Shah & Mitch, 2011; Bond et al., 2014), free amino acids are probably not the primary precursors for HANs, mainly because their actual concentrations in natural waters are too low to sufficiently account for the amounts of HANs that can actually occur in finished water supplies (Reckhow et al., 2001; Bond et al., 2012). For instance, aspartic acid was detected in the source waters for 16 US drinking water treatment plants at concentrations between 0.3 μg/L to 1.6 μg/L (Mitch et al., 2009). This could only account for 0.08 μg/L DCAN production based on a maximal DCAN formation potential of 6% (i.e., mole/mole) for aspartic acid (Bond et al., 2009). On the other hand, in surface water, around 60% of recoverable dissolved amino acids are combined in peptides and proteins, with another 20% associated with humic substances (Thurman, 1985). Thus, those combined amino acids are generally 4 to 5 times as common as free amino acids in natural waters (Hureiki et al., 1994).

Unlike free amino acids, the majority of the amino nitrogens in combined amino acids are bound in peptide linkages and therefore are orders of magnitude less reactive with chlorine than amine nitrogens (Hawkins and Davies, 1999). In fact, many have shown that amide nitrogens in peptide bonds are unreactive with aqueous chlorine (Pereira et al., 1973; Hureiki et al., 1994). For this reason, due to the absence of an active amine group, an aspartyl residual that is incorporated in a peptide may be inaccessible to chlorine to form the corresponding DCAN. However, when the aspartyl residual is at the *N*-terminal end, its unprotected amine group can be chlorinated in the same way as the α-amine in free aspartic acid, leading to the formation of an *N,N*-dichloramine (Bieber & Trehy, 1983; *Figure* 26). Since peptides cannot readily undergo decarboxylation (Nweke &

Scully, 1989; McCormick et al., 1993; Conyers & Scully, 1993; Conyers & Scully, 1997), following dehydrohalogenation of this dichloramine yields an *N*-chloroimine, which can undergo C-C cleavage to remove a cyanoacetic acid from the peptide backbone (Bieber & Trehy, 1983). The resulting cyanoacetic acid will then convert rapidly into DCAN via the aforementioned dichlorination and decarboxylation pathways (*Figure 25*). Subsequently, the chlorination reaction will proceed to the next amino acid residue with the generation of a new amine group at the *N*-terminus from isocyanate hydrolysis (Keefe et al., 1997; Fox et al., 1997; *Figure 26*). As a result, the peptide will be degraded in a slow stepwise fashion (Goldschmidt et al., 1927; Bieber & Trehy, 1983; Keefe et al., 1997; Fox et al., 1997) and DCAN can be produced at any point when the remaining peptide contains an *N*-terminal aspartyl residue that can be chlorinated to generate cyanoacetic acid as an essential DCAN precursor.

Because aspartyl residue is well represented in peptides and proteins, DCAN formation in drinking water will thus be readily accounted for if chlorine can produce appreciable amount of cyanoacetic acid via stepwise peptide degradation. However, no empirical evidence has been presented so far showing the actual formation of DCAN from chlorination of bound aspartyl residues. Therefore, the reactivity of combined aspartic acid with chlorine needs to be evaluated and its potential contribution to DCAN formation has to be validated. Moreover, in addition to its continuous formation in treated drinking waters, DCAN will undergo simultaneous decomposition due to its metastability in water (Reckhow et al., 2001; Chapter 1). As DCAN degrades, it leaves the corresponding *N-chloro-2,2*-dichloroacetamide (*N-Cl*-DCAM) and dichloroacetic acid

(DCAA) in its place (Chapter 3). For this reason, understanding the role of combined amino acids in the formation of those secondary DBPs is also of great importance.

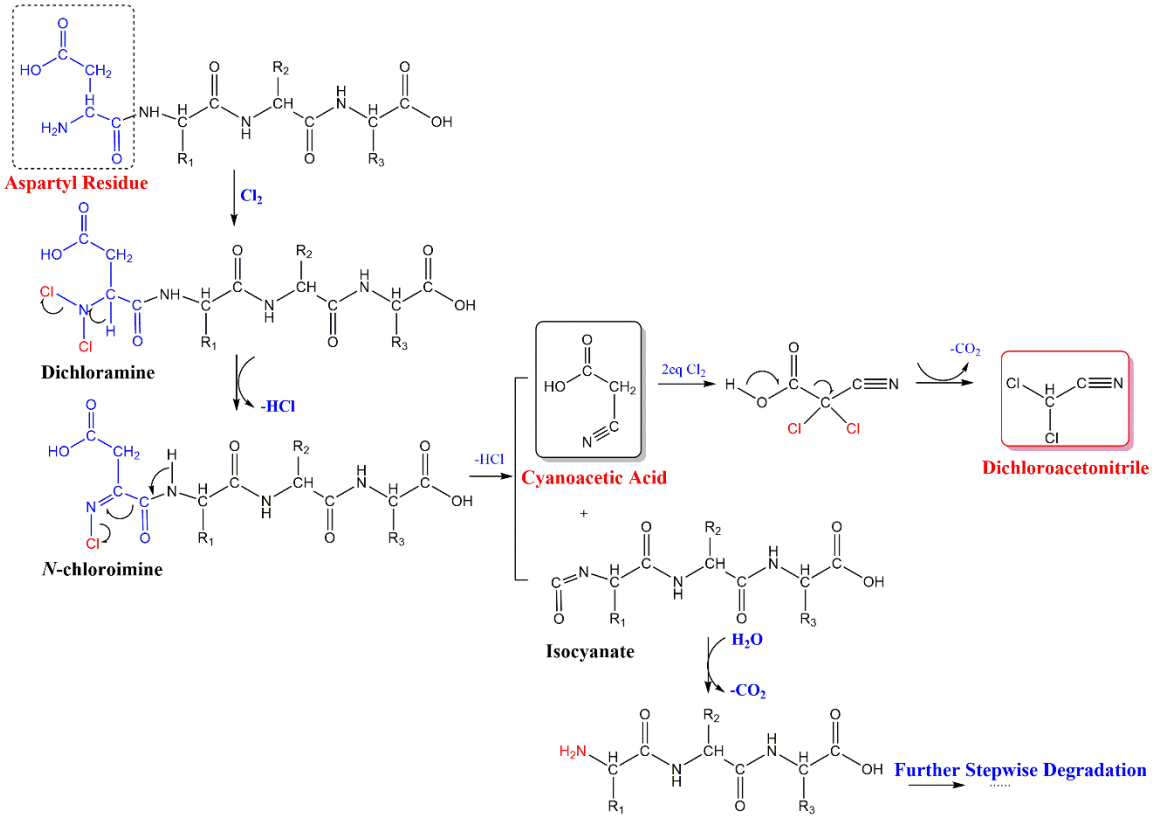

Figure 28. Proposed DCAN formation mechanism from the chlorination of a generic peptide possessing an aspartyl residual at the *N*-terminus (summarized from Bieber & Trehy, 1983; Keefe et al., 1997; Fox et al., 1997).

The purpose of this study was to compare the formation of DCAN and its degradation products (i.e., *N*-*Cl*-DCAM and DCAA) from free aspartic acid and two aspartyl-containing model peptides during chlorination so as to clarify the reactivity of bound aspartyl residues in combined amino acids and their role as potential HAN precursors.

4.2. Materials and Methods

4.2.1. Selection of Model Peptides

As has been mentioned above, chlorination and removal of an aspartyl residue during stepwise peptide degradation is the key to DCAN formation. Therefore, two commercially available model peptides that particularly contain aspartyl residues were studied. Tetra-aspartic acid (i.e., Asp-Asp-Asp-Asp) is a small-size oligopeptide that simply consists of four aspartyl residues and the one at the *N*-terminus should be initially reactive with chlorine due to the presence of an α-amine. The other peptide that was investigated in this study was Arg-Gly-Asp-Ser. Unlike Asp-Asp-Asp-Asp, Arg-Gly-Asp-Ser contains only one aspartyl residue, which is located in the middle of the peptide backbone. Hence, this aspartyl residue won't contribute to DCAN formation unless the prior two amino residues are both degraded.

4.2.2. Chemicals and Reagents

L-Aspartic acid (reagent grade, ≥ 98%), Asp-Asp-Asp-Asp (≥ 97%), Arg-Gly-Asp-Ser (≥ 95%), and all purified DBP standard compounds, including dichloroacetonitrile (DCAN), dichloroacetamide (DCAM), and dichloroacetic acid (DCAA) were all purchased from Sigma-Aldrich (St. Louis, MO). General laboratory chemicals including Optima LC/MS grade organic solvents and formic acid (FA) were obtained from Fisher Scientific (Pittsburgh, PA). *N-chloro-2,2*-dichloroacetamide (*N-Cl*-DCAM) was prepared by reacting equal stoichiometric amount (Cl_2/N=1:1) of free chlorine with dichloroacetamide (DCAM), with pH of both solutions adjusted to 9.0 before mixing. The formation of *N-Cl*-DCAM in the stock solution was confirmed using ultra

performance liquid chromatography/quadrupole time-of-flight mass spectrometry (ACQUITY UPLC/Xevo G2-XS qTOF, Waters; Chapter 3).

4.2.3. Experimental Conditions

All reaction solutions were prepared in ultrapure Milli-Q water (EMD Millipore Corp.), containing 10 mM phosphate buffer and were adjusted to the desired pHs with sodium hydroxide or hydrochloric acid. At the start of each chlorination experiment, certain amount of model compound was introduced individually into three liters of buffered solutions, so that the respective initial concentrations for free aspartic acid, Asp-Asp-Asp-Asp, and Arg-Gly-Asp-Ser were 20 μM, 10 μM, and 10 μM. Chlorine solutions were prepared on the day of use by diluting the sodium hypochlorite stock solution (5.65%-6%, laboratory grade, Fisher Scientific), followed by acidification to the target pHs using hydrochloric acid. The actual chlorine concentration was standardized using the *N,N*-diethyl-*p*-phenylene diamine (DPD)-ferrous ammonium sulfate (FAS) titrimetric method (EPA Method 330.4). Chlorination of individual model precursors was conducted by adding small volumes of acidified sodium hypochlorite solutions to reach a fixed dose of 15 mg/L as Cl_2. Immediately after the introduction of chlorine, samples were partitioned off into 300 mL BOD bottles and were stored without headspace in a dark 20 °C constant temperature incubator until the prescribed reaction times. At each reaction time, one bottle of sample would be sacrificed for instant chlorine residual determination and DBP analysis. All samples were analyzed in duplicates to account for measurement uncertainties.

4.2.4. Sample Pretreatment and Chromatographic Analysis

After the prescribed chlorine contact time, the chlorine residual in each sample was quenched using ammonium chloride (100 mg/L NH_4Cl). Subsequent DCAN analysis was performed according to EPA Method 551.1. To prevent DCAN from base-catalyzed hydrolysis (Chapter 1) during sample pretreatment, 20 mL aliquots of quenched samples were first acidified to pH 6 using hydrochloric acid. DCAN was extracted by adding 4 mL of pentane with an internal standard (i.e., 1,2-dibromopropane), together with 15 g anhydrous sodium sulfate. Then the samples were shaken at 300 rpm for 15 minutes, and the upper organic layer was collected for subsequent analysis by an Agilent 6980 gas chromatography with a linearized micro-electron capture detector (μ-ECD) (*Table 2*). DCAA was quantified following EPA Method 552.2. In brief, 30 mL aliquots of each sample were acidified to pH ~2 using 1.5 mL of concentrated sulfuric acid (95.0-98.0% W/W, ACS grade, Fisher Scientific), followed by liquid-liquid extraction with 3 mL methyl *tert-butyl* ether and methylation using 5% acidic methanol at 60 °C for two hours. The final extract, which contained the derivatized methyl dichloroacetate was analyzed using GC- μECD (*Table 2*).

N-Cl-DCAM was quantified according to solid phase extraction (SPE)-ultra performance liquid chromatography/electrospray ionization/quadrupole time-of-flight mass spectrometry (UPLC/ESI/qTOF MS) method that was described in Chapter 3. Before analysis, *N-Cl*-DCAM in aqueous samples was first concentrated using Oasis mixed-mode, reversed-phase, strong anion-exchange (MAX) cartridges (60 mg, 3 mL, 30 μm; Waters, Milford, MA) that were mounted on an Agilent VacElut SPS 24 SPE manifold. Prior to sample loading, each MAX cartridge was conditioned with 3 mL

methanol, followed by one Milli-Q water wash (3 mL). Each sample (100 mL) was drawn through the cartridges under vacuum at a flow rate of approximately 1 mL/min. After sample loading, the cartridges were washed with 2 mL of methanol/NH_4OH (v/v=95/5) and then dried for 1 minute under vacuum. Subsequently, the retained *N-Cl*-DCAM was eluted with 2 mL of acetonitrile/water (v/v=90/10, with 25% formic acid). The acetonitrile extract was reconstituted by adding 0.5 mL of water/NH_4OH (v/v=85/15) and was then evaporated down to 1.0 mL under a gentle nitrogen stream (TurboVap LV).

An ACQUITY UPLC (Waters, Milford, MA) system was used for LC separation with an ACQUITY UPLC HSS T3 column (1.8 μm, 100 Å, 2.1×100 mm; Waters), coupled with a 1.8 μm, 2.1×5 mm VanGuard pre-column (ACQUITY UPLC HSS T3; Waters). The column temperature was maintained isothermally at 35 °C. The mobile phases were 5 mM ammonium acetate (solvent A) and 100% methanol (solvent B) at a constant flow rate of 0.3 mL/min. The initial gradient was 0-2 min, 5% B, curve 6; increased from 5% to 90% B between 2 and 7 min, curve 6; 7-8 min 90% B, curve 6; switch back to 5% B in 0.1 min, curve 11; 11-15 min for equilibration, 5% B. The injection volume for each sample was 5 μL. A quadrupole time-of-flight mass spectrometer (Xevo G2-XS qTOF; Waters) with an electrospray ionization (ESI) source was used to obtain accurate mass measurements of the parent ions of *N-Cl*-DCAM. Negative ESI-TOFMS mode was applied with typical conditions optimized as follows: capillary voltage 2.50 kV; sampling cone, 25 arbitrary units; source offset, 80 arbitrary units; source temperature, 120 °C; desolvation temperature 20 °C; cone gas, 80 L/hour; desolvation gas flow, 800 L/hour. The retention time of *N-Cl*-DCAM is 1.289 min and the method detection limit is 0.39 μg/L.

4.3. Results and Discussion

4.3.1. Dichloroacetonitrile Formation from Free and Combined Aspartic Acid

Figure 27 shows the formation of DCAN as a function of reaction time and pH during the chlorination of free aspartic acid, Asp-Asp-Asp-Asp, and Arg-Gly-Asp-Ser. Regardless of the reaction pH, temporal DCAN formation profiles followed many similar trends among the three model precursors. In general, the yields of DCAN increased rapidly at the beginning of each chlorination reaction, but significantly decreased at longer reaction times especially under high pH conditions. This non-monotonic relationship between DCAN yield and chlorine contact time is indicative of its simultaneous formation and decomposition over the entire reaction period. As a result, the amount of DCAN that was initially formed may be substantially greater than what was instantaneously measured (indicated by the solids dots in *Figure 27*). In order to compare the actual DCAN formation potentials between free and combined aspartic acid, the amount of DCAN that was degraded also needs to be considered.

Although developing a mechanistic kinetic model to predict byproduct formation meanwhile reflecting the underlying precursor chlorination chemistry can be practically very challenging, the amount of DBP formation can instead be back simulated based on their decomposition kinetics, which are often adequately characterized and in some cases, are well modeled (Reckhow et al., 2001). In Chapter 1, the DCAN degradation kinetics have been fully characterized, which can be described by the following rate law:

$$\frac{d[DCAN]}{dt} = -k_{H_2O}[DCAN] - k_{OH}[OH^-][DCAN] - k_{OCl}[OCl^-][DCAN] \quad (28)$$

In the above equation, k_{H_2O} and k_{OH} are the second-order neutral and basic hydrolysis rate constants, and k_{OCl} is the hypochlorite chlorination rate constant, which were estimated to be (1.68±1.02) $\times 10^{-4}$ hr^{-1}, (5.60 ± 0.31) $\times 10^{3}$ $M^{-1}hr^{-1}$, and (6.85± 0.45) $\times 10^{2}$ $M^{-1}hr^{-1}$, respectively (Chapter 1). *Equation 28* can be further formulated as follows using the hypochlorous acid dissociation constant (i.e., K_a=$10^{-7.582}$ at 20°C; Morris, 1966) to reflect the fraction of total free chlorine (i.e., C_t) that is actually in the form of hypochlorite (i.e., OCl^-) at any given pH.

$$\frac{d[DCAN]}{dt} = -\left(k_{H_2O} + k_{OH}[OH^-] + k_{OCl}\alpha_1 C_t\right) \cdot [DCAN] \qquad (29)$$

$$\alpha_1 = \frac{K_{a,HOCl}}{K_{a,HOCl} + [H^+]} \qquad (30)$$

When both DCAN and residual chlorine concentrations were monitored over reaction time, the amount of DCAN that decomposed in a discretized time step from "t" to "t+1" can be quantitatively determined using *Equation 31*, where intermediate DCAN and free chlorine concentrations were approximated by linear interpolation (i.e., $\frac{[DCAN]_t + [DCAN]_{t+1}}{2}$ and $\frac{C_{t,t} + C_{t,t+1}}{2}$).

$$\Delta[DCAN] = \left(k_{H_2O} + k_{OH}[OH^-] + k_{OCl}\alpha_1 \cdot \frac{C_{t,t} + C_{t,t+1}}{2}\right) \cdot \frac{[DCAN]_t + [DCAN]_{t+1}}{2} \cdot \Delta t \quad (31)$$

As a result, if there wasn't any DCAN decomposed, the cumulative DCAN formation (denoted as $[DCAN]_F$) can be back calculated as follows by augmenting the amount of DCAN that was instantaneously measured with the amount that had been degraded.

$$[DCAN]_{F,t+1} = [DCAN]_{F,t} + ([DCAN]_{t+1} - [DCAN]_t) + \Delta[DCAN]$$
$$Initial\ Condition: [DCAN]_{F,t}|_{t=0} = 0 \qquad (32)$$

Solid lines in *Figure 27* represent the results of this calculation based on the kinetic DCAN and C_t measurements (i.e., solid dots shown in *Figure 27* and *Figure 28*). It is evident in *Figure 27* that large amounts of DCAN initially formed but subsequently degraded during the chlorination of all three model precursors, especially at high pH levels.

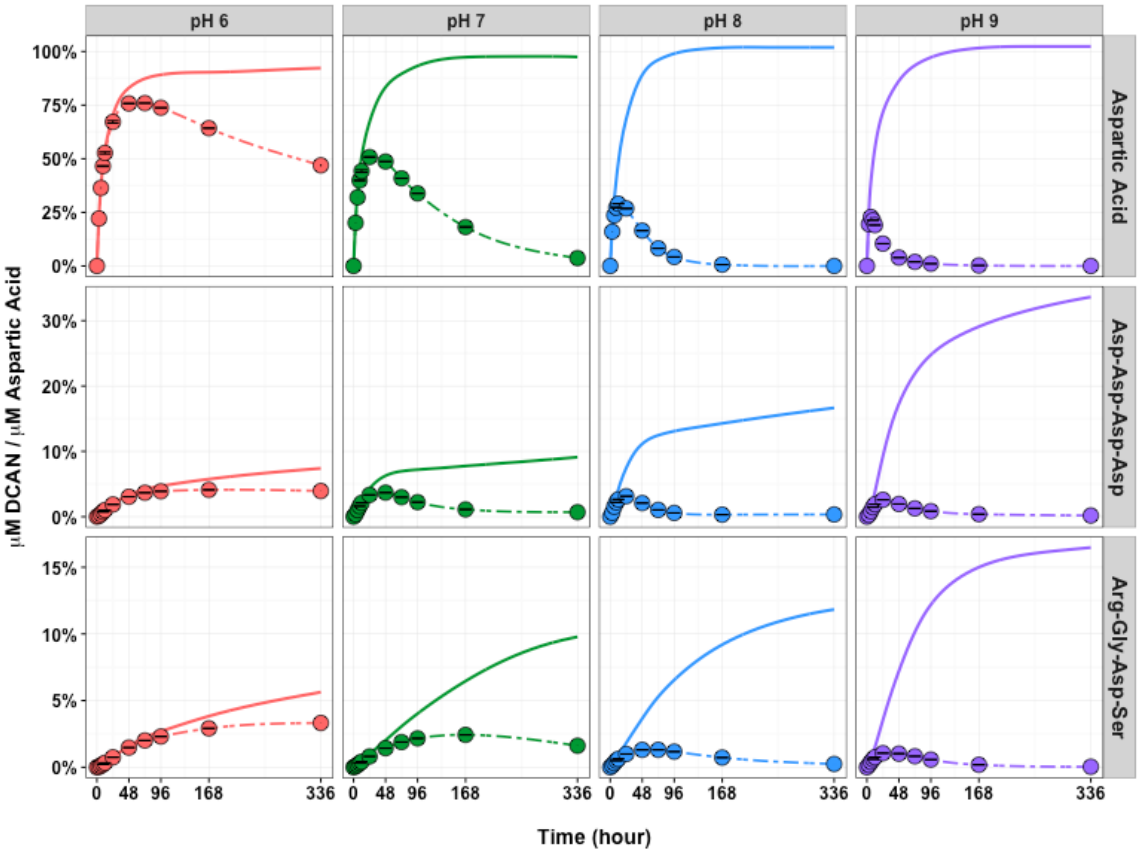

Figure 29. Formation of DCAN as a function of reaction time during the chlorination of free aspartic acid, Asp-Asp-Asp-Asp, and Arg-Gly-Asp-Ser at four different pH levels (i.e., pH 6, 7, 8, and 9). DCAN yields are shown in percentage on the y-axis, which were calculated by normalizing the amount DCAN formed with the initial aspartic acid content in each model compound. Solid dots represent the actual time-based DCAN measurements, with error bars showing the standard deviation between the two

duplicates. Dashed lines in the figure interpolate the kinetic DCAN formation potential profiles. Solid lines indicate the calculated cumulative DCAN formation potentials.

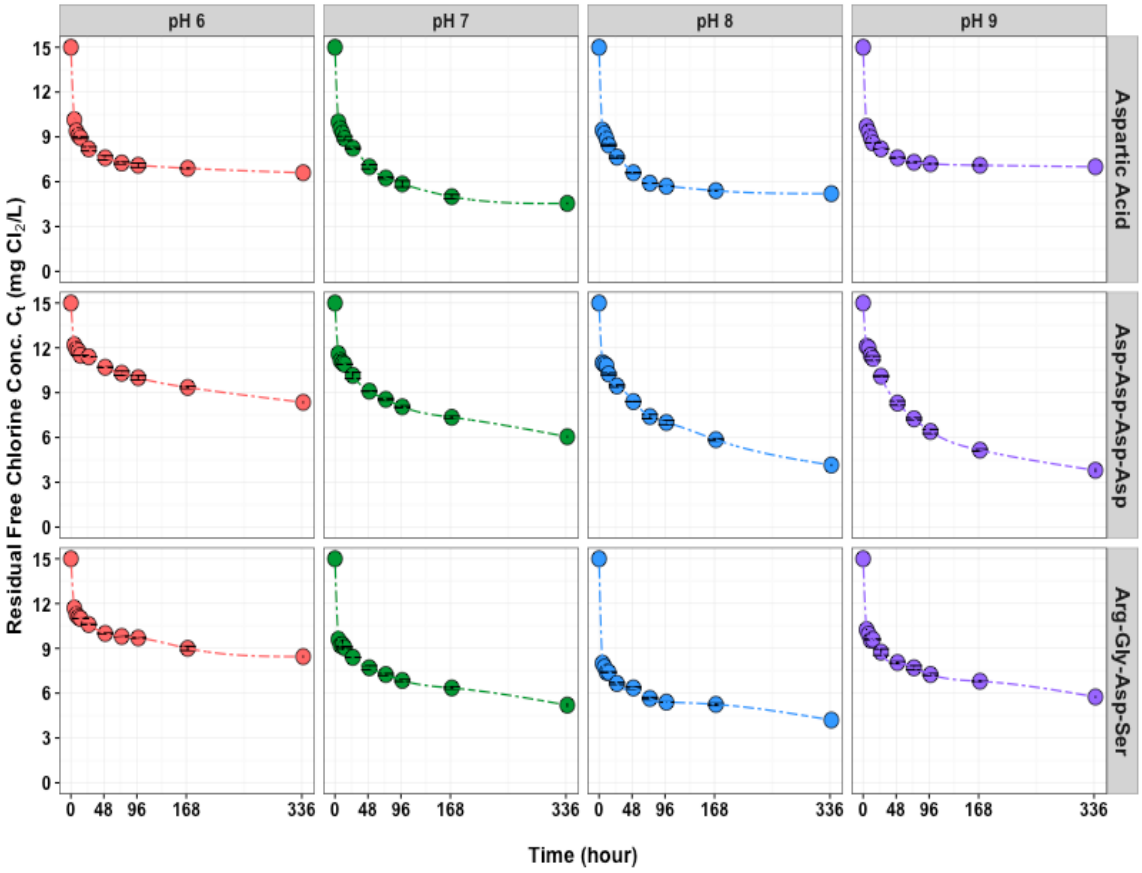

Figure 30. Residual chlorine concentrations over reaction time during the chlorination of free aspartic acid, Asp-Asp-Asp-Asp, and Arg-Gly-Asp-Ser.

4.3.2. Reactivity of Free vs. Combined Aspartic Acid

To elucidate the different reactivity between free and combined aspartic acid, cumulative DCAN formation potentials of the three model compounds are further compared in *Figure 29* under identical pH conditions. As is shown in the figure, about 90% of total free aspartic acid was transformed to DCAN after 72 hours at pH 6, which compares to 97%, 100%, and 100% maximum DCAN formation at pH 7, 8, and 9,

respectively. This agrees with the expected high reactivity of free aspartic acid when chlorine is in excess (Alouini & Seux, 1987). Perhaps most importantly, results indicated that the actual DCAN formation potential of free aspartic acid was almost 100% when pH was above neutral, although apparent DCAN yields (solid dots in *Figure 27*) were suppressed at higher pHs mainly by its simultaneous degradation. Therefore, over increasing reaction pH, the decreased DCAN yields shown in *Figure 27* are attributed to its more substantial self-decomposition and not to the lower reactivity of free aspartic acid to form less DCAN.

Given the same reaction time and pH, both Asp-Asp-Asp-Asp and Arg-Gly-Asp-Ser produced approximately one order of magnitude less DCAN compared to free aspartic acid (*Figure 29*). Furthermore, the yields of DCAN from both peptides increased not only with increasing reaction time, but also with increasing reaction pH. Since peptide degradation is a slow and base-catalyzed process (Bieber & Trehy, 1983; Goldschmidt et al., 1927), these trends clearly suggest that bound aspartyl residues in peptides are also reactive with chlorine to form DCAN, but the rate of DCAN formation is dependent on how fast reactive *N*-terminal aspartyl residue can be generated via peptide degradation. Therefore, more DCAN formation was observed at higher pHs when peptide degradation was accelerated. Moreover, because only *N*-terminal aspartyl residue is reactive with chlorine (Bieber & Trehy, 1983), the rate of DCAN formation from each aspartyl residue will follow a descending trend when this residue is located in a peptide closer towards the *C*-terminal end. In Asp-Asp-Asp-Asp, the first aspartyl residue contains the α-amine group and therefore is initially reactive with chlorine. Hence, the rate of DCAN formation from this first aspartyl residue should be the highest. As the second aspartyl

residue in Asp-Asp-Asp-Asp won't be reactive until the *C-C* bond is cleaved and the isocyanate intermediate is hydrolyzed, the DCAN formation rate will be determined by those steps and thus becomes much slower. Continuing this trend, the third and the last aspartyl residue in Asp-Asp-Asp-Asp will form DCAN at even slower rates. Compared to Asp-Asp-Asp-Asp, Arg-Gly-Asp-Ser contains only one aspartyl residue near the *C*-terminal end, and thus DCAN formation from this peptide is expected to be much slower. As is obvious in *Figure 29*, all kinetic data well supported the expected DCAN formation trends from the two investigated tetrapeptides and the corresponding DCAN formation mechanisms can therefore be proposed as shown in *Figure 30 & 31*.

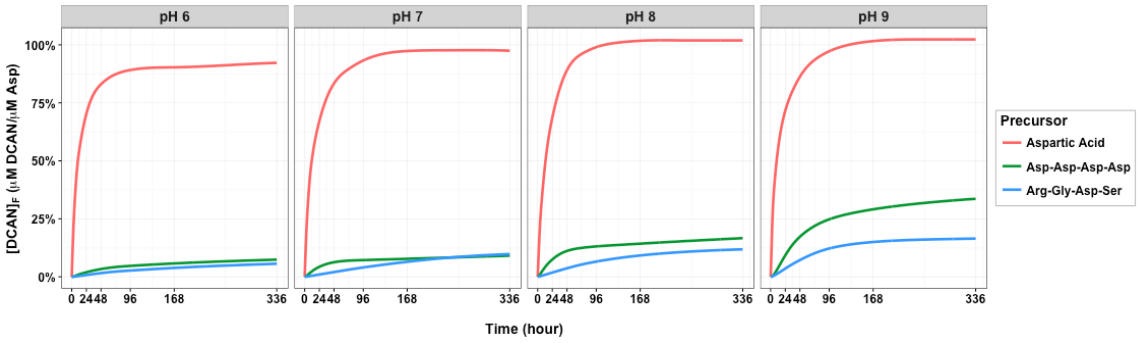

Figure 31. Comparison of cumulative DCAN formation potentials (calculated using *Equation 32*) of free aspartic acid Asp-Asp-Asp-Asp, and Arg-Gly-Asp-Ser under four pH conditions.

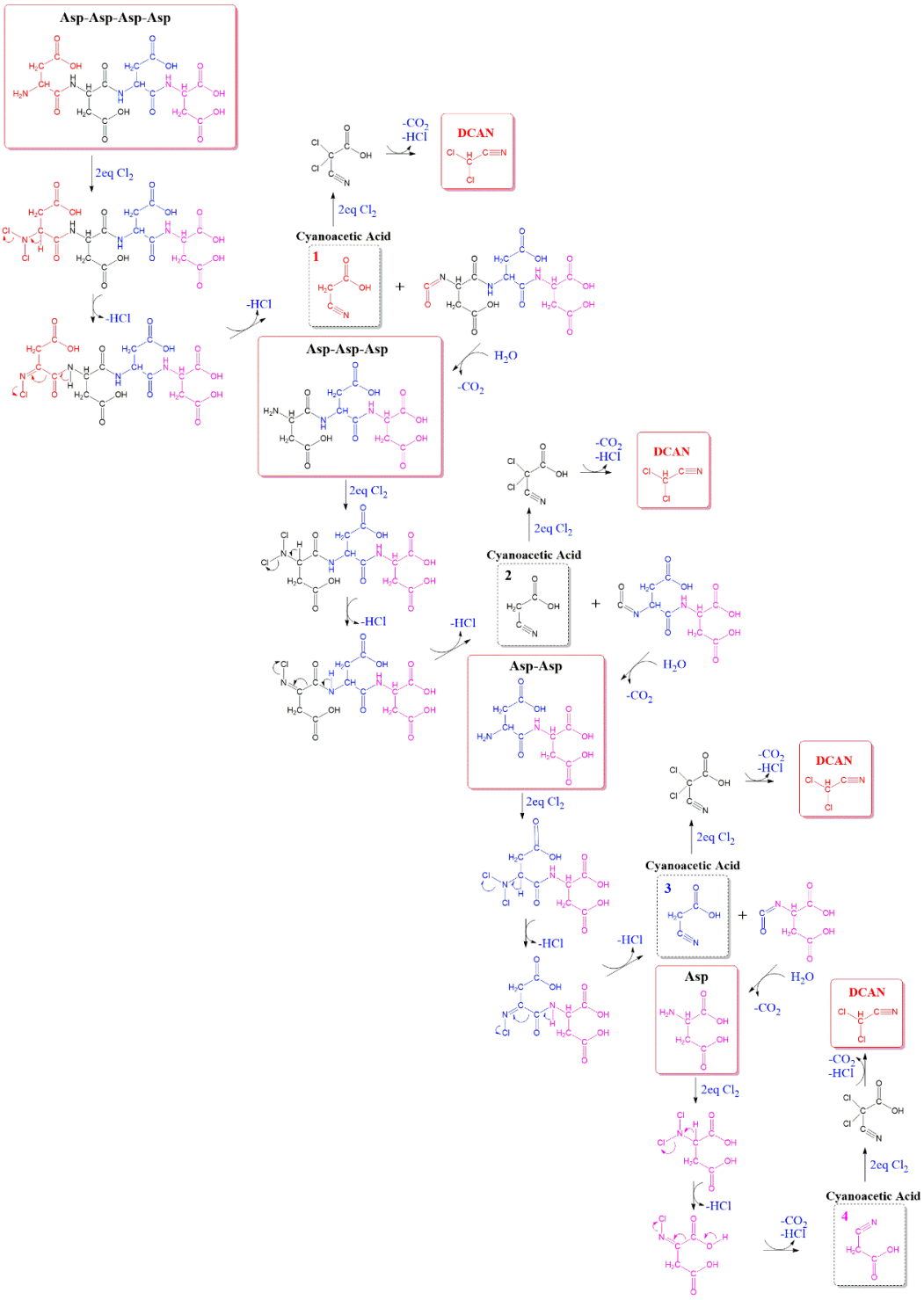

Figure 32. Proposed DCAN formation pathways from chlorine-induced Asp-Asp-Asp-Asp degradation. Four aspartyl residues in this peptide are indicated by different colors.

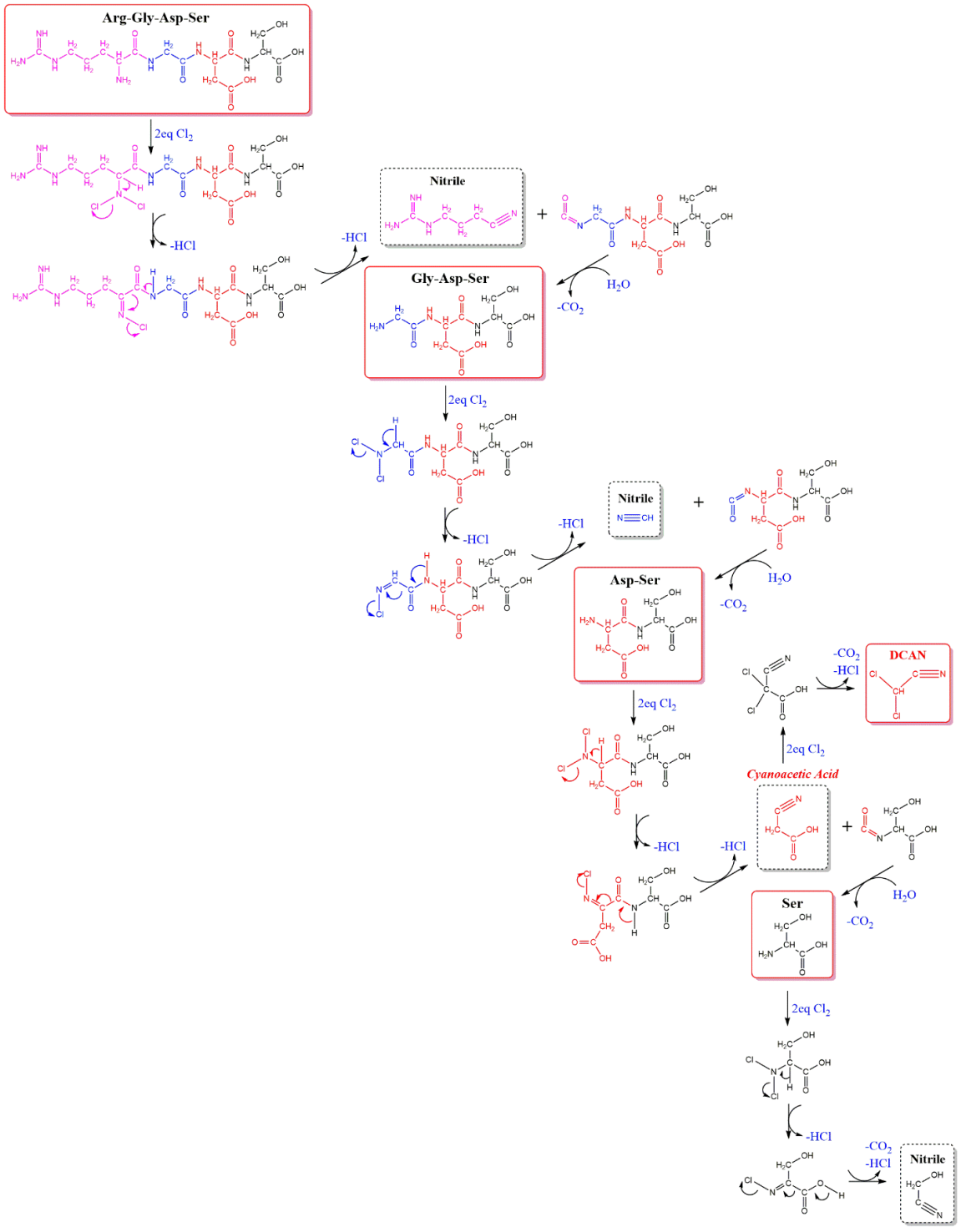

Figure 33. Proposed DCAN formation pathways from chlorine-induced Arg-Gly-Asp-Ser degradation. The four amino acid residues are indicated by different colors.

4.3.3. *N-chloro-2,2*-dichloroacetamide and Dichloroacetic Acid Formation from Free Aspartic Acid

As has been demonstrated above, large quantities of DCAN can initially form but subsequently degrade during the chlorination of all three model precursors. Thus, it is necessary to understand both the identities and quantities of these secondary degradation products. In Chapter 3, *N-Cl*-DCAM and DCAA were found to be the major DCAN decomposition products in chlorinated drinking waters and therefore these two compounds were also quantified during the course of aspartic acid chlorination.

Figure 32 shows that both *N-Cl*-DCAM and DCAA were formed, which considerably accounted for the loss of DCAN under all pH conditions. In general, *N-Cl*-DCAM formation increased not only with increasing reaction time but also with increasing pH. At lower pHs (i.e., pH 6 and 7), *N-Cl*-DCAM was barely measurable. However, when pH was increased to 8, its formation became much more substantial, albeit its yield exhibited some slight decrease at longer reaction times. At pH 9, more *N-Cl*-DCAM was formed and its yield quickly reached a plateau of 62% (mol/mol of aspartic acid) within the first 72 hours. These trends can be explained by the dual dependence of *N-Cl*-DCAM formation and degradation on pH (Chapter 3). In brief, high pH favors *N-Cl*-DCAM formation while inhibits its decomposition. For this reason, greater amount of *N-Cl*-DCAM was formed at higher pHs, under which conditions it also persisted longer.

On the other hand, the formation of DCAA continuously increased over reaction time but significantly decreased with increasing pH with the exception of pH 6. At this slightly acidic pH, only a small amount of DCAN was initially degraded so that the formation of both *N-Cl*-DCAM and DCAA was relatively insignificant compared to the other pH

conditions. In Chapter 3, it has been confirmed that DCAN will degrade to form DCAA mainly through an acid-catalyzed *N-Cl*-DCAM chlorination pathway (*Figure 20*). Therefore, when pH was below or close to neutral, *N-Cl*-DCAM degradation was accelerated so that the amount of DCAN decomposed was mostly offset by the amount of DCAA formed. However, at pH 9, considerable DCAA formation was still observed when the formed *N-Cl*-DCAM wasn't degraded (*Figure 32*). This is indicative of another DCAA formation pathway that is independent of *N-Cl*-DCAM decomposition. More importantly, the aggregate DCAN, *N-Cl*-DCAM, and DCAA formation (shown by purple diamonds in *Figure 32*) fully accounted for the amount of DCAN that was initially formed (shown by solid black lines in *Figure 32*), suggesting that the rapid DCAA formation at pH 9 was also a result of DCAN degradation. For these reasons, a new DCAA formation pathway can be proposed as follows in *Figure 33.* In this pathway, DCAN will undergo sequential reactions with hydroxide and hypochlorite to form an *N-chloro-2,2*-dichloroethane-*1,1*-diol. Following hydrolysis of this *N-Cl*-DCAM hydroxyl adduct eventually yields a DCAA. Due to the participation of both a hydroxide ion and a hypochlorite ion, this reaction is presumed to be base-catalyzed, and thus was only noted in this case at the highest reaction pH (i.e., pH 9)

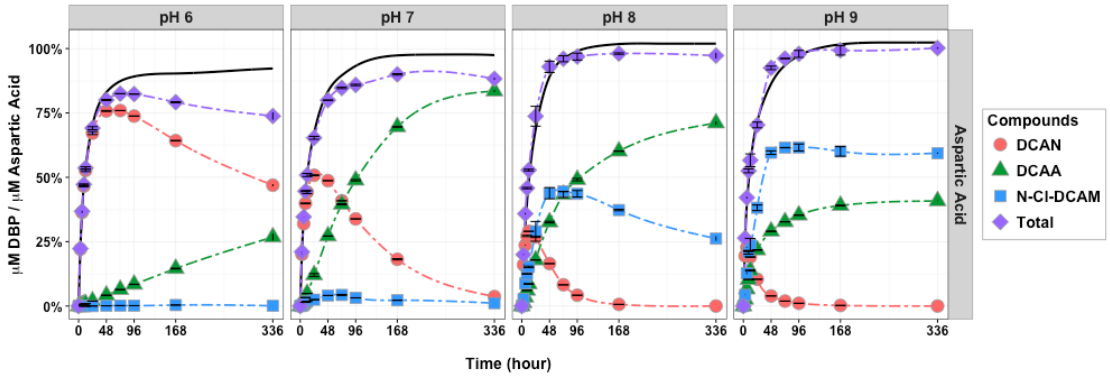

Figure 34. DCAN, *N-Cl*-DCAM, and DCAA formation as a function of reaction time and pH during the chlorination of free aspartic acid. Purple diamonds represent the aggregate formation potentials of all three dichloro species. Black solid lines indicate the cumulative DCAN formation potentials (i.e., $[DCAN]_F$) that were calculated based on *Equation 32*. All solid symbols are actual time-based measurements, with dashed lines interpolating the corresponding kinetic profiles.

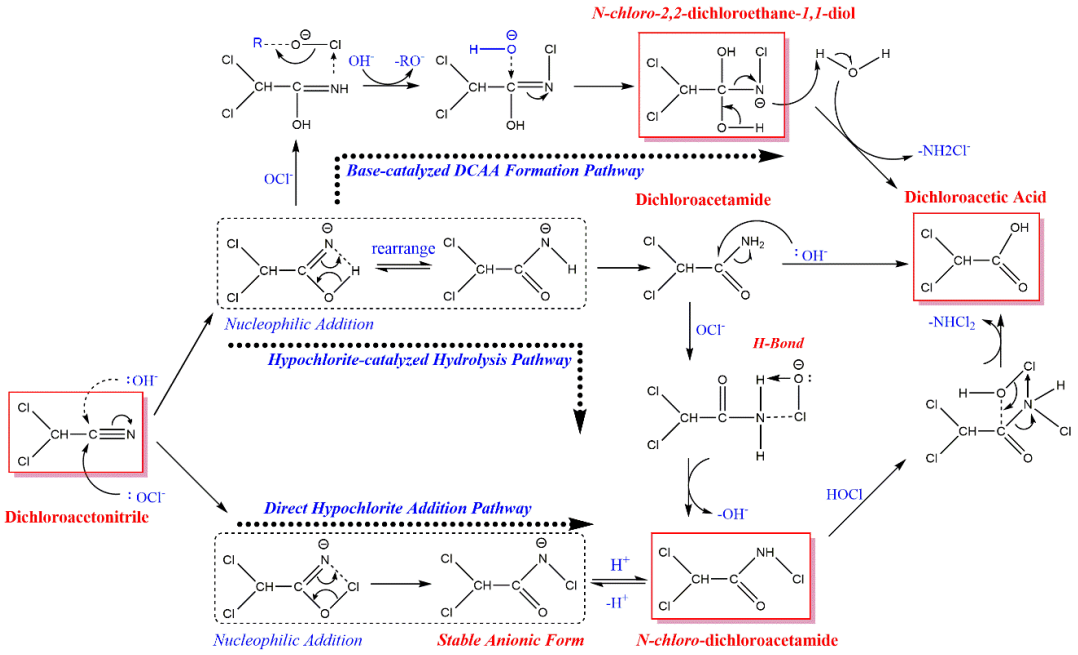

Figure 35. Proposed *N-Cl*-DCAM and DCAA formation pathways from DCAN degradation.

4.3.4. *N-chloro-2,2*-dichloroacetamide and Dichloroacetic Acid Formation from Aspartyl-containing Tetrapeptides

Significant *N-Cl*-DCAM formation was also observed during the chlorination of Asp-Asp-Asp-Asp and Arg-Gly-Asp-Ser (*Figure 34*), which exhibited many of the similar trends as noted previously for free aspartic acid. At pH 6 and 7, only trivial amount of *N-Cl*-DCAM was formed. This is probably because peptides were less reactive with chlorine to form DCAN at lower pHs, whereas the formed DCAN either didn't substantially degrade (e.g., pH 6), or decomposed to form DCAA instead. When pH was above neutral, the yields of *N-Cl*-DCAM increased with both increasing reaction time and pH as its formation was accelerated while decomposition was retarded under these more alkaline conditions. More importantly, *N-Cl*-DCAM yields were consistently lower than the amount of DCAN that could have cumulatively formed without degradation (i.e., $[DCAN]_F$). For this reason, it is highly likely that *N-Cl*-DCAM was produced exclusively from DCAN decomposition other than from some other peptide or intermediate chlorination pathways.

Furthermore, it is obvious in *Figure 34* that both Asp-Asp-Asp-Asp and Arg-Gly-Asp-Ser yielded large amounts of DCAA under all pH conditions, which positively deviated from the cumulative DCAN formation potentials that were predicted during prior discussions. Therefore, the prevailing DCAN degradation pathways (*Figure 33*) will not fully account for the amount of DCAA that was produced by these two peptides. On the other hand, in the chlorination of peptides, certain active amino acid side chains may be oxidized by chlorine independently of the stepwise peptide degradation pathway, thus giving rise to additional DCAA formation. For example, it is chemically plausible that

the side chain of an aspartyl residue (i.e., -CH_2-C(O)-OH) can be chlorinated and then cleaved to form DCAA. Moreover, both free arginine and serine exhibited certain DCAA formation potentials (0.569 ± 0.014% and 0.063 ± 0.009%, respectively) when chlorinated with excess chlorine at pH 7 (Hong & Liang, 2008). Hence, these two amino acid monomers may still be able to contribute to DCAA formation once they are removed from the peptide structure. Nonetheless, to fully understand the DCAA formation mechanisms during the chlorination of Asp-Asp-Asp-Asp and Arg-Gly-Asp-Ser, further research using isotopically labeled model compounds is needed.

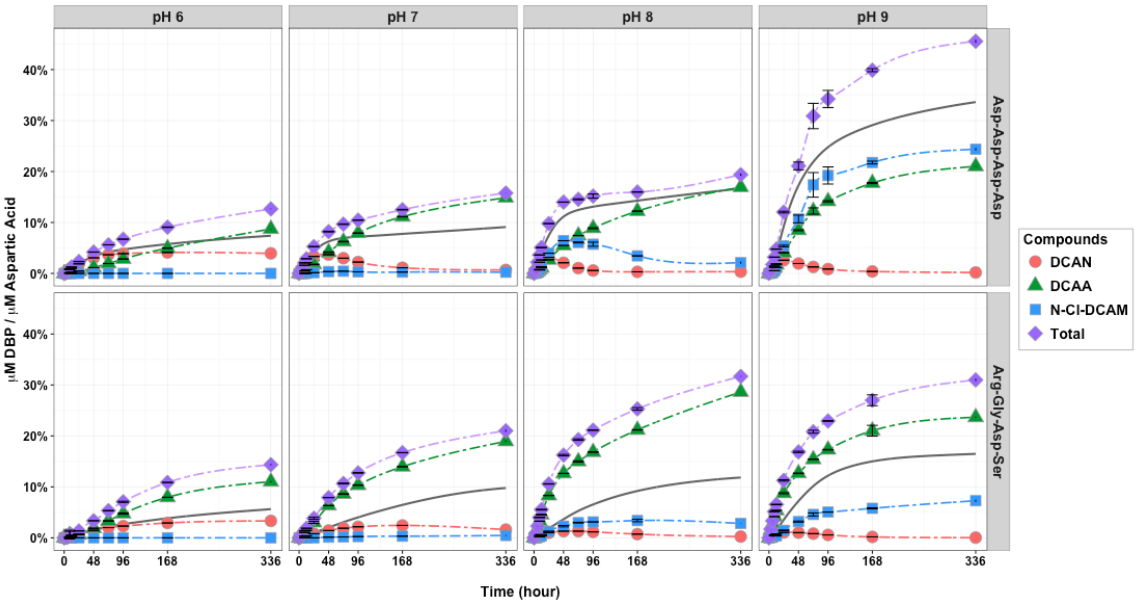

Figure 36. DCAN, *N-Cl*-DCAM, and DCAA formation during the chlorination of Asp-Asp-Asp-Asp and Arg-Gly-Asp-Ser at four pH levels. Purple diamonds represent the aggregate formation potentials of all three dichloro species. Black solid lines indicate the cumulative DCAN formation potentials (i.e., $[DCAN]_F$) that were calculated based on *Equation 32*. All solid symbols are actual time-based measurements, with dashed lines interpolating the corresponding kinetic profiles.

4.3.5. Implications with Respect to Precursor Removal during Drinking Water Treatment

As was confirmed in this study, combined amino acids (i.e., peptides) actually have significant reactivity to form both nitrogenous and carbonaceous DBPs under conditions that are typical for drinking water treatment. The nitrogenous DBPs (i.e., DCAN and *N*-*Cl*-DCAM) were mainly derived via chlorine-induced stepwise peptide degradation so that the amino nitrogens served as the nitrogen source for both N-DBPs. However, the carbonaceous byproduct (i.e., DCAA) tended to form independently through halogenative oxidation of the amino acid side chains in addition through the aforementioned DCAN as its decomposition product. Perhaps most importantly, proteinaceous material, including peptides, proteins, and amino acids that are associated with humic substances, are usually found in hydrophilic neutral or base fractions of NOM (Westerhoff & Mash, 2002), which are poorly removed by conventional drinking water treatment processes (e.g., coagulation; Scully et al., 1988), compared to the hydrophobic fractions that usually harbor most THM precursors. For this reason, it may be important for treatment plant operators to develop different treatment techniques to control the formation of different types DBPs, especially if these emerging N-DBPs (i.e., HANs and *N*-*Cl*-HAMs) are soon to be considered for future regulation.

CHAPTER 5

CONCLUSIONS

The fate of HANs in drinking waters from their precursors in natural waters to their degradation products in consumers' tap were systematically investigated in this study.

Combined amino acids were proved reactive with chlorine to form DCAN under typical drinking water conditions. However, the rate of DCAN formation from bound aspartyl residues was much slower compared to free aspartic acid. The key to DCAN formation from combined amino acids was a chlorine-induced peptide degradation process, which slowly degraded the peptide backbone to continuously produce reactive amine functional groups at the *N*-terminal end. Particularly, when an *N*-terminal aspartyl residue is chlorinated, it will form an *N*-chloroimine, which can undergo C-C cleavage to remove a cyanoacetic acid from the peptide structure. This cyanoacetic acid will then transform to DCAN as an essential intermediate precursor.

Simultaneous to their continuous formation, HANs were found to be chemically unstable and can undergo considerable decomposition via several types of degradation reactions. The rate of HAN loss generally increased with increasing pH but varied among different HAN analogues depending on the nature of their halogenated substituents. Additionally, free chlorine was shown to be an important facilitator and HAN degradation was accelerated in its presence. Perhaps most importantly, a mathematical kinetic model was established for seven chlorinated and brominated HAN species and their second-order hydrolysis and chlorination reaction rate constants were estimated

using a Bayesian modeling framework, so that their lifetimes under typical sets of drinking water conditions can be quantitatively predicted

As HANs degrade, they leave other reaction products in their place. In the absence of chlorine, HANs decomposed to form the corresponding HAMs as reaction intermediates and HAAs as endpoint products. When chlorine was present, a group of previously unreported compounds, the *N*-*Cl*-HAMs were proved to be the HAN chlorination intermediates. However, *N*-*Cl*-HAMs are often misidentified in chlorinated drinking waters in the form of HAMs because the nitrogen-bound chlorine in *N*-*Cl*-HAMs is highly labile and thus can be readily dechlorinated by common reducing agents during sample preservation. *N*-*Cl*-HAMs are weakly acidic and they exhibited very high stability in water under a wide range of pH conditions without the presence of chlorine. On the other hand, it can undergo acid-catalyzed chlorination by hypochlorous acid to form the corresponding DCAA. Lastly, an analytical method using ultra performance liquid chromatography (UPLC)-quadrupole time-of-flight mass spectrometry (qTOF) was developed for a family of seven *N*-*Cl*-HAMs. Combined with solid phase extraction, the occurrence of *N*-*Cl*-DCAM and its two brominated analogues (i.e., *N*-*Cl*-BCAM and *N*-*Cl*-DBAM) in real tap waters was quantitatively determined for the first time.

CHAPTER 6

RECOMMENDATIONS FOR FUTURE WORK

Since the formation of *N*-*Cl*-THAMs from THAM chlorination has been confirmed by UPLC/ESI/qTOF MS, it becomes important to understand their relations with the corresponding THANs and THAMs by quantitatively characterizing their formation kinetics. It was noticed in the preliminary study that the chlorination reaction rates of all four THAMs were faster than the maximum detectable rate that can be achieved by a regular spectrophotometric system. Therefore, a spectrophotometer coupled with a rapid mixing stopped-flow accessory may be a more appropriate setup to obtain more reliable kinetic data for the estimation of those second-order THAM chlorination rate constants.

For a more complete description of the formation and degradation of *N*-*Cl*-HAMs in chlorinated drinking waters, the stability of *N*-*Cl*-BCAM, *N*-*Cl*-DBAM, and *N*-*Cl*-THAMs needs to evaluated. For this reason, a more comprehensive kinetic analysis is needed to investigate *N*-*Cl*-HAM degradation kinetics under a range of pH conditions with and without the presence of chlorine. Residual *N*-*Cl*-HAM concentrations can be determined over reaction time using the UPLC/ESI/MS method that was developed in this study. Ideally, a mathematical kinetic model can also be established to predict their lifetimes in drinking water on time scales relevant to system residence times.

Lastly, more *N*-*Cl*-HAM occurrence data has to be collected to understand their relative importance compared to HANs and HAMs. More importantly, cytotoxicity and genotoxicity of *N*-*Cl*-HAMs need to be quantitatively determined and the impact of HAN

transformation, to *N*-*Cl*-HAMs, and ultimately to HAAs on aggregate drinking water toxicity has to be assessed.

REFERENCES

1. Alouini, Z.; Seux, R. Kinetics and mechanisms of hypochlorite oxidation of alpha-amino-acids at the time of water disinfection. *Water Res.* **1987,** *21* (3), 335-343.

2. Bieber, T.I.; Trehy, M.L. Dihaloacetonitriles in chlorinated natural waters. *Water chlorination: environmental impact and health effects.* **1983,** *4*.

3. Blank, V.; Shukairy, H.; McLain, J.; McGuire, M.; McLain, J.; Obolensky, A. Unregulated organic DBPs in ICR finished water and distribution systems. *Information Collection Rule Data Analysis.* **2002,** 277-297.

4. Bond, T.; Henriet, O.; Goslan, EH.; Parsons, S.A.; Jefferson, B. Disinfection byproduct formation and fractionation behavior of natural organic matter surrogates. *Environ. Sci. Technol.* **2009,** *43* (15), 5982-9.

5. Bond, T.; Templeton, M.R.; Graham, N. Precursors of nitrogenous disinfection by-products in drinking water—a critical review and analysis. J. Hazard. Mater. **2012**, 235, 1-16.

6. Bond, T.; Kamal, N.H.M.; Bonnisseau, T.; Templeton, M.R. Disinfection by-product formation from the chlorination and chloramination of amines. *J. Hazard. Mater.* **2014,** *278*, 288-296.

7. Bond, T.; Templeton, M.R.; Kamal, N.H.M.; Graham, N.; Kanda, R. Nitrogenous disinfection byproducts in English drinking water supply systems: Occurrence, bromine substitution and correlation analysis. *Water Res.* **2015,** *85*, 85-94.

8. Bull, R.J.; Reckhow, D.A.; Li, X.; Humpage, A.R.; Joll, C.; Hrudey, S.E. Potential carcinogenic hazards of non-regulated disinfection by-products: Haloquinones, halo-cyclopentene and cyclohexene derivatives, N-halamines, halonitriles, and heterocyclic amines. *Toxicology.* **2011,** *286* (1), 1-19.

9. Carlin, Bradley. P.; Louis, Thomas. *A Bayesian methods for data analysis, third edition* .2008.

10. Chen, B. Hydrolytic Stabilities of Halogenated Disinfection Byproducts: Review and Rate Constant Quantitative Structure-Property Relationship Analysis. *Environ. Eng. Sci.* **2011,** *28* (6), 385-394.

11. Choy, S.L.; O'Leary, R.; Mengersen, K. Elicitation by design in ecology: using expert opinion to inform priors for Bayesian statistical models. *Ecology*. **2009,** *90* (1), 265-277.

12. Chu, W.; Gao, N.; Deng, Y. Formation of haloacetamides during chlorination of dissolved organic nitrogen aspartic acid. *J. Hazard. Mater.* **2010b,** *173* (1), 82-86.

13. Chu, W.; Gao, N.; Deng, Y.; Krasner, S.W. Precursors of dichloroacetamide, an emerging nitrogenous DBP formed during chlorination or chloramination. *Environ. Sci. Technol.* **2010a,** *44* (10), 3908-3912.

14. Conyers, B.; Scully Jr, F.E. N-chloroaldimines. 3. Chlorination of phenylalanine in model solutions and in a wastewater. *Environ. Sci. Technol.* **1993,** *27* (2), 261-266.

15. Conyers, B.; Scully, F.E. Chloramines V: products and implications of the chlorination of lysine in municipal wastewaters. *Environ. Sci. Technol.* **1997,** *31* (6), 1680-1685.

16. Deborde, M.; von Gunten, U. Reactions of chlorine with inorganic and organic compounds during water treatment—kinetics and mechanisms: a critical review. *Water Res.* **2008,** *42* (1), 13-51.

17. Englezos, Peter.; Kalogerakis, Nicolas. *Applied parameter estimation for chemical engineers.* M. Dekker: New York, 2001.

18. Fox, T.C.; Keefe, D.J.; Scully, F.E.; Laikhter, A. Chloramines VII: chlorination of alanylphenylalanine in model solutions and in a wastewater. *Environ. Sci. Technol.* **1997,** *31* (7), 1979-1984.

19. Gao, Zhenglei.; Green, John W.; Vanderborght, Jan.; Schmitt, Walter. Improving uncertainty analysis in kinetic evaluations using iteratively reweighted least squares. *ETC Environmental Toxicology and Chemistry.* **2011,** *30* (10), 2363-2371.

20. Gelman, Andrew.; Rubin, Donald. B. Inference from Iterative Simulation Using Multiple Sequences. *Statistical Science.* **1992,** *7* (4), 457-472.

21. Gelman, Andrew.; Hill, Jennifer. *Data analysis using regression and multilevel/hierarchical models.* Cambridge University Press: Cambridge; New York, 2007.

22. Gelman, A. *Bayesian data analysis.* Chapman & Hall: London; New York, 1995.

23. Glezer, V.; Harris, B.; Tal, N.; Iosefzon, B.; Lev, O. Hydrolysis of haloacetonitriles: linear free energy relationship, kinetics and products. *Water Res.* **1999,** *33* (8), 1938-1948.

24. Goldschmidt, S.; Wiberg, E.; Nagel, E.; Martin, K. About Proteins. *Justus Liebigs Ann. Chem.* 1927**,** *456*, 1-38.

25. Görlitz, L.; Gao, Z.; Schmitt, W. Statistical analysis of chemical transformation kinetics using Markov-Chain Monte Carlo methods. *Environ. Sci. Technol.* **2011,** *45* (10), 4429-37.

26. Hand, V.C.; Margerum, D.W. Kinetics and mechanisms of the decomposition of dichloramine in aqueous solution. *Inorganic Chem.* **1983,** *22* (10), 1449-1456.

27. Hansch, C.; Leo, A.; Taft, R. A survey of Hammett substituent constants and resonance and field parameters. *Chem. Rev.* **1991,** *91* (2), 165-195.

28. Hawkins, C.L.; Davies, M.J. Hypochlorite-induced oxidation of proteins in plasma: formation of chloramines and nitrogen-centered radicals and their role in protein fragmentation. *Biochem. J.* **1999,** *340 (Pt 2)*, 539-548.

29. Hayes-Larson, E.L.; Mitch, W.A. Influence of the method of reagent addition on dichloroacetonitrile formation during chloramination. *Environ. Sci. Technol.* **2009,** *44* (2), 700-706.

30. Hong, H.; Wong, M.; Liang, Y. Amino acids as precursors of trihalomethane and haloacetic acid formation during chlorination. *Arch. Environ. Contam. Toxicol.* **2009,** *56* (4), 638-645.

31. Hrudey, E.J. *Safe drinking water: Lessons from recent outbreaks in affluent nations.* IWA publishing: 2004.

32. Hua, G.; Reckhow, D.A. Evaluation of bromine substitution factors of DBPs during chlorination and chloramination. *Water Res.* **2012,** *46* (13), 4208-4216.

33. Hureiki, L.; Croue, J.; Legube, B. Chlorination studies of free and combined amino acids. *Water Res.* **1994,** *28* (12), 2521-2531.

34. Keefe, Daniel J.; Fox, T. Christopher.; Conyers, Barbara.; Scully, Frank E. Chloramines VI: Chlorination of Glycylphenylalanine in Model Solutions and in a Wastewater. *Environmental Science & Technology.* **1997,** *31* (7), 1973-1978.

35. Kimura, S.Y.; Komaki, Y.; Plewa, M.J.; Mariñas, B.J. Chloroacetonitrile and N,2-dichloroacetamide formation from the reaction of chloroacetaldehyde and monochloramine in water. *Environ. Sci. Technol.* **2013,** *47* (21), 12382-12390.

36. Kimura, S.Y.; Vu, T.N.; Komaki, Y.; Plewa, M.J.; Mariñas, B.J. Acetonitrile and N-Chloroacetamide Formation from the Reaction of Acetaldehyde and Monochloramine. *Environ. Sci. Technol.* **2015,** *49* (16), 9954-9963.

37. Krasner, S.W.; McGuire, M.J.; Jacangelo, J.G.; Patania, N.L.; Reagan, K.M.; Aieta, E.M. The occurrence of disinfection by-products in US drinking water. *Journal-American Water Works Association.* **1989,** *81* (8), 41-53.

38. Krasner, S.W.; Weinberg, H.S.; Richardson, S.D.; Pastor, S.J.; Chinn, R.; Sclimenti, M.J.; Onstad, G.D.; Thruston, A.D. Occurrence of a new generation of disinfection byproducts. *Environ. Sci. Technol.* **2006,** *40* (23), 7175-7185.

39. Kuhnert, P.M.; Martin, T.G.; Griffiths, S.P. A guide to eliciting and using expert knowledge in Bayesian ecological models. *Ecol. Lett.* **2010,** *13* (7), 900-914.

40. Lawson, A., *Bayesian disease mapping: hierarchical modeling in spatial epidemiology.* CRC Press: Boca Raton, 2009.

41. Lee, W.; Westerhoff, P.; Croué, J. Dissolved organic nitrogen as a precursor for chloroform, dichloroacetonitrile, N-nitrosodimethylamine, and trichloronitromethane. *Environ. Sci. Technol.* **2007,** *41* (15), 5485-5490.

42. Lowry, T.H.; Richardson, K.S. Mechanism and theory in organic chemistry. 1981.

43. Lunn DJ, Aarons, L. The pharmacokinetics of saquinavir: a Markov chain Monte Carlo population analysis. *J. Pharmacokinet. Biopharm.* **1998,** *26* (1), 47-74.

44. McCormick, E.F.; Conyers, B.; Scully Jr, F.E. N-chloroaldimines. 2. Chlorination of valine in model solutions and in a wastewater. *Environ. Sci. Technol.* **1993,** *27* (2), 255-261.

45. McKinney, J.; Mauer, R.; Haas, J.; Thomas, R. Possible factors in the drinking water of laboratory animals causing reproductive failure. *Identification and Analysis of Organic Pollutants in Water (LH Keith, Ed.), Ann Arbor Science Publishers, Ann Arbor, MI.* 1976**,** 417-432.

46. Menard, H.; Lessard, J. Acidities of some N-haloamides (ZCONHX) in water and ethanol-water mixtures at 25 degree C. *J. Chem. Eng. Data.* **1978,** *23* (1), 64-65.

47. Mitch, W.A.; Krasner, S.W.; Westerhoff, P.; Dotson, A. Occurrence and formation of nitrogenous disinfection by-products. **2009.**

48. Morris, J.C. The acid ionization constant of HOCl from 5 to 35. *J. Phys. Chem.* **1966,** *70* (12), 3798-3805.

49. Morris, J. The Chemistry of Aqueous Chlorine in Relation to Water Chlorination. Water Chlorination: Environmental Impact and Health Effects. *Ann Arbor Sci. Publ., Ann Arbor, Michigan,* **1975.**

50. Muellner, M.G.; Wagner, E.D.; McCalla, K.; Richardson, S.D.; Woo, Y.; Plewa, M.J. Haloacetonitriles vs. regulated haloacetic acids: are nitrogen-containing DBPs more toxic? *Environ. Sci. Technol.* **2007,** *41* (2), 645-651.

51. Nweke, A.; Scully Jr, F.E. Stable N-chloroaldimines and other products of the chlorination of isoleucine in model solutions and in a wastewater. *Environ. Sci. Technol.* **1989,** *23* (8), 989-994.

52. Oliver, B.G. Dihaloacetonitriles in drinking water: algae and fulvic acid as precursors. *Environmental Science & Technology.* **1983,** *17* (2), 80-83.

53. Pereira, W.; Hoyano, Y.; Summons, R.; Bacon, V.; Duffield, A. Chlorination studies II. The reaction of aqueous hypochlorous acid with α-amino acids and dipeptides. *Biochimica et. Biophysica Acta (BBA)-General Subjects* **1973,** *313* (1), 170-180.

54. Peters, Ruud J. B., De Leer, Ed W. B.; De Galan, Leo. Chlorination of cyanoethanoic acid in aqueous medium. *Environmental Science & Technology.* **1990,** *24* (1), 81-86.

55. Plewa, M.J.; Muellner, M.G.; Richardson, S.D.; Fasano, F.; Buettner, K.M.; Woo, Y.; McKague, A.B.; Wagner, E.D. Occurrence, synthesis, and mammalian cell cytotoxicity and genotoxicity of haloacetamides: an emerging class of nitrogenous drinking water disinfection byproducts. *Environ. Sci. Technol.* **2007,** *42* (3), 955-961.

56. Plewa, M.J.; Wagner, E.D.; Jazwierska, P.; Richardson, S.D.; Chen, P.H.; McKague, A.B. Halonitromethane drinking water disinfection byproducts: chemical characterization and mammalian cell cytotoxicity and genotoxicity. *Environ. Sci. Technol.* **2004,** *38* (1), 62-68.

57. Plummer, J.D.; Edzwald, J.K. Effect of ozone on disinfection by-product formation of algae. *Water science and technology* **1998,** *37* (2), 49-55.

58. Plummer, M. rjags: Bayesian graphical models using MCMC. *R package version* **2011,** *2* (0).

59. Reckhow, D.A.; Platt, T.L.; MacNeill, A.; McClellan, J.N. Formation and degradation of DCAN in drinking waters. *Journal of Water Supply Research and Technology, AQUA.* **2001,** *50* (1), 1-13.

60. Richardson, S.D.; Postigo, C. Drinking water disinfection by-products, In *Emerging organic contaminants and human health,* Anonymous; Springer: 2011; pp. 93-137.

61. Rook, J.J. Formation of haloforms during chlorination of natural waters. *Water Treat. Exam.* **1974,** *23*, 234-243.

62. Schwarzenbach, R.; Gschwend, P.; Imboden, D. Environmental chemistry. *Environmental chemistry.* 2003

63. Scully, F.E.; Howell, G.D.; Kravitz, R.; Jewell, J.T.; Hahn, V.; Speed, M. Proteins in natural waters and their relation to the formation of chlorinated organics during water disinfection. *Environ. Sci. Technol.* **1988,** *22* (5), 537-542.

64. Shah, A.D.; Mitch, W.A. Halonitroalkanes, halonitriles, haloamides, and N-nitrosamines: A critical review of nitrogenous disinfection byproduct formation pathways. *Environ. Sci. Technol.* **2011,** *46* (1), 119-131.

65. Silverman, R.A.; Gordon, G. Variation of the absorbance spectra of hypochlorous acid with perchlorate concentration. A hypochromic effect. *J. Phys. Chem.* **1980,** *84* (6), 625-629.

66. Stedinger, J.R.; Tasker, G.D. Regional hydrologic analysis: 1. Ordinary, weighted, and generalized least squares compared. *Water Resour. Res.* **1985,** *21* (9), 1421-1432.

67. Steinschneider S.; L.U. A hierarchical Bayesian regional model for nonstationary precipitation extremes in Northern California conditioned on tropical moisture exports. *Water Resources Research.* **2015,** *51* (3), 1472-1492.

68. Stevens, A.A.; Moore, L.A.; Slocum, C.J.; Smith, B.L.; Seeger, D.R.; Ireland, J.C. By-products of chlorination at ten operating utilities. *Water Chlorination: Chemistry, Environmental Impact and Health Effects.* **1990,** *6*, 579-604.

69. Taft Jr, R.W. Polar and steric substituent constants for aliphatic and o-Benzoate groups from rates of esterification and hydrolysis of esters1. *J. Am. Chem. Soc.* **1952,** *74* (12), 3120-3128.

70. Taft Jr, R. *Separation of Polar, Steric and Resonance Effects in Reactivity in Steric Effects in Organic Chemistry.* John Wiley and Sons, New York, 1956.

71. Tellinghuisen, J., A Monte Carlo Study of Precision, Bias, Inconsistency, and Non-Gaussian Distributions in Nonlinear Least Squares. *JOURNAL OF PHYSICAL CHEMISTRY A*. **2000,** *104*, 2834-2844.

72. Thomm, Ernest Wing Chup Wong; Wayman, M. N-chlorination of secondary amides. II. Effects of substituents on rates of N-chlorination. *Canadian Journal of Chemistry* **1969,** *47* (18), 3289-3297.

73. Thurman, E. *Organic geochemistry of natural waters.* Springer Science & Business Media: 1985.

74. Trehy, M.L. *The formation of dihaloacetonitriles by chlorination of natural water.* Florida Atlantic University. 1980.

75. Trehy, M.L.; Bieber, T.I. Detection, identification and quantitative analysis of dihaloacetonitriles in chlorinated natural waters. *Advances in the Identification & Analysis of Organic Pollutants in Water.* **1981,** *2*.

76. Trehy, M.L.; Yost, R.A.; Miles, C.J. Chlorination byproducts of amino acids in natural waters. *Environ. Sci. Technol.* **1986,** *20* (11), 1117-1122.

77. Ueno, H.; Moto, T.; Sayato, Y.; Nakamuro, K. Disinfection by-products in the chlorination of organic nitrogen compounds: By-products from kynurenine. *Chemosphere.* **1996,** *33* (8), 1425-1433.

78. USEPA; Stage 2 Disinfectants/Disinfection Byproducts Rule; Proposed Rule. Fed. Reg., 68:159:49548. 2003.

79. Wayman, M.; Thomm, E. N-Chlorination of secondary amides. I. Kinetics of N-chlorination of N-methyl acetamide. *Canadian Journal of Chemistry.* **1969,** *47* (14), 2561-2567.

80. Weinberg, H.S.; Krasner, S.W.; Richardson, S.D.; Thruston Jr, A.D. *The occurrence of disinfection by-products (DBPs) of health concern in drinking water: results of a nationwide DBP occurrence study.* 2002.

81. Westerhoff, P.; Mash, H. Dissolved organic nitrogen in drinking water supplies: a review. *Aqua.* **2002,** *51*, 415-448.

82. Wikle, C.K. Hierarchical Bayesian models for predicting the spread of ecological processes. *Ecology.* **2003,** *84* (6), 1382-1394.

83. Yang, X.; Fan, C.; Shang, C.; Zhao, Q. Nitrogenous disinfection byproducts formation and nitrogen origin exploration during chloramination of nitrogenous organic compounds. *Water Res.* **2010,** *44* (9), 2691-2702.

84. Yang, X.; Shen, Q.; Guo, W.; Peng, J.; Liang, Y. Precursors and nitrogen origins of trichloronitromethane and dichloroacetonitrile during chlorination/chloramination. *Chemosphere* **2012,** *88* (1), 25-32.

85. Young, M.S.; Uden, P.C. Byproducts of the aqueous chlorination of purines and pyrimidines. *Environ. Sci. Technol.* **1994,** *28* (9), 1755-1758.

86. Yu, Y.; Steinschneider, S.; Reckhow, D.A. Evaluation of Environmental Degradation Kinetics Using Hierarchical Bayesian Modeling. *J. Environ. Eng.* **2015**, 06015008.

87. Zhang, X.; Minear, R.A. Decomposition of trihaloacetic acids and formation of the corresponding trihalomethanes in drinking water. *Water Res.* **2002,** *36* (14), 3665-3673.